L S Z
9 000004 122440

OF 1915

ANALELE UNIVERSITATII BUCURESTI

FIZICĂ

ANUL XXVII — 1978

FIZICĂ

COMITETUL DE REDACŢIE

Redactor responsabil :	Prof. dr. doc. *Gheorghe Brătescu*
Redactor responsabil adj. :	Prof. dr. *Ion Petrea*
Membri :	Prof. dr. doc. *Vasile Mihu*
	Conf. dr. *Constantin Vrejoiu*
	Conf. dr. *Dumitru Ciobotaru*
	Conf. dr. *Grecu Voicu*
Secretar de redacţie :	Lector dr. *Ion Licea*

REDACŢIA
TIPOGRAFIA UNIVERSITĂŢII BUCUREŞTI
Şoseaua Panduri, nr.90
Telefon 314000/132

~~F 8482~~ OF 1915

ANALELE UNIVERSITĂȚII BUCUREȘTI

1989

BUDAPESTI MŰSZAKI ÉS GAZDASÁGTUDOMÁNYI EGYETEM
Országos Műszaki Információs Központ és Könyvtár
2001

FIZICĂ

SUMAR ● CONTENTS

PLASMA PHYSICS

G. G. BRĂTESCU : Paschen's Potentials in Cadmium-Vapours and the Light Emitted in this Electrical Discharge 3
G. G. BRĂTESCU, MAGDA CAZAN-CORBASCA : Sparking Potentials and Ionization Coefficients in N.—Propanol Vapour ($CH_3-CH_2-CH_2OH$) 11
N. GHERBANOVSCHI : Negative Ions in Ionospheric Plasma 17

POLYMER PHYSICS

I. C. PETREA, C. A. STĂNESCU, TATIANA ALEXOIU-POP : Aspects cinétiques et morphologiques de la cristallinité de certains polymèrs. 21
M. COJOCARU, I. C. PETREA, C. A. STĂNESCU : Sur la relaxation des formations supramoleculaires dans le caoutchouc rétifié . . . 29
LIVIA MARIA IONESCU : La conformation des chaines macromoléculaires dans la phase lamellaire des copolyméres séquencés polystyrène-polysoprène a l'état solide 35

LIQUID STATE PHYSICS

CLEOPATRA GHERBANOVSCHI : Determination of some Physical Parameters of the Binary Liquid Acetic-Acid-Acetone Mixture. . 41

BIOPHYSICS

ALEXANDRINA STIRBEȚ, H. VAIS, V. GHEORGHE : Photosynthesis Redox Reactions Investigated by a Photocalorimetric Method 47
LILIANA RADU, V. GHEORGHE : Quantitative Estimation of the Structure of Nucleohistone Complexes : A Spectrophotometric and Spectrophotofluorometric Study 53

SOLID STATE PHYSICS

V. P. MIHU, VETURIA RASZILLIER : Attenuation and Velocity of Rayleigh Waves on the Surfaces of some Ferrous materials . . . 59
NICOLETA GRECU, V. GRECU, JANA BLUM : EPR'Study of Cu^{2+} Ions in Mordenite-Type Zeolites 69
I. LICEA, V. RUXANDRA : Non-Ohmic Electrical Conduction in Polycrystalline semiconducting CdS Thin Films. 77
V. RUXANDRA, I. LICEA, B. POPESCU : Curent-Field Characteristics of Smmal Conducting Thin Films in Strong Electric Field 83
G. G. BRĂTESCU, ELENA ZAMFIR, ZINCA MARIŞ : The Influence of Support Roughness on the Optical Constants of the PbTe Films Studied by Internal Reflection Ellipsometry 91

EARTH PHYSICS

ELENA DECU, ST. LASCU, D. EŞEANU : The Influence of the Meteorological Factors on the Concentration of Atmospheric Aerosol . 97
ST. LASCU : Some Notices on Intermediate Earthquakes Producing in Vrancea 103
ELENA DECU, D. VRAPCEA, GH. STĂNCĂLIE : Cosiderations synoptiques et statistiques sur les chutes de grêle en Roumanie . . . 109

GENERAL PHYSICS

G. G. BRĂTESCU, T. TUDOR : The investigation of the Three-Dimensional light distribution near focus with Laser Beam 121

BME KÖZPONTI KÖNYVTÁRA
F
8482
FOLYÓIRAT OSZTÁLY

Budapesti Műszaki Egyetem
Központi Könyvtára
Folyóiratleltár
8275/1978

BUDAPESTI MŰSZAKI EGYETEM KÖZPONTI KÖNYVTÁR 1848

ANALELE UNIVERSITĂȚII BUCUREȘTI, FIZICA, XXVIII, 1978, pag. 3–9

PASCHEN'S POTENTIALS IN CADMIUM-VAPOURS AND THE LIGHT EMITTED IN THIS ELECTRICAL DISCHARGE*

G. G. BRĂTESCU

Department of Optics, Spectroscopy and Plasma Physics
Faculty of Physics, University of Bucharest **

ABSTRACT

In cadmium vapours and with nickel plane electrodes the sparking potentials V_s were determined as a function of the reduced electrode distance p_0d (reduced pressure at 0°C x electrode distance), the Paschen's curve was plotted and the following minimum values were found: $V_{s,\min} = 439.5$ volts and $(p_0d)_{\min} = 0.69$ mm.Hg.0°C.cm. The luminous zones, that appear before the sparking voltage (in the Townsend's discharge) and after it (in the glow discharge), are the same with those previously observed by the author in similar discharge in potassium and cesium vapours. A broader discharge channel appeared and then a discharge of a different shape could be observed, namely the hindered abnormal glow discharge. Moreover, a second discharge channel in cadmium vapours stood out, narrower than the former and situated inside it.

1. Introduction

In 1957 and 1962, the author has determined the sparking potentials in kalium and cesium vapours [1], [2], [3], [4].

At the same time, the intense and clear luminous effects, that appeared in the stage of Townsend's discharge and then in the normal glow discharge have been investigated too [5]. A discharge channel stood out [6], [7].

By increasing the electrical potential between the electrodes, the normal glow discharge turns into a new one which the author called the hindered abnormal glow discharge [8], [9].

In the present work the author is carrying on the researches on metallic plasmas and determining the sparking potentials in cadmium vapours, evincing and describing the luminous effects that also appeared with alkali metals.

---

* This work has been presented at the "Conference on Plasma Physics", "Al. I. Cuza" — University, Jassy (Romania), Faculty of Physics, on November 25–26, 1977.

** National Centre of Physics, P. O. Box, 5211, Măgurele, Bucharest. Permanent adress: Str. Cpt. Preotescu 16, Sector 5, Bucharest, cod 75112.

However, in cadmium vapours other new shapes of discharge appeared.

2. Experimental method and results

Many experiments have been made in different discharge tubes.

The experimental results concerning this work have been obtained in a discharge tube having nickel plane electrodes, a Rogowski's profile and 7.5 cm in diameter. The diameter D of the electrode plane section was about 6.0 cm and the distance *d* between them was 1.91 cm.

The tube was cleaned up in vacuum at a pressure of 10^{-6} mm. Hg. and at a temperature of 550°C during 50 hours, using also a trap with liquid nitrogen. After a repeated distillation in vacuum, cadmium was introduced in the discharge tube, then the tube was closed in vacuum and mounted in an oven with no temperature gradient. The temperature was measured with a mercury thermometer of 650°C which was further checked with a crom-alumel thermo-couple. The thermometer was standardized by means of Pb (327.5°C), Zn (419.45°C) and Sb (630.5°C) melting points. Cadmium melting point is at 320.9°C.

The cadmium vapours saturated pressure in torrs was calculated as a function of abslute temperature T and A, B, C and D cadmium constants as follows [10] :

$$\log \mathrm{p}_{\mathrm{sat}} = -\frac{A}{T} + \mathrm{B} + \mathrm{C} \log T + DT.$$

The reduced pressure p_0 at 0°C was calculated by the formula

$$\mathrm{p}_0 = \mathrm{p}_{\mathrm{sat}} \frac{273}{273 + t}.$$

The electrical upset used was a classical one. The variable electrical potential between the electrodes was obtained by means of a variable potentiometer [11, p. 419].

The instant of the striking discharge at the sparking (breakdown) potential V_s was observed by the appearance of the negative glow in the normal glow discharge. Table I shows the obtained experimental values. The curve reproducing the values of the sparking potentials V_s as a function of (p_0, d), shows the minimum value of the sparking potentials $V_{s.\mathrm{min}} = 439.5$ volts at $(p_0 d)_{\mathrm{min}} = 0.69$ mm.Hg.0°C. cm for cadmium vapours and nickel electrodes plunged into the saturated cadmium vapours. The ratio between the electrode diameter D and the dis-

Table I

The sparking potentials V_s as a function of (p_0 d) for cadmium vapours and nickel electrodes

t°C	(p_0d) mm.Hg.0°C. cm	V_s volts	t°C	(p_0d) mm. Hg.0°C. cm	V_s volts
360.0	0.355	469.6	384.1	0.684	439.6
361.0	0.362	465.2	385.9	0.705	439.6
363.0	0.386	460.4	386.9	0.720	439.8
363.0	0.386	464.0	388.8	0.750	440.0
364.0	0.394	461.6	402.9	1.028	452.8
365.0	0.409	460.0	403.9	1.057	456.0
369.0	0.464	458.0	404.8	1.079	460.0
369.7	0.471	452.0	407.6	1.159	464.8
370.7	0.487	449.6	410.5	1.253	469.2
370.6	0.487	450.0	411.9	1.296	472.4
376.4	0.570	443.6	412.9	1.340	476.4
379.4	0.616	442.0	414.3	1.406	478.8
380.3	0.631	440.8	415.2	1.442	480.0
381.2	0.639	440.4	415.8	1.463	481.6
382.2	0.654	440.8	425.8	1.839	514.0
383.1	0.669	440.0			
d = 1.91 cm (D/d) = 3					

tance d between the electrodes was $\frac{D}{d} \approx \frac{60}{19} \approx 3$. *Figure* 1 reproduces Paschen's curves for cadmium and for other metals, namely :

$$1 - \mathrm{Cd(Ni)}\left(\frac{D}{d} = 3\right); \quad 2 - \mathrm{Cs(Ni)}\left(\frac{D}{d} = 1{,}4\right); \quad 3 - \mathrm{Cs(Ni)}\left(\frac{D}{d} = 3.0\right);$$

$$4 - \mathrm{Cs(Ni)}\left(\frac{D}{d} = 8.8\right); \quad 5 - \mathrm{K(K)}\left(\frac{D}{d} = 1\right); \quad 6 - \mathrm{K(Al)}\left(\frac{D}{d} = 1\right);$$

$$7 - \mathrm{Hg(Fe)}\left(\frac{D}{d} = 1.4\right); \quad 8 - \mathrm{Hg(Hg)}\left(\frac{D}{d} = 1.6\right), \quad [11,\ p.\ 421].$$

Table II shows the values of $V_{s.min}$ and $(p_0d)_{min}$ for different gases and vapours [11, p. 423], [12], [13], [14].

The different values of $V_{s.min}$ obtained for Cs refer to the different values of the ratio D/d. By increasing the ratio D/d, the losses of energy due to the diffusion of the electrons will be greater and so will be the values of the sparking potentials [12].

Experiments were also made with a liquid cadmium cathode to establish the sparking potentials. But no conclusive results could be reached because of the cadmium cathode. Once melted, cadmium must maintained all the time in this state for when it cools, owing to its ensuing solidification, at about 100°C, as a result of its allotropical modifications, a sudden thermal dilatation of about 8% occured and thus the glass tube broke due to the power stroke of cadmium [15].

3. The luminous phenomena in the discharge

In the electrical discharge in cadmium vapours, before and after the sparking (in Townsed's and in the glow discharge conditions), luminous effects with well outlined regions appeared, *figure* 2 (luminous

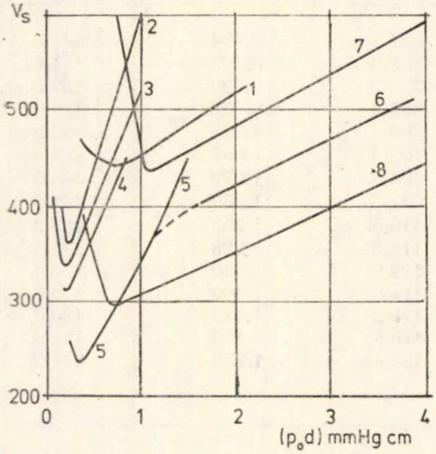

Figure 1. Pashen's curves for cadmium and for other metals vapours.

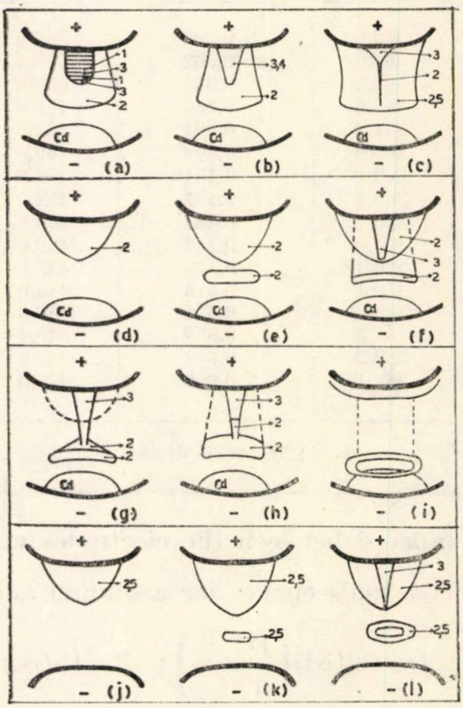

Figure 2. Luminous effects in the electrical discharge in cadmium vapours.

Table II

The minimum sparking potentials for several gases and vapours

gas	cathode	$V_{s.min}$ volts	(pd) mm.Hg. cm	gas	cathode	$V_{s.min}$ volts	(pd) mm.Hg. cm
He	Fe	150	2.50	Hg	W	425	1.80
Ne	Fe	244	3.00	Hg	Fe	497	1.07
Ar	Fe	265	1.50	Hg	Hg	295	0.70
N_2	Fe	275	0.75	Na	Na, Ni	335	0.04 (?)
O_2	Fe	450	0.70	K	K	230	0.33
H_2	Pt	295	1.25	Cs	Ni	360	0.24
air	Fe	330	0.57	Cs	Ni	330	0.22
CO_2	?	420	0.5	Cs	Ni	310	0.22
H_2O	brass	518.7	1.87	Cd	Ni	439.6	0.69
CH_4	brass	435	0.41				
CCl_4	Al	380.5	0.75				
n-propanol	Ni	471.5	0.315				
n-propanol	Al	456.5	0.305				

effects in the electrical discharge in cadmium vapours). The colours which appeared are: 1 – red, 2 – pink, 3 – green, 4 – blue, 5 – violet.

The luminous aspects (a), (b) and (c) correspond to $(pd) < (pd)_{min}$, when the discharge tented to deviate from the axis of the electrodes. The luminous aspects (d) and (j) correspond to $(pd) > (pd)_{min}$ and these were the stages of Townsend's discharge before the sparking discharge, i. e. for $V < V_s$. A broad discharge channel like region appeared near the anode as well as the potassium and cesium vapours. This channel appeared as a result of the elementary processes of ionization and excitation, α and ε [11, p. 397, 417] and the weakly inhomogenous structure of the electrical field between the electrodes. Its shape, the way of setting up and its development were studied in works [6] and [7].

The luminous aspects (e) and (k) correspond to the moment of the sparking and setting up of the glow discharge when the negative glow appeared in front of the cathode for $V = V_s$.

At higher potential differences, the normal glow discharge, i. e. the luminous aspects (f), (g) and (h) turned into a hindered abnormal glow discharge, i. e. the luminous aspects (i) and (l), when the negative glow desintegrated in the middle (where the electrical field is stronger) and moved towards the cathode edge (where the electrical field is weaker). This kind of discharge was also observed in potassium and cesium vapours and it was studied in works [8] and [9].

A new effect was observed in these discharge in cadmium vapours namely the setting up of the new, narrow discharge channel (the second channel) inside the broad channel (the first channel formed in the beginning in the luminous aspects (d), (j)). The (second) narrow central channel from (a), (b), (c), (f), (g), (h) and (l) originated from the broader channel initially formed. The second channel set up in the central region between the electrodes where the electrical field was stronger.

The layer, the region in front of the cathode of the first channel would constitute a sort of "plasma cathode" (not a metallic cathode) concerning the second channel.

The green colour, 3, of this new channel showed the existence of some greater energy electrons in this discharge region. In the luminous aspects (a), (c) and (h) this second channel showed green and red coloured layers. In the stage (a) the succesive green and red layers seemed to be of the same thickness. The shape and the succesion of these layers would suggest a process of the setting up similar to the luminous aspects observed by Holst and Oesterhuis in the noble gases [16], [17] taking into account the Seeliger's rule [11, p. 451].

These luminous effects revealed the formation of a plasma inside another plasma due to the inhomogeneous structure of the electrical field. The new plasma shape produced a still stronger distortion of the electrical field in the respective region and so the volume where the new plasma is moulded, would be outlined and well separated from the rest of the plasma.

4. Conclusions

The researches concerning the metal vapours plasmas, the potassium and cesium vapours plasmas and the mercury and cadmium metal vapours plasmas give new information about the features of these plasmas, especially revealed through the luminous effects coming out in the discharge.

The electrical field between the elctrodes, as a weakly inhomogenous one, acts like a separator of the different plasma regions formed between the electrodes. In this way the different kinds of plasma can easily be separated and studied.

This is the justification for the continuation and intensification of the researches in concerning this field of the metal vapours plasma physics.

REFERENCES

1. G. G. BRĂTESCU, *Über die Zündspannung in K-Dämpfen* Rev. Phys. Acad. R. P. R., Nr. 1 (1957), 87
2. G. G. BRĂTESCU, *Zündspannung und Kathodenstruktur in K-Dämpfen* Rev. Phys. Acad. R. P. R. IV (1) (1959), 33
3. G. G. BRĂTESCU, *Zündspannung in Cäsium-Dämpfen* Rev. Phys. Acad. R. P. R. Nr. 1 (1962), 131
4. G. G. BRĂTESCU, *Elektrische Entladungen in Alkalimetall-Dämpfen* Acta Polytechnica – Práce CVUT v Praze 14 (IV, 7, 1975)
5. G. G. BRĂTESCU, *On the formation of the glow discharge in alkali-metals vapours,* Anal. Univ. C. I. Parhon *25* (1960) 229 (in Romanian, with abbreviated texts in Russian and German)
6. G. G. BRĂTESCU, *On the discharge channel at the formation of the glow discharge,* Anal. Univ. Bucureşti, Seria St. Nat. Mat. Fiz. *39*-XII (1963), 119 (in Romanian, with abbreviated texts in Russian and French)
7. G. G. BRĂTESCU, *On the discharge channel of the preglow discharge* (II), Anal. Univ. Bucureşti XVI (1966), 19 (in Romanian, with abbreviated texts in Russian and French)
8. G. G. BRĂTESCU, *A new glow discharge,* Ses. Com. Şt. Platforma Măgurele 26–27 sept. (1974), 92 (a note in Romanian)
9. G. G. BRĂTESCU, *A new glow discharge : the hindered abnormal discharge,* Anal. Univ. Bucureşti, Şt. Nat. An. XXV (1976), 21
10. LANDOLT-BÖRNSTEIN, *Zahlenwerte und Funktionen aus Physik, Chemie, Astronomie, Geophysik, Technik,* II-Band, 2 Teil, S. 1, 2, 3, Berlin, Göttingen, Heidelberg, Springer Verlag, 1960
11. G. G. BRĂTESCU, *Plasma Physics* Ed. Did. Ped., Bucureşti 1970 (in Romanian, 590 pages, with 382 figures and 801 bibliographical references)
12. A. A. W. M. GARAMOON and N A. SURPLICE, J. Phys. D. Apll. Phys., *6* (1973), 206

13. G. G. BRĂTESCU, M. CAZAN-CORBASCA, *Sparking potentials in propilic alcohol vapours*, Ses. Com. St. Platf. Măgurele 26—27 sept. (1974), 93 (a note in Romanian)

14. G. G. BRĂTESCU and MAGDA CAZAN-CORBASCA, *Sparking potentials and ionization coefficients in n-propanol vapours* ($CH_3-CH_2-CH_2-OH$), Anal. Univ. Bucureşti, Fizica, XXVII (1978), 11

15. GMELINS HANDBUCH der ANORGANISCHEN CHEMIE, Achte Auflage, Cadmium System Numer, 33, 1925, Leipzig, Berlin, Verlag Chemie G. m. B. H. S. 33; Cadmium Ergänzungsband 1959, S. 33, 106, 108

16. G. HOLST and OOSTERHUIS, Physica *1* (1921), 78

17. J. G. A. HOLSCHER, Thesis, 1964, Eindhoven; Physica *35* (1967), 129

Received December 17, 1977.

ANALELE UNIVERSITAŢII BUCUREŞTI, FIZICA, XXVII, 1978, pag. 11–16

SPARKING POTENTIALS AND IONIZATION COEFFICIENTS IN N-PROPANOL VAPOUR ($CH_3-CH_2-CH_2OH$)

G. G. BRĂTESCU and MAGDA CAZAN-CORBASCA
Faculty of Physics, Bucharest University*

ABSTRACT

The sparking potentials were experimentally determined in n-propanol vapour and Paschen curves were drawed. Townsend coefficients α and γ were computed for $\frac{E}{p_0}$ over a range about 300 to 3.700 $V.cm^{-1}.Torr^{-1}$. Two types of electrodes were used : aluminium and nickel since the object of the work was also to emphasize the role of the electrode nature in the case of such a discharge.

1. Introduction

M. Narayana Swamy and J. A. Harrison determined experimentally the Townsed α coefficient, by measuring the discharge current in the vapours of : *n*-buthanol, hydrogen and mixtures of *n*-buthanol and hydrogen. (Narayana Swamy and Harrison, 1966) [1] as well as in the vapours of : *n*-propanol, benzene, hydrogen and mixtures of *n*-propanol and hydrogen (Narayama Swamy and Harrison, 1967) [2].

In the case of *n*-propanol vapour, they represented $\frac{\alpha}{p_0}$ as a function of $\frac{E}{p_0}$ by using the equation :

$$\frac{\alpha}{p_0} = Ae^{-\frac{B}{\frac{E}{p_0}}} \qquad (1)$$

where constants A and B deduced from the experimental data, were $A = 25.1\ cm^{-1}.Torr^{-1}$, $B = 369\ V.cm^{-1}.\ Torr^{-1}$ over a range about

---

* National Center of Physics, P. O. Box 5211, Măgurele, Bucharest.

80 to 500 Vcm^{-1}.Torr, E is the electric field and p_0 the pressure reduced at 0°C.

In this paper the authors propose to represent $\frac{\alpha}{p_0}$ as a function of $\frac{E}{p_0}$ in *n*-propanol vapours within a $\frac{E}{p_0}$ range of 300–3 700 $\mathrm{V.cm}^{-1}$. Torr^{-1}. They made use of equation (1), where constant A determined by M. Narayana-Swamy and J. A. Harrison, depends on the nature of gas. Constant B was deduced from the experimental data obtained by the authors by means of relations:

$$B = \left(\frac{V_s}{pd}\right)_{\min} \tag{2}$$

where V_s is the sparking potential, d is the electrode separation and p the vapour pressure. It is assumed that B depends on both the gas nature and the electrode materials.

2. Equipment.

It is used a spherical glass discharge tube of 10.9 cm diameter.

Two pairs of plane-parallel Rogowsky profile electrodes (alluminium and nickel) were used with a 3.08 cm diameter. These electrodes were very often cleaned with benzene and alcohol and polished with speical brushes.

The electrode separation was maintained constant all through the determinations in order to keep up paralellism between their faces. It was measured by a cathetometer.

The vapour pressure was varied from 0.7 to 10 Torr and was measured by a differential manometer with silicone oils.

The error affecting the product p. d did not exceed 0.1 cm Torr.

The high voltage current was supplied by an ORION stablized voltage generator with output voltages going from 0 to 900 V. To this generator an electric filter was associated consisting in two 1 μF condensers and a 990 KΩ resistance.

The air was evacuated with an oil diffusion pump. The equipment was also provided with a liquid nitrogen trap so that before introducing the vapours, the vapour pressure was about 10^{-6} Torr.

A 0.5 class voltmeter with a 150 divisions scale measured voltages up to 600 V. In series with the discharge tube a 1.3 MΩ resistance and a multiflex galvanometer of 10^{-9} A/div sensitivity, were connected.

3. Experimental determinations and results

The sparking potentials for the Al and Ni electrodes were experimentally determined and the dependence on product p. d of the sparking potential was studied. The electrode separation was maintained constant during a whole series of determinations while varying the vapour pressure within the tube.

It was established that $V_s = f(p.d)$ is a Paschen curve (fig. 1 and 2).

The values of the minimum sparking potential supplied by the Paschen curves are: 471.50 ± 1 V for the Ni electrodes and 456.50 ± 1 V for the Al electrodes. The corresponding values of products p.d are: 3.15 ± 0.01 mm Torr and 3.05 ± 0.01 mm Torr.

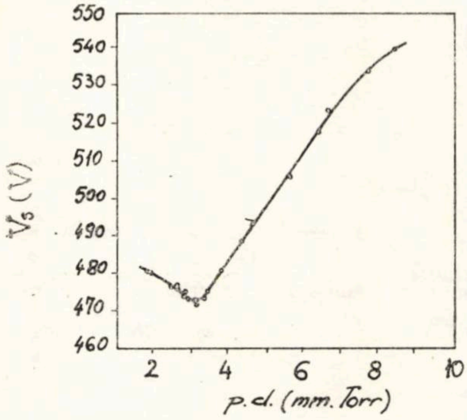

Figure 1. Sparking potential as a function of the product p. d for Ni electrodes in n-propanol vapour.

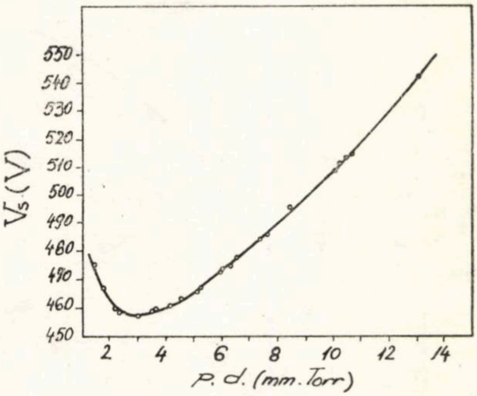

Figure 2. Sparking potential as a function of the product p. d for Al electrodes in n-propanol vapour.

It is found that the value of the minimum sparking potential as well as the slope of the right branch of the Paschen curves depend on the nature of the electrodes. The various values of the sparking potentials were ascribed by the authors to the surface emission of the cathode which depends partly on the output work φ of the electrons in the metal ($\varphi = 4.96$ eV for Ni and $\varphi = 4.20$ eV for Al).

Constants B were computed by means of relation (2) which supplied: $B = 1494\ \mathrm{V.cm^{-1}.Torr^{-1}}$ for the Ni electrodes and $1497\ \mathrm{V.cm^{-1}.Torr^{-1}}$ for the Al electrodes.

Figures 3 and 4 represent curves $\frac{\alpha}{p_0} = f\left(\frac{E}{p_0}\right)$ supplied by equation (1) and curves $\frac{1}{\eta} = f\left(\frac{E}{p_0}\right)$, where $\eta = \frac{\alpha}{E}$. Quantity $\frac{e}{\eta} = \frac{eE}{\alpha}$ represents the mean energy consumed by an electron in an electrostatic field when it traverse a 1 cm distance to from a pair positive ion-electron.

It was observed that the minimum points on curves $\frac{1}{\eta}$ agrees with the Stoletov point on the corresponding curves $\frac{\alpha}{p_0}$ [3].

Figures 5 and 6 point out the dependence of the secondary emission coefficient γ on ratio $\frac{E}{p_0}$. Coefficient γ was computed by the relation:

$$V_s = \frac{1}{\eta} \ln\left(1 + \frac{1}{\gamma}\right) \tag{3}$$

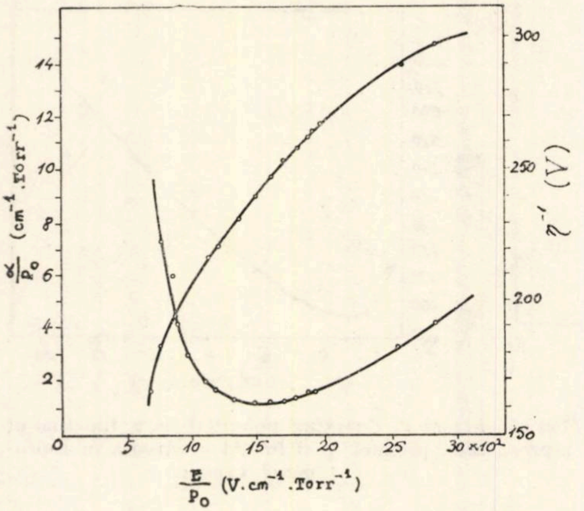

Figure 3. $\frac{\alpha}{p_0}$ as a function of $\frac{E}{p_0}$ and η as a function of $\frac{E}{p_0}$ in n-propanol vapour, for Ni electrodes

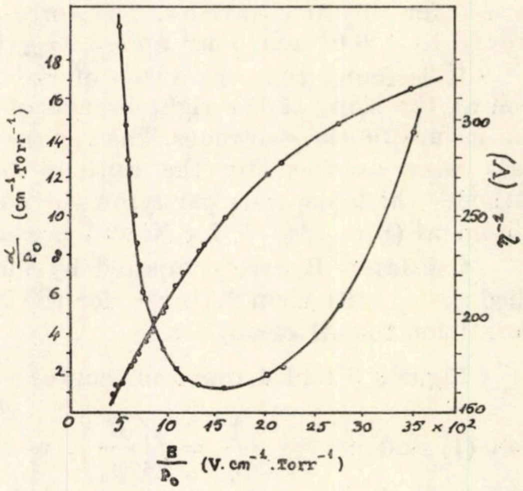

Figure 4. $\frac{\alpha}{p_0}$ as a function of $\frac{E}{p_0}$ and η as a function of $\frac{E}{p_0}$ in n-propanol vapour, for Al electrodes.

4. Conclusions

It is found that dependance $V_s = f(p.d)$ is a Paschen curve just as in the case of gases with a simple molecular structure which is moreover confirmed in the case of other vapours of organic substances. [4, 5, 6, 7].

The values of the minimum sparking potential are higher than in the case of simpler molecular structure gases because a part of the electron energy that interacts with the gas molecules is used in a number of elementary processes such as excitations and disociations non-followed by ionization.

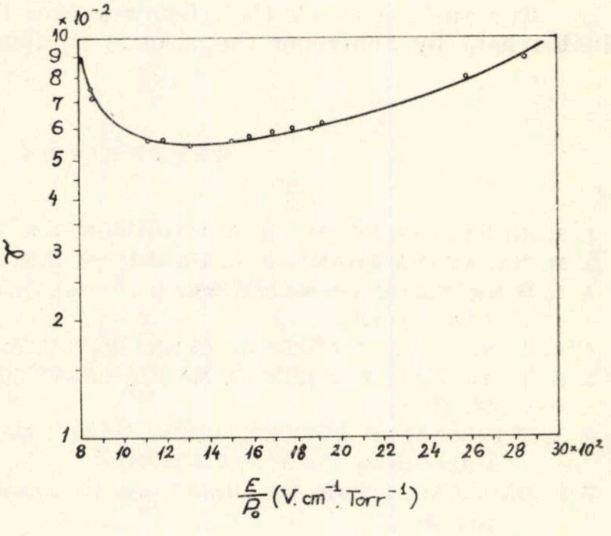

Figure 5. γ — coefficient as a function of $\frac{E}{p_0}$ in n-propanol vapour for Ni electrodes.

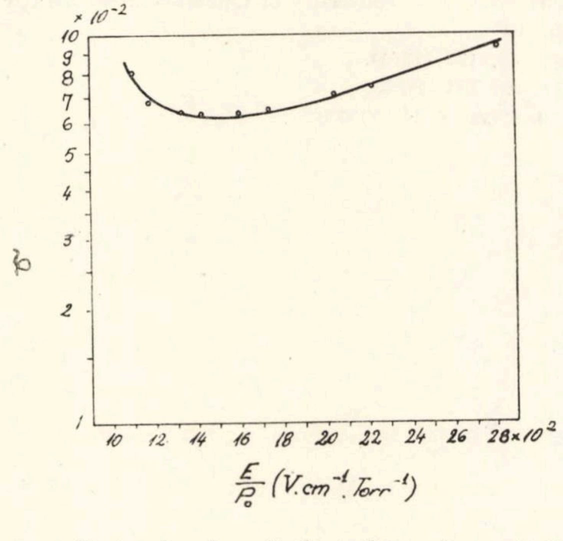

Figure 6. γ coefficient as a function of $\frac{E}{p_0}$ in n-propanol vapour for Al electrodes.

It is also found that the values of the minimum sparking potential and the Paschen curves forms depend on the nature of the electrodes.

The curves $\frac{\alpha}{p_0}$, η and γ as a function of $\frac{E}{p_0}$ are similar to the ones found in literature. [8, 3, 9, 10, 11].

From the study of the Townsend discharge in *n*-propanol vapour there results that they behave in the same way as within vapours of other organic substances, the greatest role being played here by the molecule complexity that produces a multitude of elementary processes contributing to the phenomenon.

Acknowledgement.

The authors thank their fellow-worker C. Stănciulescu for his valuable help by achieving the electric equipment for measurements.

REFERENCES

1. M. NARAYANA SWAMY, J. A. HARRISON, Brit. J. Appl. Phy. *17*, 123 (1966).
2. M. NARAYANA SWAMY, J. A. HARRISON, Brit. J. Appl. Phys. *18*, 781 (1967).
3. G. G. BRĂTESCU. *Plasma Physics* (in Romanian), Ed. Didactică şi Pedagogică, Bucureşti, 1970 pag 403.
4. A. T. NICOLAU, P. POPESCU, ELENA PASCU, Anal. Univ. Bucureşti, *16* 51 (1966)
5. A. T. NICOLAU, P. POPESCU, MAGDA CAZAN-CORBASCA, Anal. Univ. Bucureşti 53, (1968)
6. A. T. NICOLAU, P. POPESCU, ELENA PASCU, MAGDA CAZAN-CORBASCA, Studii şi Cercetri de Fizică *20*, 799 (1968)
7. E. BĂDĂRĂU, I. POPESCU, *Ionized Gases* (in Romanian) Ed. Tehnică, Bucureşti 1965 pag. 25.
8. L. LOEB, *Basic Processes in Gaseous Electronics*, University of California Press Berkley and Los Angeles 1945 pag. 647.
9. A. E. D. HEYLEN, J. Chem. Phys. *35*, 169 (1961).
10. A. E. D. HEYLEN, J. Chem. Phys. *38*, 764 (1963).
11. A. E. D. HEYLEN, Brit. J. Appl. Phys. *1*, 179 (1968).

Primit la redacţie la 2 iulie 1977

ANALELE UNIVERSITĂȚII BUCUREȘTI, FIZICA, XXVII, 1978, pag. 17—20

NEGATIVE IONS IN IONOSPHERIC PLASMA

NICOLAE GHERBANOVSCHI

Faculté de Physique, Université de Bucharest[*]

RÉSUMÉ

Une courte présentation de la théorie des ions négatifs. L'on montre la contribution des ions négatifs moleculaires dans l'explication des quelques réflexions critiques en ionosphére, en acord avec la théorie unitaire de l'ionosphére donée par le prof. Th. V. Ionescu.

In order to explain electromagnetic waves propagation round the earth, Kennelly and Heaviside supposed that the upper layers of the atmosphere higher than 80 Km are ionised. These layers are called ionosphere.

Ionosphere (70—900 Km) was specially researched since the short (< 100 m) waves were used in radiocommunications. These waves are able to traverse long distances with a low emission power.

Whereas the signals transported by these radiowaves were easily received at great distance even at antipodes, there was round the emitter a region where these signals could not be received (so called quiet zone).

The most interesting results obtained by various physicist who dealt with these phenomena, were obtained by ionospheric echo method : a short signal of a few microseconds is registred both at emission and reception on a moving photoband in a special receiver. In this manner the apparent heights where the waves are reflected, $h = 1/2\, c\Delta t$ in ionosphere for certain critical frequencies can be deduced. The heights are apparent because the group velocity in ionised medium is lower than the propagation velocity in vacuum or in ionised air ; as a consequence the electromagnetic wave penetrating in ionosphere is reflected after a longer time.

In close connection with the explanation of the ionosphere properties many labor-experiments were made in ionised gases. The commonest mode to produce the gas ionisation is the electric current. The majority of the ions appearing in plasma of an ionised gas is made of positive ones. The free electrons and negative ions are negative charge carries that together with the positive ions give the electrical quasineutrality characteristic of the gaseous ionised medium.

---

[*] *National Center of Physics*, P. O. Box 5211, Măgurele, Bucharest.

BUDAPESTI MŰSZAKI EGYETEM 1848

The fact that some stable negative ions are observed (O^-, O_2^-, NO_2^-, OH^- and H^-) — whereas other are not (N^-, N_2^-, He^-, Ar^-) — explains their formation opportunity.

For an ion to the stable it is necessary that his energy in normal state W_- to be smaller than that of the atom or of the neutral molecule in normal state W_0. The difference $W_0 - W_-$ is called atom electronic affinity.

Atoms or molecules with positive affinity are able to produce stable negative ions.

Under what conditions can the affinity be positive?

If an external electron can approach the atom up to the outer zone of the electronic cloud, let this distance from the nucleus be r_1, then the electronic cloud inside the sphere of radius r_1 together with the nucleus charge, are producing an effective positive charge that attracts the external electron. This electron is moving on stationary orbits according to Schrödinger equation. The electronic cloud from outside the sphere r_1 has a small influence on the external electron. It is to be remarked that the attractive force is not coulombian but varies aproximately with r^{-5} and in consequence the number of stationary states is finite and not infinite as in the case of coulombian potential.

Certainly, the attached electron cannot approach to any distance from the nucleus because of the exclusion principle of Pauli.

As a general rule, it can be said that the atoms with complet electronic layers cannot form stable negative ions because in this case the attached electron should be bound in a state with a quantum number bigger with 1 than that of the atom perispheral electrons.

Apart from the stable negative ions, the labile ones in fundamental state have no smaller energy than the free molecule. In other words, the attached electron is in no bound state but is gravitating a relative short time round the molecule and leaving it on a simmetrical trajectory to that of approach. Langevin has studied this movement in the potential

$$V(r) = -\frac{\alpha e^2}{2r^4}$$

where α is molecular polarisability. Two orbite types are possible in this potential. The orbits corresponding to high kinetic momenta are similar to hyperbolas whereas for small kinetic momenta the trajectory represents a spiral movement towards the centre until a repulsive force inverses it (fig. 1).

In Langevin theory is shown that for a b considered as a collision parameter, smaller than a kinetic value $b_0 \left[= \left(\frac{4\alpha e^2}{m_r v_0^2} \right)^{1/4} \right]$, the attached electron orbit is a double symmetrical spiral. For b_0 as limit value of b the spiral becomes a circular orbit. The orbits for $b < b_0$ pass trough the origin in the absence of a repulsive core, whereas the ones corresponding to $b \geqslant b_0$ approach no more than $r_0 = b_0/\sqrt{2}$.

Until now it was not considered the nature of the force centre. The collision theory in frame of which the above considerations were made, supposs the force center as a material point. The electrons can pass through it or eventually canbe reflected on it as on a rigid sphere.

Physically we have to consider both force center-polarised molecule-influence on electron and electron influence on movement state. Equally in these interactions quantic effects are felt.

He who deepened the study on negative ion formation is acad. Th. V. Ionescu. He shows that whereas in stable negative ions the attached electron is indiscernible with respect to the others of considered element, in labile ones the electron replace an atom because there is energy equipartition on them. Th. V. Ionescu quantifies the kinetic momentum of attached electron for the enough long time when he describes a circular movement round the nucleus, his kinetic energy being $\frac{h^2 l(l+1)}{8\pi^2 m r^2}$.

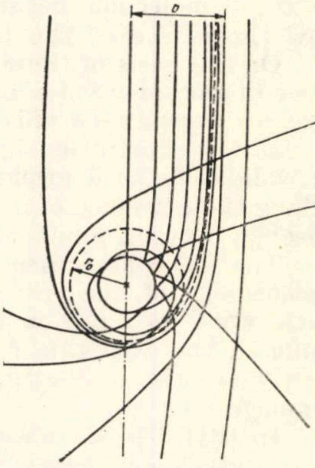

Fig. 1

Kinetic rotation energy of the molecule is hcBK(K + 1), where K is rotation quantum number, B-spectral constant. By equalizing the two energies it results for l = 1 the orbit radius for H_2^- and O_2^- as a function of the discreet values for K = 1 ; 2 ; 3 ...

$$r_{H_2} = 3{,}219.10^{-7}\,[K(K+1)]^{-1/2}\,\mathrm{cm}$$

$$r_{O_2} = 2{,}070.10^{-6}\,[K(K+1)]^{-1/2}\,\mathrm{cm}$$

($B_{H_2} = 60{,}87\ \mathrm{cm}^{-1}$, $B_{O_2} = 1{,}56\ \mathrm{cm}^{-1}$).

There are, therefore, for the attached electron more trajectories dependent on the molecular rotation number. Consequently and absorbtion or (stimulated) emission spectrum is ascertained. These absorbtions or stimulated emissions correspond to the magnetic energy variation of the negative ions. This energy is dependent on the attached electron trajectory and on the direction of molecular magnetic dipole with respect to the magnetic field created by the attached electron. (The molecular magnetic dipole of the electrons that produces the oxygen paramagnetism or the magnetic dipole of the coupled protons from hydrogen molecule).

The proper frequencies of the O_2 labile negative ion, calculated according to Th. V. Ionescu theory, are in total agreement with the critical frequency spectrum resulted from ionosphere study, also measured in labor in ionised air by Th. V. Ionescu in collaboration with Octav C. Gheorghin and D. Ionescu for 1 to 44 MHz frequency range.

Opposed to what it was believed for a long time, i. e. that about 100 Km height there is atomic oxygen only, Th. V. Ionescu asserted even since 1950 that molecular oxygen must be found up to 300 Km height because "critical" reflections at this heights indicate the presence of oxygen molecular negative ions. The knowledge of these frequencies allow the choice of the best wave lengths for radio communications.

On the basis of these researches Th. V. Ionescu ascertains the existance in ionosphere of a single ionised layer, previous determined strata being an appearance only.

Direct registration by satellites and rockets or by Thomson diffusion validated the ionospheric model proposed by Th. V. Ionescu, establishing the existence of a single ionsied layer and the presence of a high molecular oxygen amount up to 300 Km.

The ionosphere theory given by Th. V. Ionescu explains that the displacement of the critical frequences towards high values when an elastic wave go along in ionosphere, produced by a nuclear explosion, is due to the adiabatic compression rising th etemperature and consequently negative ions appear with absorbtion frequencies corresponding to ionograms.

In 1941, Th. V. Ionescu, publishes a study concerning the electrical waves reflexion in ionosphere, produced by the free electrons from the regions where the collision frequency with the molecules and atoms are negligible with respect to the electrical waves frequency. In it is shown that theoretically had to exist characteristic reflexions not only on gyromagnetic frequency of the earth magnetic field but as well on multiple frequencies of this fundamental frequency. After 25 years the registrations made by canadian satellite Alouette, from 1 000 Km height put into evidence these singular frequencies considered unexpected. Later these cyclotronic absorbtions were experimentally found in labor by Th. V. Ionescu.

BIBLIOGRAPHY

1. Papers published by acad. TH. V. IONESCU in *Comptes Rendus de l'Academie des Sciences — Paris* tome *199*, p. 1301; 1934; *199*, 1389, 1934; *250*, 2182, 1960; *257*, 2268, 1963; *262*, 944, 1966; *263*, 899, 1966.
2. *Eights International Conference on Phenomena in Ionized Gases*, 1967, Viena, p. 170, Th. V. Ionescu in collaboration with M. Comănescu
3. TH. V. IONESCU, Bul. Acad. R. P. R., V, 1, 1953
4. TH. V. IONESCU, Rev. Phys., I, 1956
5. TH. V. IONESCU, Disquisitiones Mathematicae et Physicae, 1, 491, 1941
6. TH. V. IONESCU, Rev. Phys., VI, 2, 1961
7. TH. V. IONESCU, Rev. Roum. Phys., 10, 2, 1965
8. TH. V. IONESCU, O. C. GHEORGHIU, Rev. Phys., IV, 1959
9. TH. V. IONESCU, D. C. IONESCU, Rev. Roum. Phys., 12, 9, 1967
10. A. TH. IONESCU, Rev. Roum. Phys., 16, 197, 1971
11. TH. V. IONESCU, A. TH. IONESCU, Rev. Roum. Phys., 20, 1007, 1975

Primit la redacţie la 28 I 1978

ANALELE UNIVERSITĂȚII BUCUREȘTI FIZICĂ XXVII, 1978, pag. 21—28

ASPECTS CINETIQUES ET MORPHOLOGIQUES DE LA CRISTALLINITÉ DE CERTAINS POLYMERES

I. C. PETREA, C. A. STĂNESCU
Faculté de Physique, Université de Bucharest*

TATIANA ALEXOIU-POP
Fabrique d'Appareils Nucléaires

RÉSUMÉ

La connaissance des interdépendances cinétiques et morphologiques des polymères policrstallins est une prémisse essentielle pour le développement de la recherche dans ce domaine, comprenant l'interprétation théorique de différents mécanismes spécifiques physico-structuraux.

La recherche scientifique de spécialité montre que les propriétés macroscopiques des polymeres dépendent de leur structure moléculaire, étant subordonnées ou même controlées par la conjoncture organisationnelle des molécules constituant les diverses formations suprastructurales de type cristallin, susceptibles d'exister dans les systémes macromoléculaires.

Le polypropyléne (PP) isotactique plus particulierement, et le polyéthylène (PE) étudiés dans ce contexte peuvent constituer des models pour la description correlée de certains aspects cinético-morphologiques et des plus importantes caracteristiques physiques et mécaniques mises en évidence par divers moyens.

On a relevé dans cet article quelques aspects remarquables de la cristallinité du polyethylene fabriqué dans la Republique Socialiste de Roumanie et d'un polypropylène provenant du Japon. La photomicrographie des aspects morphologiques générés dans de diverses conditions cinétiques de la cristallisation des polymères peut constituer un support pour les éventuelles recherches dans ce genre.

Notions introductives

L'existence simulatnée des centres de nucléation cristalline et des tendances de formation des microblocs ou structures supramoléculaires ayant un degré accentué d'organisation, favorise d'habitude, l'amélioration de certaines caractéristiques physiques et structurales des poly-

---

* *Centre National de Physique*, Măgurele, Bucharest, CP 5211 Roumanie.

mères, généralement amorphes, mais capables de cristalliser dans des conditions appropriées de laboratoire ou technologiques. La cristallinité des polymères est stimulée par la capacité d'association intermoléculaire des entités structurales fondamentales par la propriété des segments de chaîne proches de s'orienter en faisceaux tout en formant des microdomaines avec une accentuée ordonnabilité stérique, dispersés dans la matrice amorphe des macrochaînes, prédominante avant que le processus de cristallisation commence.

Le caractère coopératif unidimensionnel des macrochaînes et leur rigidité partielle d'orientation devient définitoire pour les mécanismes de constitution et restructuration, pour les processus élémentaires qui concourent à l'évolution de la cristalliation des polymères.

Les formations cristallines, les cristallites, les sphérulites, etc. présentent des directions ou des axes d'orientation qui leur sont propres, à caractère polydispersé sous le rapport de leur disposition réciproque dans la masse du polymère cristallin-amorphe. De ce point de vue la fonction d'orientation qui suit devient significative et utile :

$$f_x = \frac{3 < \cos^2 x > -1}{2} \tag{1}$$

Elle exprime, d'habitude, la distribution angulaire des cristallites par rapport au choix d'une direction adéquate. La valeur $< \cos^2 x >$ indique la moyenne des valeurs du cosinus carré de l'angle x de la direction de référence de l'échantillon examiné et de l'axe cristallographique de la formation cristalline [1].

Dans un polymère polycristallin la disposition de position et d'orientation des entités structurales, de même que celle des formations supramoléculaires, joue un rôle à part dans l'extériorisation de ses caractéristiques physiques et mécaniques. Souvent, l'organisation des molécules, leur disposition réciproque, est plus significative de ce point de vue que l'arrangement des sousentités le long d'une chaîne moléculaire. Néanmoins, dans le cas du polypropylène isotactique il est nécessaire de tenir compte des particularités qui découlent de sa conformation du type helix 3_1 et des effets du repliement lamellaire des macromolécules du polymère fondu et refroidi ensuite afin de cristalliser.

Les processus de nucléation cristalline provoquent dans le polypropylène isotactique l'apparition des structures macromoléculaires sphérulitiques qui peuvent atteindre des dimensions qui varient entre 1 micron et plusieurs centimètres. La déformation des sphérulites au cours des épreuves équivaut à une réorientation qui peut être exprimée par la relation (1), tenant compte de l'altération de quelques-unes des propriétés mécaniques qui dérivent de la coexistence des domaines amorphes et des microblocs cristallins.

La provocation dirigée et stimulée des processus afférents à la cristallinité du polyéthylène (PE) de haute pression et du polyprophylène isotactique (PP) peut constituer les prémisses de quelques propriétés physiques et mécaniques imprimées à ces systèmes dans certaines conditions expérimentales. Les conséquences scientifiques et technologiques de l'exploration de telles interdépendences sont parmi les plus difficiles.

Dans ce sens l'objet de ces travaux est constitué par l'analyse de quelques aspects et interdépendences cinétiques et morphologiques capables de mettre en évidence les particularités du comportement des polymères étudiés.

Ont été examinés par analyse microscopique, sous lumière polarisée, l'action et les effets de diverses modalités de traitement thermique corrélées avec la température de cristallisation, la durée des processus essentiels et des mécanismes d'interface polymère — support.

Considerations theoriques fondamentales

La détermination des dimensions et de leur variation temporelle et celle des caractéristiques cinétiques et morphologiques de la formation des microdomaines cristallins dans les polymères étudiés est basés sur les principaux éléments de la théorie d'Avrami. La cristallisation des polymères est subordonnée aux lois qui s'ensuivent de cette thèorie fondamentale pour l'analyse dilatométrique des structures des polymères cristallins.

Il est connu que les systèmes macromoléculaires susceptibles de cristalliser sont caractérisés par des vitesses de développement unidimensionnel des formations cirstallines en fonction de température T, exprimés par la relation :

$$V_t = V_{eo} \exp\left(-\frac{A}{T} - \frac{B}{T\Delta T}\right) \qquad (2)$$

dans laquelle A est un coefficient qui caractérise l'énergie libre du contact de repliement des chaînes macromoléculaires et B est le coefficient qui caractérise l'énergie libre de transfert de l'interface polymère fondu — support.

On distingue dans ce processus une température de cristallisation influencée par les particularités du traitement thermique, de la nature du spport, en général par l'histoire de l'échantillon. Les propriétés du polymère cristallin dépendent de la fraction cristalline massique :

$$m_c = \frac{\rho_a(\rho - \rho_c)}{\rho(\rho_c - \rho_a)} \qquad (3)$$

dans laquelle ρ est la densité mesurée de l'échantillon, ρ_c et ρ_a les densités des fractions cristallines et amorphes.

Procédés et techniques de laboratoire

Les caractéristiques physiques et structurales des échantillons obtenus dans les conditions exigées par l'exactitude des études effectuées ont été mises en évidence par l'investigation microscopique en lumière transmise ou polarisée.

L'épaisseur des échantillons était comprise entre 20 —360 μm; parmi celles-ci les plus indiquées ont été sélectionnées pour la microphotographie avec divers grossissements et expositions, à l'aide du microscope MC-1 (produit par l'Industrie Optique Roumaine).

Les pellicules ont été préparées par les méthodes d'évaporation d'une solution concentrée, ou, de laminage du polymère fondu. Les pelicules obtenues par évaporation ont été préparées avec des solutions de concentration variable de PE en xylène et de PP dans le même solvent.

Les polymères fondus ont été pressés entre des lamelles de verre, maintenues à une distance contrôlée pour permettre l'évaluation exacte des épaisseurs, en évitant ainsi de déterminer directement l'épaisseur à l'aide de l'indice de réfraction, puisque les pellicules n'ont pas des épaissurs uniformes. Après la formaion les pellicules ont été soumises au traitement thermique dans l'intervalle de température 200°C—300°C, pour une très courte durée, afin d'effacer l'histoire thermo-mécanique des préparations antérieures.

Le processus de cristallisation proprement dit est caractérisé par l'intervalle de température 115°C—145°C et des délais différents. On a examiné les modalités les plus appropriées pour refroidir le système de la température de cristallisation. Ainsi on a refroidi brusquement les échantillons dans de la glace, comme cas extrème, ou on les a laissé refroidir lentement pendant plusieurs heures à la temperature environnante.

Données et resultats expérimentaux

Les échantillons de PP soumis au traitement thermique 5 minutes à 250°C présentent après l'arrêt du processus de cristallisation, (à 130°C avec des délais très variés) un accroissement des dimensions des cristallites, simultanément avec la durée de cristallisation. La figure numéro 1 représente un échantillon de 60 μm dont les spherulites se sont développées dans la matrice amorphe du polymère sans se contacter trop souvent. Le processus simultané de cristallisation secondaire met en évidence néanmoins une déformation du profil des sphérulites dues aux contacts produits pendant leur croissance.

La durée de cristallisation influence sensiblement la morphologie des formations caractéristiques. Ainsi, pour les durées courtes on remarque une structure fine, fibrilaire ou aciculaire (fig. 1). Simultanément au prolongement du temps de cristallisation la texture devient moins conturée, par le grossissement des zones amorphes allongées et l'apparition des formations paracristallines.

Les échantillons de PE indiquent une dépendence de la cinétique de cristallisation de leur épaisseur, tandis que le PP ne présente pas une telle dépendence que dans le cas des pellicules minces (30 μm, 40 μm, 50 μm) [3]. Les sphérulites formées sont caractérisées pas des rayons moyens pratiquement égaux, quand les conditions de préparation ne diffèrent pas. Les films à une épaisseur plus grande de 200 μm ne peuvent plus être examinés au microscope à cause de la perte de transparence.

Pour étudier l'influence de la température de cristallisation sur la vitesse de croissance et sur la morphologie des sphérulites on a cristallisé des pellicules minces de PP à 115°C, 127°C, 130°C, 140°C. Ainsi on a constaté l'accroissement du diamètre des sphérulites et une diminution du nombre de centre de nucléation, en augmentant la température. Ces constatations mettent en évidence l'accroissement de la vitesse de cristallisation, concomitante à la baisse de la vitesse de nucléation, quand on augmente la temperature. De la figure 2 résulte la dépendence de nombre de spérulites de leur rayon et aussi de la température de cristallisation. On observe à 140°C, la plus élevée des températures investiguées, que le nombre total des sphérulites est minime, tandis que l'apparition des sphérulites de grandes dimensions est la plus fréquente. Mais on constate qu'à des températures plus basses on obtient aussi des sphérulites à grand rayon, bien qu'à une fréquence diminuée. Les grandes sphérulites apparaissent surtout dans les zones marginales des échantillons probablement à la suite d'un traitement initial hétérogène. Le gradient des pertes de chaleur dans l'échantillon est aussi responsable de cette répartition des sphérulites selon leur dimensions.

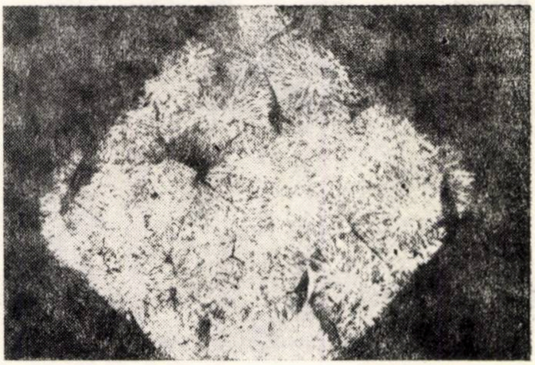

Fig. 1. Echantillon de PP cristallisé à 130°C pendant 6 heures (épaisseur 60 μ)

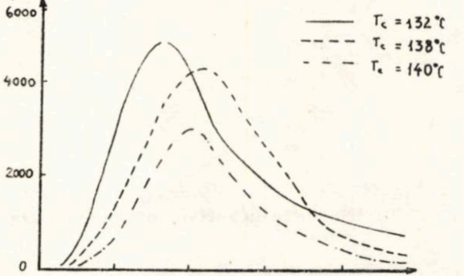

Fig. 2. Dépendence du nombre de sphérulites du rayon et de la température de cristallisation sation pour le PP

Le refroidissement contrôlé des échantillons a mis en évidence la cristallisation secondaire dans le cas d'une lente diminution de la température ou d'une interruption brusque du processus de cristallisation par l'introduction en eau glacée. (Figure 3).

On a pu observer distinctement quatre types de sphérulites, remarquables par leur biréfringence et morphologie, correspondant aux quatre températures de cristallisation. Avec la variation de la température de cristallisation les chaînes s'orientent par rapport à la direction de développement des formations sphérulitiques, ce qui représente en effet, le processus élémentaire qui détermine les quatre types distincts.

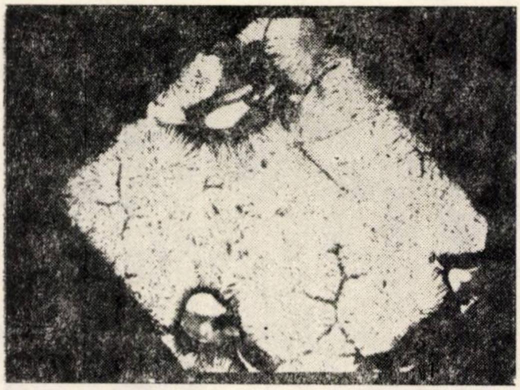

Fig. 3. Echantillon de 80 μm de PP tenu 3 minutes à 300°C et cristalisé 4 heures à 140°C, refroidi ensuite lentement 24 heures. On observe de nombreux centres de nucléation, comme des points lumineux, à la suite du processus de cristalisation secondaire.

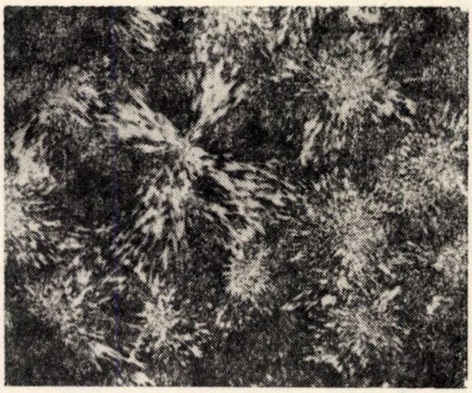

Fig. 4. Sphérulite de type I de PP avec biréfringence négative, obtenu à 140°C.

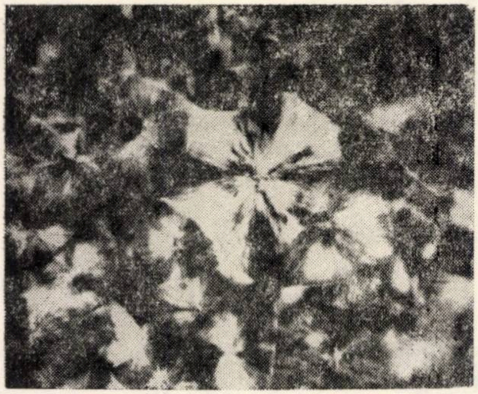

Fig. 5. Type II de sphérulite de PP avec biréfringence négative, obtenu à 140°C.

En examinant les mécanismes cinétiques et morphologiques caractéristiques du processus de cristallisation on a tenu compte aussi de l'influence du support (verre, metal, huile siliconique).

En cristallisant les échantillons entre deux lamelles (sandwich), on a pu constater une augmentation du nombre des centres de nucléation par rapport à la même situation, mais avec une seule lamelle pour support. Pour confirmer cette constatation, on a effectué des sections transversales dans les échantillons à l'aide d'un microtome sans l'inclusion du polymère. On a remarqué la distribution décroissante des centres de nucléation de la surface du support vers la surface libre. Dans le cas de deux lamelles sandwich, on peut discerner une symétrie des centres de nucléation.

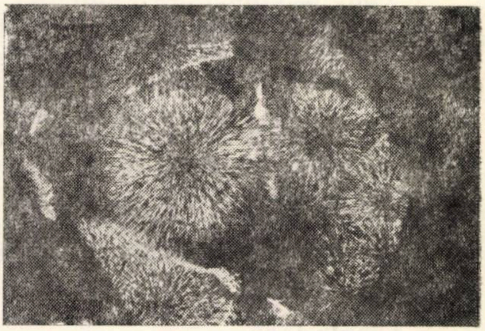

Fig. 6. Type III de sphérulite de PP positive dans le centre obtenu à 115°C.

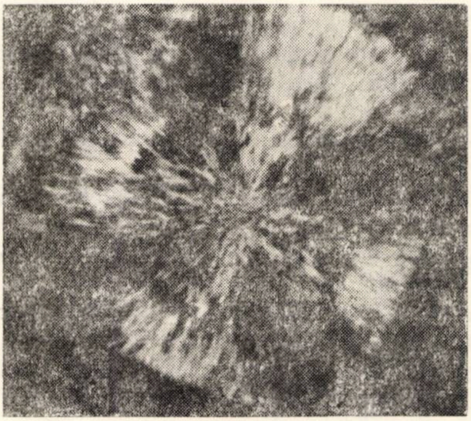

Fig. 7. Le type IV de sphérulite de PP annelé, obtenu à 130°C.

Dans le cas de la cristallisation sur support de zinc, à différentes températures le grand nombre de centres de nucléation ne permet pas le développement intégral des sphérulites. Les petites sphérulites apparaissent dans le champs microscopique comme de petits points lumineux capables de biréfringence en lumière polarisée.

La présence de l'huile siliconique sur le support produit une modification des centres de nucléation, réduisant leur nombre et augmentant les dimensions des sphérulites par comparaison à l'absence de l'huile.

On peut ainsi affirmer, [1, 2], comme conséquence de cette étude que l'influence du support sur les mécanismes cinétiques et morphologiques est correlée à l'énergie libre de sa surface.

L'influence des concentrations initiales des solutions de xylène a été examinée pour le domaine 0,01–0,5%. Avant 0,1% la présence des sphérulites n'a pas été mise en évidence. A 0,5% on a observé les formations dendritiques. Les pellicules obtenues des solutions plus concentrées (1—2%) ont cristallisé de la même manière que les feuilles de PE obtenues du polymère fondu.

Pour examiner les influences réciproques du PE sur la cristallisation du PP, on a étudié des mélanges en proportion de 1/1, 1/2, et 1/3. Les pellicules ont été préparées par évaporation des solutions de 2,5% en xylène. On constate une interinfluence des morphologies de formation des composants. Une influence plus évidente est exercée sur le composant ayant la plus basse température de cristallisation, dans notre cas, le PE. Les sphérulites de PE se développent moins que les autres, car le PP a une plus grande vitesse de cristallisation. Même si on prolonge le processus de cristallisation en le ralentissant, les sphérulites de PE ne disposent plus de conditions spéciales pour se développer normalement

Conclusions

De l'examination des facteurs qui influencent la cristallisation du PP et du PE, du point de vue cinétique et morphologique il résulte que :

— la diminution de la durée de cristallisation entraîne la diminution du rayon des sphérulites ;

— l'augmentation du rayon (moyen) est associé généralement à des changements dans la morphologie ;

— la cinétique de cristallisation des échantillons de PP sur verre n'est influencée par l'épaisseur de l'échantillon que jusqu'à 50 μ ;

— dans le cas du PE cette cinétique est influencée par l'épaisseur des échantillons, même dans des conditions de préparation industrielle ;

— l'élévation de la température implique l'augmentation du rayon des sphérulites et la diminution de la concentration des centres de nucléation ;

— le support influence la cinétique par l'énergie libre de surface ;

— la structure morphologique dans le cas de la présence simultanée de PE et PP est caractérisée par leur influence réciproque ;

— la distribution des centres de nucléation dépend des conditions de cristallisation.

BIBLIOGRAPHIE

1. ROBERT JOEL SAMUEL, *Structured polymer properties*, John Wiley, 1974
2. I. C. PETREA, *Structura polimerilor*, E. D. P., Bucureşti, 1971
3. C. A. STĂNESCU, I. C. PETREA, M. COJOCARU, ELENA LUTIC-SANDU, Comunicare la Sesiunea ştiinţifică ICEFIZ, 1976, p. 86.

Primit la redacţie la 12 ianuarie 1978

ANALELE UNIVERSITĂŢII BUCUREŞTI FIZICĂ, XXVII, 1978 pag. 29—34

SUR LA RELAXATION DES FORMATIONS SUPRAMOLECULAIRES DANS LE CAOUTCHOUC RÉTIFIÉ

M. COJOCARU, I. C. PETREA, C. A. STĂNESCU

Faculté de Physique
Université de Bucarest*

RÉSUMÉ

L'étude expérimentale et l'analyse théorique des résultats obtenus en suivant systématiquement la précision et la corrélation des particularités physicomécaniques du système élastomère butadiène-acrylonitryle, à une température constante, et dans des conditions de modification controlée du temps de vulcanisation, relève la présence et l'influence sur la relaxation de certaines formations structurales supramoléculaires.

On met en evidence dans ce contexte l'existence certe des formations supramoléculaires dans l'élastomère examiné et la manifestation de certains processus élémentaires aux effets distincts au niveau de la relaxation lente. Les courbes expérimentales obtenues dans le cas d'un tel caoutchouc rétifié avancent l'idée de la coexistence de deux relaxations : une rapide et l'autre lente ; la relaxation lente peut être identifiée par la période de relaxation la plus élevée. La nature et les dimensions des formations supramoléculaires reflétées dans une série de particularités cinéticostructurales expliquent la non concordance remarquée entre les processus élémentaires de relaxation spécifiques pour les élastomères avec, ou sans noir de fumée comme remplissage. Les caoutchoucs vulcanisés, mais sans remplissage, présentent une relaxation phénoménologique moins diversifiée que les systèmes équivalents contenant, en plus, noir de fumée. Le temps de relaxation déterminé dans cet article est de l'ordre de 3×10^3 secondes et il correspond au stade de regroupement des structures supramoléculaires, c'est-à-dire, à la période de relaxation lente.

Notions introductives

Dans les systèmes élastomères, capables d'états et de particularités physicomécaniques déterminées par les procédés préalables de rétification et de plastification, se produisent des phènomènes de relaxation qui impliquent de divers types d'unités cinetique-structurales. Cettes entités interviennent dans le mécanisme de relaxation de la tension mécanique par l'intermède de quelques processus élémentaires distincts [1].

---

* *Centre National de Physique* Magurele, Bucharest B. P. 5211.

On sait qu'un système soumis à une déformation initiale ε_0 peut être caractérisé dans des conditions données par une tension σ relaxée au moment t d'après la loi :

$$\sigma(t) = \sum_{i=1}^{n} \sigma_i(t), \qquad (i=1, 2, ... 5) \tag{1}$$

Les composantes σ_i de la tension relaxée peuvent être examinées séparément et corrélées d'après leur signification physique et les effets au niveau du comportement macroscopique du système relaxé. Ces composantes interviennent toutefois dans le processus de relaxation globale du système élastomère composé, par des poids statistiques dépendantes de la nature, la configuration et les dimensions des entités structurales ou des formations systématiques spécifiques pour un état donné du système.

L'étude de la relaxation globale comme une somme des processus élémentaires influents suppose, dans le cas d'un élastomère, l'investigation dans des conditions d'équilibre statistique, de la liaison existente entre le caractére macroscopique des propriétés élastiques et les particularités de la mobilité micro et macrobrownienne des entités structurales constituantes. Le procédé de synthèse de l'élastomère, sa mise en oeuvre ultérieure appropriée aux exigences d'exploitation pratique de celui-ci, ainsi-que toute son histoire précédant la réalisation de certaines proprétés thermomécaniques préconisées par une recherche de spécialité, comme dans ce cas, compliquent, par des diverses coséquences, la corrélation des particularités de structure locale avec d'intéressants paramètres macroscopiques.

Considérant la relaxation comme une composante des manifestations cinétiques — moléculaires du système étudié il faut tenir compte, en même temps, du fait que la vitesse des processus élémentaires du même genre diminue en temps. La coexistance de certaines entités structurales ou des formations supramoléculaires dans les élastomères du même type que celui étudié pour être utilisé à l'étanchement des dispositifs à longue soliciation cyclique, pose de problèmes pratiques difficile à résoudre, étant donnée la réaction particulière des differentes formations moléculaires ou microblocs.

Les propriétés mécaniques remarquables d'un tel système avec une structure complexe, peuvent être ainsi exprimées obligatoirement par l'intermède d'un paramètre structural généralisé γ, qui rejoint la température ambiante T, la fréquence ν de la solicitation périodique, la déformation ε, la tension σ et d'autres grandeurs au rôle d'argument dans une fonction implicite :

$$P = t(\gamma, \mathrm{T}, \varepsilon, \sigma) \tag{2}$$

Dans les élastomères, la dépendence déformation-tension, examinée en consensus avec les particularités du module d'élasticité pour l'état caoutchoutique, nécessite aussi la considération des processus de relaxation afférents aux solicitations mécaniques périodiques, de fréquence plus ou moins élevée. La manifestation distincte d'un des deux processus qui composent la relaxation globale peut-être atribuée au phénomène de résonance qui se produit, dans des conditions spéciales, pour les entités de dimensions convenables à la fréquence de solicitation mécanique du système.

Treloar [2] a le mérite d'avoir contribué essentiellement à l'élaboration de la théorie statistique des élastomères, dans des conditions de comportement mécanique suffisament réversible, en faisant des exprériences sur des systèmes complexes de caoutchouc vulcanisé soumis à des diverses types de déformations mécaniques. Thirion et Chasset [3] ont mis en évidence l'influence du tau de rétification sur les courbes de relaxation de certains caoutchoucs naturales vulcanisés avec péroxyde de dicumyl. La présence de certains ingrédients dans la phase amorphe des chaînes suffisament régulières transforme sensiblement le comportement élastique des vulcanisats plastifiés qui deviennent ainsi, des systèmes complexes difficilement à analyser seulement à l'aide de la théorie statistique. La diffraction des rayons X, la biréfringence optique, le hystérésis mécanique etc. peuvent aider effectivement la connaissance approfondie descrelations, qui deviennent caractéristiques après certains processus technologiques, entre la structure modifiée du point de vue physicochimique et les propriétés macroscopiques.

Donnees experimentales

Le présent travail fait partie d'un ensemble de préoccupations concernant l'analyse physicostructurale de certains systèmes élastomères déstinés à l'utilisation immédiate dans des conditions avantageuses du point de vue économique.

L'étude expérimentale du caoutchouc butadiène-acrylonitryle a été initié par les auteurs de cet article en procédant à une vulcanisation typique, efféctée aux intérvales de temps convenablement échalonnés, et sans changer la température.

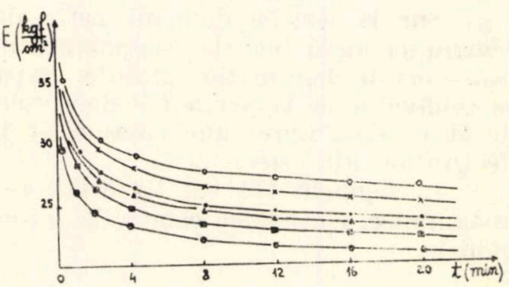

Fig. 1. Le module d'élasticité E en fonction du temps de solicitation mécanique, pour les diverses échantillons.

Les échantillons de caoutchouc vulcanisé se présentent sous forme d'éprouvettes de 1,5 cm largeur et 2—3 mm épaisseur.

La précision des mésures ne dépasse pas 1%.

La figure 1 comprend les résultats expérimentaux intervenant dans l'étude du module d'élasticité E en fonction de la durée de solicitation, pour des échantillons caractérisés par des temps différents de vulcanisation. Chacune des cinq courbes tracées à l'aide des résultats de laboratoire présente, d'une mainère commune, deux régions distinctes, à savoir AB non-linéaire et l'autre BC — linéaire. De telles courbes décrivent généralement, dans les termes mentionnés, le comportement caractéristique des matériaux caoutchoutiques amorphes.

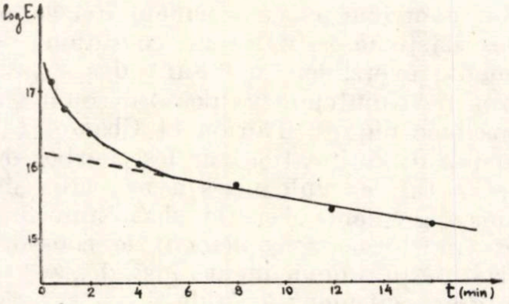

Fig. 2. Le module d'élasticité E en fonction du temps de vulcanisation pour les échantillons vulcanisé pendant 25 minutes.

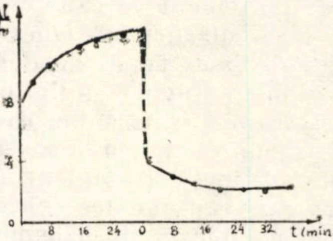

Fig. 5. La déformation reiative $\Delta 1/ll_0$ en fonction du temps de solicitation mécanique pour l'échantillon vulcanisé pendant 25 minutes.

La courbe représentée dans la figure 2 a le but d'illustrer, par l'extrapolation, le module Young d'équilibre E ; l'éxtrapolation de la partie linéaire CB donne sur l'axe OY le segment OD qui s'identifie en effet avec E , grandeur qui dépend strictement de la structure interne du caoutchouc nitrlique étudié. L'échantilon choisi pour ce graphique a été découpé dans un caoutchouc nitrylique vulcanisé pendant 25 minutes et le teste a été efféctué à 23°C.

Dans la figure 3 est représentée la déformation relative en fonction de la durée de solicitation de l'échantillon, pour les conditions $\sigma =$ const. et T = const.

Sur la courbe donnant cette dépendence fonctionnelle on peut remarquer aussi bien la composante réversible, que celle iréversible du processus de déformation globale. La partie rémanente de la déformation se confond avec la partie CE de la courbe, correspondant à la relaxation de la tension, après que l'action de la force constante d'étirement de l'échantion ait cessé.

Le segment OA sur l'axe OY représente la déformation élastique instantanée, considérée comme la seconde composante de la déformation globale.

Discution des resultats

On connaît que les systèmes élastomères plastifiés avec noir de fumée présentent des processus de relaxation non-linéaires caractéristiques [4]. C'est le cas, d'ailleurs, du caoutchouc nitrylique étudié par les auteurs de cet article.

La concurence des processus élémentaire de relaxation et des particularités physicostructurales qui découlent de la coexistence des différentes entités structurales composant le système, est reflétée de manière caractéristique, par la forme des courbes trassées dans le but d'obtenir des informations concernant le phénomène de relaxation globale [5]. La concomitance de ces processus favorise la mise en évidence du temps maximum de relaxation $\tau_{\max}$ correspondant au module d'élasticité $E_{\max}$. L'interprétation des interdépendences microphysiques qui se trouvent à l'origine de la déformation et de la relaxation macroscopique du système élastomère rétifié et plastifié ne s'inscrit pas de manière simple dans la corrélation des prévisions théorətique cantitatives et le comportement mécanique réel d'un tel système.

Le module Young, aussi bien que d'autres constantes physiques utilisées pour la description phénomènologique des liaisons existentes entre les grandeurs macroscopiques de type force déformatrice déformation et relaxation doit être introduit dans le calcul comme un coefficient moyen. La moyenne nécessite des approximations successives et des modèles qui peuvent faciliter la corrélation des propriétés de résistence et de haute élasticité avec les processus de relaxation soit, par exemple, les pertes mécaniques. La stabilité des formations supramoléculaires diminue sous les actions déformatrices et aux températures relativement élevées, tot en gardant le caractère de la disposition réciproque des segments de chaîne et des chaînes élémentaires du réseau de base.

La théorie cinétique moléculaire et la spectromètrie des relaxomères pour un système constitué par plusieurs types d'unités cinétiques attribue chaque processus élémentaire de relaxation une énergie d'activation $\mathscr{E}_i$, dont dépend le temps de vie individuelle τ_i du relaxomère impliqué dans la relaxation globale, d'après la relation :

$$\tau_i = B \exp\left(\mathscr{E}_i / kT\right) \qquad 3)$$

A une température T les relaxomères entraînés dans le processus i ont, de manière caractéristique, un temps de vie et un seuil de sensibilité B_i concordant à l'énergie d'activation $\mathscr{E}_i$.

Pour le type i de relaxomères ou d'unités cinétiques participans au processus élémentaire de relaxation on peut écrire au moment t la relaxation de la tension σ en accord avec l'équation de Maxwell :

$$\sigma_i = \sigma_i \exp\left(t - / \tau_i\right) \qquad (4)$$

Compte tenu des possbilités offertes par la confrontation des paramètres cinetique-moléculaires intervenant dans les relations mentionnées ici et en nous placeant dans les limites de la théorie visco-élastique de la relaxation [6], quand $\varepsilon = \text{const.}$, s'impose la réconsidération de la relation fondamentale :

$$\sigma = E(t) . \varepsilon \qquad (5)$$

oú apparaît, avec de nouvelles implications et significations, le module de relaxation $E(t)$.

Ce module contient et refléte les effets de la distribution des temps de relaxation, qui diminuent de manière continue en temps:

$$E(t) = \int_{-\infty}^{+\infty} W(\ln \tau) \exp(-t/\tau) \, d \ln \tau \qquad (6)$$

$W(\ln \tau)$ représente la fonction de distribution des temps de relaxation τ. A l'aide de données expérimentales obtenues par l'étude des dépendences $E(t)$ ou $\sigma(t)$ on peut calculer $W(\ln \tau)$.

La dépendence $\log E(t) = f(t)$ représentée dans la figure 2 a, elle aussi, un segment linéaire, important par sa pente au rôle déterminant pour l'estimation du temps maximum de relaxation $\tau_{\max}$. Pour le caoutchouc nitrylique étudié, ce temps a la valeur 3×10^3 s environ, indiquant par son ordre de grandeur un regroupement des formations supramoléculaires. On aprécie ainsi la situation du cas examiné dans les limites du temps de relaxation lente. On peut considérer donc que la relaxation globale possède, à côté de la composante rapide, et une lente.

La composante rapide découle de l'orientation et la mobilité des segments macromoléculaires libres, alors que la relaxation lente apparait comme une conséquence de l'existence des formations supramoléculaires.

Les processus de relaxation non linéaire dépendants de la tension et du temps, comme on peut le voir dans les figures 1, 2 et 3, sont caactéristiques pour les matériaux caoutchoutiques avec noir de fumée. Pour de tels systèmes de nombre des processus élémentaires de relaxation est plus grand que pour les élastomères rétifiés, mais non-plastifiés.

L'éventualité de l'existence de certaines formations supramoléculaires de nature réticulaire dans le cas du caoutchouc nitrylique étudié dans ce contexte, semble impossible sion tient compte du fait que le temps de relaxation spécifique pour les formations de ce genre, est de deux-trois ordres de grandeur plus élevée que celui déterminé et indiqué plus haut.

En conclusion, on peut affirmer que les microdomaines estimés comme des relaxomères lents ont des dimensions plus grandes que les segments de chaîne libres, étant toutefois plus petits que les réticules complémentaires présents dans d'autres systèmes.

BIBLIOGRAPHIE

1. G. M. BARTENEV, IU. V. ZELENEV, (pod. red.), *Relaxaţionnie iavlenia v polimerah* Izd. Himiia, Leningrad, 1972.
2. R. L. G. TRELOAR, *The Physics of Rubber Elasticity*, Oxford Press 1958.
3. P. THIRION, R. CHASSET, Chim. Ind. Gén. Chim., 97, 617, 1967.
4. G. M. BARTENEV, N. M. LIALINA, Vis. mol. soed., 12, nr. 2, 368, 1970.
5. A. V. TOBOLSKY, *Properties and Structure of Polymers*, Princeton University, 1960.
6. G. M. BARTENEV, IU. V. ZELENEV, *Kurs fiziki polimerov*, Izd. Himiia Leningrad, 1976.

Primit la redacţie în 10.I 1978

ANALELE UNIVERSITĂŢII BUCUREŞTI FIZICA, XXVIII, 1978, pag. 35—40

LA CONFORMATION DES CHAINES MACROMOLÉCULAIRES DANS LA PHASE LAMELLAIRE DES COPOLYMÉRES SÉQUENCÉS POLYSTYRÈNE-POLYISOPRÈNE A L'ÉTAT SOLIDE

LIVIA MARIA IONESCU
Faculté de Physique, Université de Bucarest*

RÉSUMÉ

Les mesures de biréfringence optique, effectuées sur la structure lamellaire orientée en larges monodomaines (monocristaux) du copolymère polystyrène-polyisoprène, ont mis en évidence une anisotropie moléculaire très faible. Ces résultats semblent montrer que la distribution angulaire des segments de chaînes est pratiquement isotrope, mais ne précisent en rien la conformation globale des séquences à l'échelle macromoléculaire.

Apparament, seules les mesures, par diffusion des neutrons aux petits angles, du rayon de giration des séquences deutériées autour de la normale aux interfaces, peuvent apporter une réponse à ce problème.

1. Introduction

Cet article porte sur les monocristaux des copolymères séquencés, constitués par des structures mésomorphes macroorientées.

La caractéristique essentielle des copolymères séquencés réside dans le fait que leurs séquences, chimiquement différentes, se repoussent et se séparent spontanément, pour former dans l'espace des microdomaines distincts de forme géométrique bien précise (lamelles, cylindres, sphères) [1].

L'expérience et la théorie nous ont appris que le type d'organisation, en réseaux réguliers, des copolymères à séquences amorphes est déterminé essentiellement par l'encombrement relatif des séquences. Les macromolécules qui se composent de deux séquences de volume semblable donnent toujours naissance à des structures lamellaires [2].

La structure lamellaire (figure 1) correspond à l'empilement de feuillets parallèles et équidistants, consittués de deux couches distinctes et superposeés, contenant chacune un seul type de séquences [3].

---

* *Centre National de Physique,* Măgurele ,Bucarest, B. P. 5211.

Dans les microdomaines, les séquences jouissent d'une grande liberté. Elles y préservent, dans une large mesure, leur individualité et consèrvent leurs propritétés intrinséques [4]. Ainsi, suivant leur nature et les conditions expérimentales, elles peuvent soit garder, toutes les deux, une conformation désordonnée (figure 1), soit alors cristalliser ; elles peuvent même les unes cristalliser, pendant que les autres demeurent à l'état liquide. Cette liberté se retrouve également dans le cas oú les séquences sont "amorphes" et oú elles préservent, suivant la température, les propriétés d'un verre ou celles d'un élastomère.

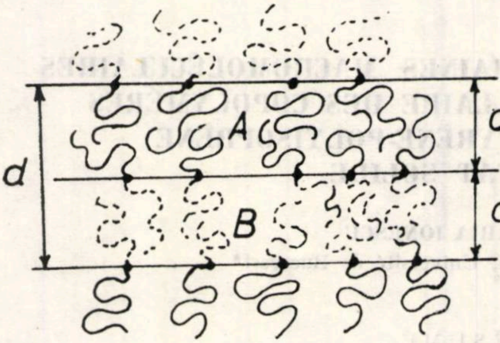

Fig. 1. Représentation schématique de la structure lamellaire : les deux séquences A et B ont une conformation désordonnée.

Les copolymères polystrène-polyisoprène, dont une des séquences est vitreuse, alors que l'autre est de type "caoutchouc", retiennent ce dernier temps l'attention, par d'intéressantes propriétés d'élastomère, vulcanisé physiquement, et moulable à chaud. Les domaines de ségrégation constitués par les séquences vitreuses jouent le rôle des nodules de vulcanisation classique ; si l'on opère à température supérieure à la température de transition vitreuse, ces nodules s'amolissent et rendent ainsi possible le moulage du produit dans les formes les plus variées. Par ailleurs, l'organisation spontanée de ces systèmes en édiffices mésomorphes permet d'envisager l'obtention de propriétés physiques et techniques nouvelles, liées à la combinaison des propriétés de chacune des séquences et au caractère "cristallin" anisotrope de l'ensemble.

La diffraction des rayons X aux petits angles de Bragg permet de déterminer la structure des copolyméres séquencés à l'état solide. Elle permet, non seulement de préciser le mode d'organisation d'un copolymère donné, mais, également, de déterminer les paramètres géométriques qui le caractérisent. Ainsi, on peut déterminer, par exemple, dans le cas de la structure lamellaire, l'équidistance des lamelles d (figure 1), qui se trouve typiquement dans un domaine de valeurs comprises entre 100 et 1 000 Å [5, 6].

A partir de ce paramètre, fourni directement par l'expérience, et moyennant certaines hypothèses, notamment sur l'aditivité des volumes spécifiques partiels $\bar{v}_A$ et $\bar{v}_B$ des entités présentes dans le système, on peut calculer d'autres paramètres fort intéressants, telles les épaisseurs respectives d_A et d_B des souscouches (figure 1), qui forment la lamelle élémentaire [3, 7] :

$$d_A = \left(1 + \frac{1 - x_A}{x_A} \cdot \frac{\bar{v}_B}{\bar{v}_A}\right)^{-1} \qquad (1)$$

$$d_B = d - d_A \tag{2}$$

oú x_A représente la teneur en poids des séquences A.

L'aire moléculaire, c'est-à-dire, la surface moyenne qu'occupe une macromolécule au niveau de l'interface, c'est un autre paramètre accessible par calcul; on peut l'exprimer de manière simple [4, 7], telle que:

$$S = \frac{2M_A v_A}{N \cdot d} \cdot \left(1 + \frac{1-x_A}{x_A} \cdot \frac{\bar{v}_B}{\bar{v}_A}\right) \tag{3}$$

oú M_A est la masse moléculaire moyenne des séquences A, et N — le nombre d'Avogadro.

Il est nécessaire de décrire plus en détail la conformation des chaînes macromoléculaires à l'intérieur des microdomaines de ségrégation, et d'apprécier leur degré d'enchevêtrement.

Pour préciser d'avantage la structure, nous avons fait appel à une méthode optique (biréfringence).

II. Technique experimentale

1. *Produits utilisés*

Nous avons utilisé un copolymère biséquencé polystyrène-polyisoprène (PS-PI), dont les caractéristiques moléculaires sont données dans le tableau 1.

Tableau 1

Prélèvement	M_w	$\frac{M_w}{M_n}$	Copolymère	Teneur en poids du PI (%)	M_w	$\frac{M_w}{M_n}$
PS	103000	1,15	PS−PI	51,0	210000	1,16

Tableau 1 **Caractérisation du copolymère polystyrène-polyisoprène (PS−PI) et de son prélèvement polystyrène (PS).**

La masse moléculaire moyenne en poids du prélèvement PS et celle du copolymère ont été mesurées par diffusion de la lumière en solutions dans le tétrahydrofuranne.

La polydispersité des échantillons a été caractérisée par chromatografie sur gel perméable.

La composition en poids du copolymère a été détérminée par analyse U. V.

Pour orienter les copolymères en monodomaines de dimensions suffisantes, nous avons utilisé une technique de cisaillement mise au point au Centre de Recherches sur les Macromolécules de Strasbourg [8].

Le cisaillement est réalisé par un mouvement linéaire de va-et-vient de deux plateaux parallèles métalliques, maintenus à une distance de 2,5 mm, entre lesquels est inséré le polymère préalablement moulé sous vide à 160°C. Le gradient de cisaillement est constant et de l'ordre de 10^{-2} à 10^{-1} s^{-1}. Le cisaillement est effectué à 130°C, durant quelques heures, la course étant de 4 mm. Le traitement est achevé par recuit à 130°C pendant 2 heures. Toutes ces opérations sont menées sous atmosphère inerte d'azote.

2. *Résultats*

2a) *Expériences de diffraction*

Le copolymère séquencé que nous avons étudié présente une structure lamellaire : sa composition pondérale, en effet, est voisine de 50% [2].

La périodicité d'empilement des feuillets, calculée d'après la position angulaire des taches équatoriales de diffraction, est de 860Å. Compte tenu des volumes spécifiques partiels du polystyrène ($\bar{v}_{PS} = 0{,}953\ \mathrm{cm}^3 \cdot \mathrm{g}^{-1}$) et du polyisoprène ($\bar{v}_{PI} = 1{,}106\ \mathrm{cm}^3 \cdot \mathrm{g}^{-1}$) [6, 9], ainsi que de la composition en poids du copolymère (49% PS), on peut calculer, à l'aide des formules (1) et (2), les épaisseurs respectives des couches de polystyrène et de polyisoprène qui forment la lamelle élémentaire : $d_{PS} = 380$ Å et $d_{PI} = 480$ Å. Quant à la surface spécifique S, on peut également l'évaleur, en faisant intervenir dans la formule (3), la masse moléculaire moyenne des séquences polystyrène ; on trouve $S = 426$ Å^2.

2b). *Biréfringence optique*

Le signe et la valeur de la biréfringence des échantillons ont été mesurés de manière classique, à l'aide d'un compensateur Babinet.

Nous avons trouvé que la biréfringence optique des échantillons de copolymère séquencé PS-PI a un caractère uniaxiale, à l'axe optique perpendiculaire aux lamelles de la structure orientée de ce coplymère ; pour des raisons de symètrie, on s'attendait à ce résultat [10].

Les échantillons examinés entre les polaroids croisés dans le microscope, ont montré une extinction lorsque la surface des lamelles a été placée parallèlement ou perpendiculièrement au vecteur de la lumière incidente.

En faisant usage d'un compensateur à quartz, nous avons trouvé que l'échantillon revèle une biréfringence négative par rapport à la normale aux lamelles, dont la valeur est $(24{,}0 \pm 2{,}0) \cdot 10^{-4}$.

Lorsque la lumière incidente a été perpendiculaire à la surface des lamelles, le materiel s'est montré complétement isotrope (nonbiréfringent).

III. Discussion des résultats

La biréfringence dans les polymères est normalement associée à l'orientation moléculaire, qui détermine la distribution anisotrope des polarisabilités des unités monomères dans l'espace [10].

La situation se complique dans le cas des copolymères séquencés organisés. La présence dans l'échantillon des microdomaines d'indices de réfraction différents, ayant au moins une dimension inférieure à la longueur d'onde de la lumière, fait intervenir la "biréfringence de forme", qui peut avoir une contribution notable à la biréfringence totale du système.

Cet effet depend seulement des fractions en volume v_1 et v_2 et des indices de réfraction n_1 et n_2 des deux microphases. (Nous avons substitué les indices 1 et 2 aux indices A et B pour des raisons de commodité de notation). Pour la structure lamellaire, on s'attend à une birefringence de forme négative, dont l'expression est [11] :

$$\Delta n = \frac{-\, v_1 v_2 \, (n_1^2 - n_2^2)^2}{2 \cdot (v_1 n_2^2 + v_2 n_1^2) \cdot (v_1 n_1^2 + v_2 n_2^2)^{1/2}} \qquad (4)$$

Le calcul de la biréfringence de forme, suivant la formule (4), pour le copolymère séquencé PS-PI, alors qu'on connait la composition en volume de l'échantillon et la valeur mesurée de l'indice de réfraction du polystyrène ($n_1 = 1{,}59$) et du polyisoprène ($n_2 = 1{,}52$) [12], conduit à une valeur : $\Delta n = -\, 15{,}47.10^{-4}$.

La comparison de ce résultat avec la valeur moyenne mesurée : $-\, 24{,}0.10^{-4}$, montre que la valeur observée n'est pas completement compensée par la biréfringence de forme. Ce résultat nous fait penser à l'existence d'une biréfringence supplémentaire, due à l'orientation moléculaire soit dans une ou l'autre des phases, soit dans les deux phases.

IV. Conclusions

L'ensemble de ces expériences a mis en évidence une anisotropie moléculaire très faible. Les résultats semblent montrer que la distribution angulaire des segments de chaînes est pratiquement isotrope, mais ne précisent en rien la conformation globale des séquences à l'échelle macromoléculaire.

La technique de la diffusion cohérente des neutrons aux petits angles est capable d'apporter des informations sur ce dernier point [13]. En mesurant le rayon de giration des séquences deutériées autour de la normale aux interfaces, on peut avoir une évaluation directe des dimensions latérales des chaînes et, en comparant ces dernières à l'aire moléculaire déterminée par diffraction des rayons X ou des neutrons, on peut caractériser le degré d'interpénétration des séquences. Les résultats préliminaires concernant ce sujet [13], montrent la nécessité de poursiuvre ce genre d'expériences, ce qui permettera de resoudre le problème de la conformation des chaînes dans les copolymères organisés.

RÉFÉRENCES

1. A. SKOULIOS, Informations Chimie, *120*, 41 (1973).

2. G. E. MOLAU, *Block Polymers* (S. L. Aggerwal Ed.) — Plenum Press New York, p. 79 (1970).

3. A. SKOULIOS, G. FINAZ, C. R. Acad. Sci. Paris, *252*, 3467 (1961) ; J. Chim. Phys., *59*, 473 (1962).

4. A. SKOULIOS, *Advances in Liquid Crystals*, vol. 1 C, 169 (1975).
5. A. SKOULIOS, *Reprinted from Block and Graft Copolymers* (1973).
6. L. M. IONESCU, A. SKOULIOS, Makromol. Chem., *177*, 257 (1976).
7. P. GROSIUS, Y. GALLOT, A. SKOULIOS, Makromol. Chem., *127*, 94 (1969).
8. A. MATHIS, G. HADZIIOANNOU, A. SKOULIOS, *Polymer Preprints* A. C. S., New Orleans (à paraître).
9. J. TERRISSE, *Thèse, Université de Strasbourg* (1973).
10. I. C. PETREA, L. GEORGESCU, Analele Universităţii Bucureşti (Fizică), vol. XXVI, 37 (1977).
11. M. J. FOLKES, A. KELLER, J. Polym. Sci., Phys., 14, 833 (1976).
12. *Polymer Handbook*, J. Baudrup, E. H. Immergut edtrs., Wiley-Intersci. Publish., John Wiley & Sons, New York—London—Sydney.
13. L. M. IONESCU, *Thèse, Université de Strasbourg* (1976).

Primit la redacţie în 1—XII 1977

ANALELE UNIVERSITĂŢII BUCUREŞTI FIZICA, XXVII, 1978, pag. 41—45

DETERMINATION OF SOME PHYSICAL PARAMETERS OF THE BINARY LIQUID ACETIC ACID-ACETONE MIXTURE

CLEOPATRA GHERBANOVSCHI

Faculty of Physics, University of Bucharest*

RÉSUMÉ

On a mésuré la densité, la viscosyté dynamique, l'indice de refraction et la vitese de propagation d'ultrason à 30 MHz dans le mélange binaire liquide acid acétique-acétone pour les concentrations 0,2 à 0,8 m. de l'acid acétique, dans une large interval de temperature. On a calculé la compresibilité adiabatique. On donne aussi les dépendences avec la concentration de ces paramétres physiques.

To the same aim as I had in a previous work [1], to obtain new data on the liquid mixture structure, I determined a few physical parameters of the acetic acid-acetone mixture as a function of the concentration at various temperatures.

The research, by various methods on the acetic acid, allowed the gathering of a doubtless data on structure, thermodynamics and kinetics of molecular processes in liquid acetic acid. From this point of view, the acetic acid becomes the common solvent in molecular association mechanism study through hydrogen bonds.

Experimental data

Density, dynamique viscosity, refractive index and propagation velocity of ultrasonic waves were measured in binary liquid acetic acid acetone mixtures of 0,2 ; 0,4 ; 0,6 ; 0,8 concentrations of acetic acid molar fractions. On the basis of obtained data the adiabatic compressibilities were determined.

Purification of substances was made by specific methods and purity degree was checked by density, refractive index values at 20°C and by melting and boiling temperatures.

Density, dynamic viscosity and propagation velocity of ultrasonic waves methods as well as the measurement accuracy were exposed in

---

* *National Center of Physics,* Măgurele, Bucharest, P. O. Bax 5211.

[1, 2]. Refractive index was determined with a IRF-23 refractometer, on yellow line ($\lambda = 5893 Å$) of Na spectrum. The accuracy was 10^{-4}.

In I, II, III and IV-tables the parameters values are shown.

Table I

Density of acetic acid-acetone mixtures

Concentration	ρ g/cm³		
	20° C	40° C	60° C
acetone	0,7901	0,7681	—
0,2	0,8377	0,8204	0,8024
0,4	0,8878	0,8702	0,8522
0,6	0,9398	0,9218	0,9058
0,8	0,9917	0,9752	0,9557
acetic acid	1,0489	1,0265	1,0041

Table II

Dynamic viscosity coefficients values for acetic acid-acetone mixtures

Concentration	η cp						
	60°C	40°C	20°C	0°C	20°C	40°C	60°C
acetone	0,98 (3)	0,71 (3)	0,51 (3)	0,40 (4)	0,33 (5)	0,27 (3)	0,23 (3)
0,2	1,74	1,43	1,25	1,11	0,53	0,42	0,33
0,4	—	1,75	1,44	1,23	0,64	0,49	0,38
0,6	—	—	1,73	1,50	0,80	0,59	0,45
0,8	—	—	—	1,59	1,02	0,75	—
acetic acid [6]	—	—	—	—	1,21	0,87	0,64

Table III

Refractive index values for acetic acid-acetone mixtures

Concentration	n	
	20°C	40°C
aceton	1,35898	—
0,2	1,36443	1,35593
0,4	1,36799	1,35928
0,6	1,37119	1,36259
0,8	1,37188	1,36364
acetic acid	1,37193	1,36533 [7]

Table IV

Propagation velocity values of ultrasonic waves through acetic acid-acetone mixtures

Concentration	cm/s, f = 30 MHz						
	−60°C	−40°C	−20°C	0°C	20°C	40°C	60°C
acetone	—	—	—	—	1 189	1 113	—
0,2	1 551	1 479	1 384	1 306	1 222	1 143	1 055
0,4	—	—	1 382	1 268	1 237	1 146	1 071
0,6	—	—	1 369	1 296	1 229	1 143	1 067
0,8	—	—	—	1 270	1 213	1 137	1 063
acetic acid (8)	—	—	—	—	1 149	1 080	1 010

The obtained results for the density are in agreement with the results published in [5 and 9].

For dynamic viscosity the temperature range was extended from freezing point of each concentration up to 60°C. Within the experimental error limits, the obtained data coincide with those of other authors for temperature above 0°C [9].

Refractive index was measured at 20°C and at 40°C. În literature I was not able to find data on refractive index concerning acetic acid-acetone mixture.

Data on ultrasonic wave propagation velocity are published in the paper [10] for 0,36—0,88 molar fraction concentrations of acetic acid at 25°C as well as in the paper [11]. We extended temperature range from freezing point of each concentration up to 60°C. Within experimental error limits our data coincides with those in the literature.

In 1, 2, 3 and 4 graphs, density, dynamic viscosity, refraction index and ultrasonic wave propagation velocity are shown as function of concentration.

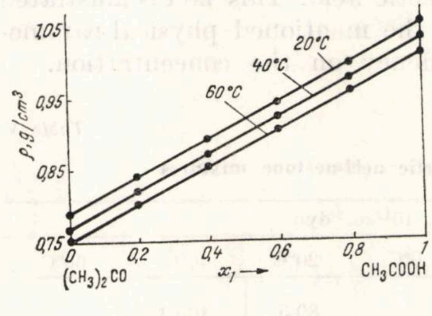

Fig. 1

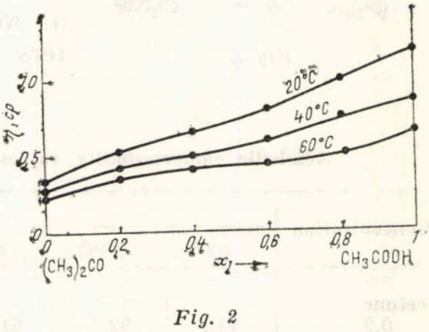

Fig. 2

As seen in fig. 1, density dependency on concentration is linear. The dependency of the other parameters on concentration presents slight deviations from ideality.

On the basis of the obtained data, from the formulae : .

$$\beta_{ad} = \frac{1}{\rho c^2}$$

the adiabatic compressibility was calculated as seen in table V.

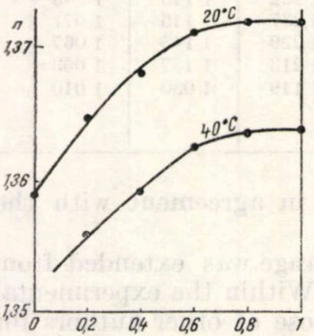

Fig. 3

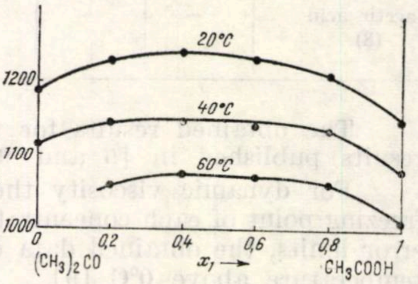

Fig. 4

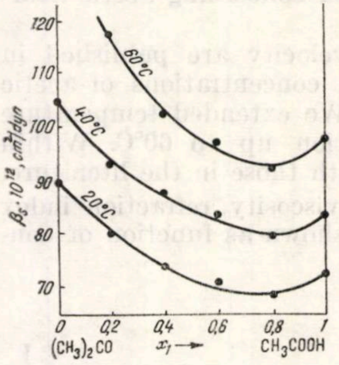

Fig. 5

In graph 5 the adiabatic compressibility is given as function of concentration. It can be observed that this dependency presents a minimum not too sharp for 0,8 molar fraction concentration, invariable with temperature.

Tacking into account other determination for these mixtures too, and the results obtained by considering data from ultrasound absorbtion coefficient study [2], we can assert that acetone interacts weakly with the acetic acid. This fact is illustrated as well by the mentioned physical parameters dependency on the concentration.

Table V

Adiabatic compressibility values for acetic acid-acetone mixtures

Concentration	β ad. 10^{12}cm²/dyn						
	−60°C	−40°C	−20°C	0°C	20°C	40°C	60°C
acetone	—	—	—	—	89,5	105,1	—
0,2	46,7	52,4	61,1	69,3	79,9	93,3	112
0,4	—	—	57,8	69,3	73,6	87,5	102,3
0,6	—	—	55,7	62,8	70,4	83,0	97,2
0,8	—	—	—	62,0	68,5	79,3	92,6
acetic acid	—	—	—	—	72,2	83,5	97,8

The minimum of adiabatic compressibility observed at a concentration where acetic acid is predominant, is due to a structural rearrangement of acetic acid molecules. The minimum maintenance with the temperature growth is indication of this structure stability.

BIBLIOGRAFIE

1. C. GHERBANOVSCHI, Analele Univ. Buc., Fizică, XXVI, 1977
2. C. GHERBANOVSCHI, *Teză de doctorat*, 1974, Univ. Lomonosov, Moscova
3. *Spravocinik himika*, vol. I, 1971, Leningrad
4. *Handbook of chemistry*, Compiled and edited by N. A. LANGE, PH. D., Revised tenth edition.
5. J. *Timmermans*, *The physico-chemical constants of binary systems* in concentrated solutions, N. Y., L, vol. 2, 1959
6. V. A. SÎRBU, *Teză de doctorat*, 1973, Univ. Lomonosov, Moscova
7. I. G. MIHAILOV, Dokladî Akad. Nauk SSSR, vol. 31, Nr. 4, 1941
8. V. A. SÎRBU, M. I. ŞAHPARONOV, Vestnik MGU, Nr. 3, 1973
9. I. M. BOHOVKIN, Jurnal obşcei himii, vol. 28, Nr. 4, 1958
10. R. D. CORSARO, G. A. ATKINSON, J. Chem. Phys., vol. 54, Nr. 9, 1971
11. M. G. SESHAGIRI RAO, RAMACHANDRA RAO B., Ind. J. Pure Appl. Phys., vol. 3, Nr. 207, 1965

Primit la redacţie în 10 – I, 1978

ANALELE UNIVERSITĂȚII BUCUREȘTI FIZICĂ, XXVIII, 1978, pag. 47—51

PHOTOSYNTHESIS REDOX REACTIONS INVESTIGATED BY A PHOTOCALORIMETRIC METHOD

ALEXANDRINA ȘTIRBEȚ
Institut of Biological Sciences, Bucharest

H. VAIS
Measuring and Industrial Electronic Instruments Factory

V. GHEORGHE
Faculty of Physics, University of Bucharest*

ABSTRACT

The preliminary results obtained in the study of the interactions of some redox systems in isolated chloroplasts from Spinacia oleracea L. are presented in this paper.

We have imaginated a photocalorimetric method for the investigation of the light photosynthesis reactions.

The redox potentials measured by our method matches the results published for ferredoxine, P 700 reaction center and HP form of cytochrom b 559.

Our method is a nondestructive one, and this is its major advantage. The measurement was made „in situ'' and in nearly physiological conditions.

1. Introduction

As it is already known, in the light stage of photosynthesis process, that takes place in green leaves, the light captured by the photopigments of the two photosystems leads to chain redox reactions coupled with photophosphorilation.

Although this process is the task of many specialised institutes in the whole world, it still presents many unknown things. So, the mechanism of those reactions is little known, representing a problem wholly unsolved, namely decoding the components and sequence of electron transporting chain.

A photocalorimetric study of interaction of some redox reagents with suspensions of isolted chloroplasts from Spinacia oleracea L. leaves is presented in this paper. The purpose was to determine the redox potentials of some transporting components of electrons in chloroplasts. The data are in full agreement with those found in the literature as well as with images regarding location of different components in the thylakoid membrane.

---

* *National Center of Physics*, P. O. Box 5211, Măgurele—Bucharest.

2. Material and method

In the experiment we used as redox reagents the following ones: NADP$^+$ (nicotinamide adenine dinucleotide phosphate) (Nutritional Biochemicals Corporation), hidroquinone (Merk), and potassium ferricyanide (Merk).

The suspension of chloroplasts, functionally isolated, of class II, was obtained by a method described in (1), using for centrifugation a cooling centrifuge of the type Janetzki K24.

The functionality of samples was tested spectrophotometrically, observing the developement of the Hill reaction (with 2,6-dichlor-phenol indophenol as Hill acceptor), and the total concentration of chlorophyll was determined by means of Arnon's method, (2). A SPECORD UV-Vis Zeiss spectrophotometer was used.

The calorimetric measurements were made with a precision calorimeter LKB-8700. By this calorimetric device we can measure the tempearature variations, ΔT, taking place as a result of thermal process induced in the reaction vessel, as well as of the caloric capacity, ε, of the investigated system.

The heat Q, absorbed or released in the studied reaction, is determinated with this two parameters:

$$Q = N\Delta H = \varepsilon \Delta T$$

where N is the number of moles of reacted substance, and ΔH is the – enthalpy variation.

The enthalpy variation is related to the variation of Gibbs's free energy by means of the well known equation:

$$\Delta G = \Delta H - T\Delta S$$

where ΔS is the entropy variation.

The approximation $\Delta H \simeq \Delta G$ was used in the present paper, assuming the fact that for a certain range of temperature ΔT, ΔH may be equal to ΔG (see Fig. 1). At the same time, is no thermodynamically reason which should indicate the size of this range for a given reaction.

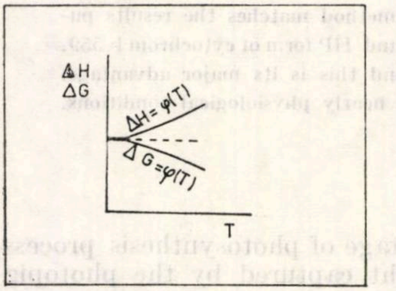

Fig. 1. The plot of ΔH and ΔG versus T.

From the equation that relate the variation of Gibbs free energy to the variation of redox potential:

$$\Delta G = -nF(E_{ac} - E_{don})$$

(where n is the number of transferred electrons, F is the Faraday number and E is the redox potential of reagents), we can obtain the redox potential of the unknown reaction partener.

The application of calorimetric method for measuring the redox potentials of some components in the thylakoid membrane of choloroplast required on the one hand the use of light (in whose absence the reaction can not take place, the respective components being reduced in darkness) and on the other hand the use of some redox reagents with special properties.

To fulfil these requirements to the calorimetric system LKB 8700 was addapted a special device for illumination (see Fig. 2), made up of a light source and a system of two mirrors titled at 45° and fixed on the bottom of the thermostate.

The passage of the light beam through the 18 l of water in the thermostate bath of the calorimeter leads to an illumination of the sample with light free of IR components from the spectrum produced by the source.

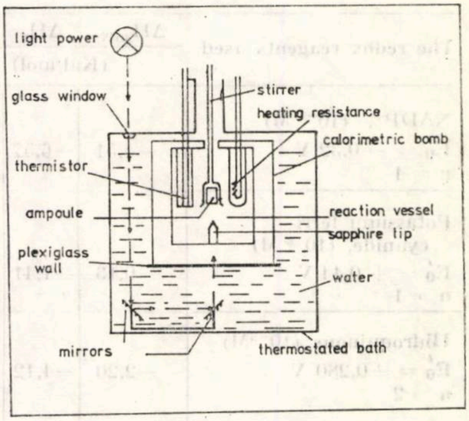

Fig. 2. Simplified diagrame of the light path through the calorimeter.

The redox reagents intended to be used in such measurements must fulfil the following conditions : (1) they must have to interact specifically with only one component in the thylakoid membrane ; (2) they have not to modified the chemical properties of this special component. Otherwise the obtained results leads to misinterpretable data.

The concentrations of redox reagents were of 10^{-6}–10^{-5} M for a total chlorophyll concentration of 2×10^{-1} mg/ml. In our calculations we considered that the whole quantity of added redox reagent was used after the reaction took place.

The enthalpy variation which follows the solving process of the redox reagent was separatelly determined.

3. Experimental results and discussions

In Table I are presented the experimental results. From this table we observe a series of redox potentials of some of electron carrier components of chloroplast. With these have interacted the redox reagents added by us. The identification of the chemical nature was made by correlating these data with those found in the literature.

The obtained result for the interaction of NADP$^+$ with chloroplast was $E'_0 = -0{,}41$ V. The good agreement between our value from E'_0 and that known from literature for classical reaction between NADP$^+$ and ferredoxine, $E'_0 = -0{,}417$ V, is a valuable argument for the applicativity of the photocalorimetric method in this kind of studies.

For a small concentration of the redox reagent and with a pH = 7,2, the interaction between potassium ferricyanide and chloroplasts occur at the PSI, (4). The redox potential $E'_0 = +0{,}5$ V which was determined for the interaction between the potassium ferricyanide and PSI allows us to mention that this interaction occur at the chloropyll reaction center P700 level. This reaction competes with the reduction of X, the primary endogene acceptor of photosystem I.

Table I

The redox reagents used	ΔH_{solv}	ΔH_r	ΔH	ΔE	E_0'	$(E_0')_{lit}$
	(Kal/mol)			(Volts)		
NADP$^+$, (10^{-5} M) $E_0' = -0,32$ V n = 1	$-4,51$	$-6,57$	$-2,06$	0,09	donor $-0,41$	ferredoxine $-0,417$ (3)
Potassium ferricyanide, (10^{-6} M) $E_0' = +0,44$ V n = 1	$-0,13$	$-1,41$	$-1,28$	0,06	donor $+0,5$	P700 $+0,5$ (5)–(8)
Hidroquinone, (10^{-5}M) $E_0' = +0,280$ V n = 2	$-2,20$	$-4,12$	$-1,92$	0,04	acc. $+0,32$	cyt b (HP form) $+0,33$ (16)

Where :

ΔH_{solv} = the solvation molar enthalpy of the redox reagent

ΔH_r = the measured molar enthalpy following the interaction between the exogen redox reagent in solid form and the illuminated chloroplasts suspension

$\Delta H = \Delta H_r - \Delta H_{solv}$

$\Delta E = (E_0')_{acc} - (E_0')$ don

E_0' = the measured redox potential

$(E_0')_{lit}$ = the redox potential found in literature

For chloroplasts and hidroquinone reaction we found $E_0' = +0,32$ V, which can be attributed for cytochrome b_{559}. We known that hidroquinone and the cytochrome b_{559} are donors for the photosystem II, (p9, 10, 11, 12 and 13). Thus, this E_0' value determined fallows us to say that the electrons from hidroquinone reach the PS II via cytochrome b_{559}, not via Z.

Some data, (14, 15) indicate that the cytochrome b_{559} is located in the reducing side of photosystem II. This ambiguity should be expleined by the fact that there are three different form of cytochrome b_{559}. Each form is characterised by different values for redox potential (HP with $E_0' = +0,3$ V; MP with $E_0' = +0,05-0,08$ V; and LP with $E_0' = 0,00$ V), (16). Each of these forms could participate in different reactions in the chloroplast.

From our results we may assume that the HP form of cytochrome b_{55} is one with an electron donor character for photosystem II, the form *MP* being a component of the intermediary electron transport chain.

It is important to mention that we used hydrophilic redox reagents which involves the localisation of endogene components on the thylakoid membrane surfaces.

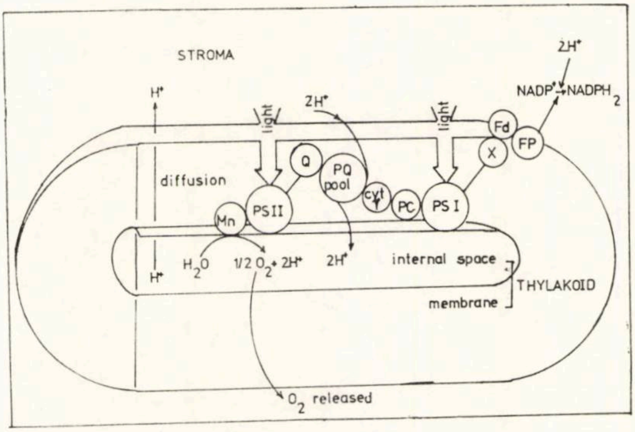

Fig. 3. The sites of the components in the thylakoid membrane, (13).

Our data for ferredoxine and P700 reaction center are in agreement with data from literature, Fig. 3 (13). For cytochrome b_{559} we should say that its two functional forms, HP and MP, are different located in the membrane structure, (HP outside and MP inside of the membrane).

REFERENCES

1. A. STIRBET, A. BREZEANU and V. GHEORGHE, (in press).
2. *Methods in Enzymology*, Vol VI, ed. Kolowick Kaplan, p 311
3. K. TAGAWA and D. I. ARNON, Biochim. Biophys. Acta, *153*, 602, (1968)
4. M. KIMIMURA and S. KATOH, Biochim. Biophys. Acta, *325*, 167, (1973)
5. H. Y. YAMAMOTO and L. P. VERNON, Biochemistry, *8*, 4131, (1969)
6. D. B. KNAFF and R. MALKIN, Arch. Biochem. Biophys., *159*, 555, (1973)
7. B. KE, K. SUGAHARA and E. R. SHAW, Biochem. Biophys. Acta, *408*, 12, (1975)
8. A. J. BEARDEN and R. MALKIN, Brookhaven Symposia in Biology, *28*, 247, (1976)
9. R. G. HILLER, J. M. ANDERSON and N. K. BOARDMAN, Biochem. Biophys. Acta, *245*, 150, (1971)
10. A. VERMEGLIO and P. MATHIS, Biochem. Biophys. Acta,*292*, 763, (1973)
11. A. VERMEGLIO and P. MATHIS, Biochem. Biophys. Acta, *314*, 57 (1973)
12. A. VERMEGLIO and P. MATHIS, Biochem. Biophys. Acta, *368*, 9, (1974)
13. A. TREBST, Ann. Rev. Plant Physiol., *15*, 423, (1974)
14. W. A. CRAMER and W. L. BUTLER, Biochem. Biophys. Acta, *143*, 332, (1967)
15. G. HIND, Photochem. Photobiol., *7*, 369, (1968)
16 D. I. ARNON and K. WADA, Proc. Natl. Acad. Sci. U. S. A., *68*, 3064, (1971)

Primit la redacție în 5–I, 1978

ANALELE UNIVERSITĂŢII BUCUREŞTI FIZICA, XXVII, 1978, pag. 53—58

QUANTITATIVE ESTIMATION OF THE STRUCTURE OF NUCLEOHISTONE COMPLEXES: A SPECTROPHOTOMETRIC AND SPRECTROPHOTOFLUOROMETRIC STUDY

LILIANA RADU
"Victor Babeş" Institute, Bucharest
V. GHEORGHE
Faculty of Physics, University of Bucharest*

ABSTRACT

Some DNA properties modified by histone-DNA binding are studied: absorption and emission spectra of dye-DNA complexes and susceptibility to DN-ase. The results permit quantitative estimation of the structure of the nucleohistone complexes.

Introduction

DNA presents a particular structural and functional complexity in eukaryotic cells, being protein bound and forming the nucleoprotein systems of chromatin. A primordial role among these proteins is played by the basic histone proteins, hence the importance of studies concerning nucleohistone complexes.

The binding of acridine dyes, with affinity for DNA, to nucleohistone complexes is influenced by the presence of histones. This effect has been appraised differently by various authors (1, 2). The action of deoxyribonuclease on chromatin and nucleohistone was studied by determining the size of the resulting fragments (3, 4).

The present paper is an attempt to determine the magnitude of zones of free DNA in nucleohistone, comparing the absorption and emission spectra of the dye in the presence of DNA and nucleohistone complexes. The action of DNA-se on nucleohistone complexes was studied by determining the activity of the enzyme.

---

* *National Center of Physics,* P. O. Box 5211, Măgurele, Bucharest.

Materials and Methods

DNA was extracted from B. subtilis WT according to the method described by Marmur (5) and histone was obtained from the rat liver by the method of Subirana (6). The purity of the DNA extract was verified by analysis of the absorbance values in the 230—280 nm range and by specific colorimetric reactions for DNA, RNA and proteins. The purity of histone was determined by analysis of the absoption and emission spectra, colorimetric reactions and electrophoresis in polyacrylamide gels. ForNA, $E_{260nm}^{0.1\,mg/ml} = 1.8$ and for histone, $E_{210nm}^{0.1\,mg/ml} = 1.7$ in water.

The dyes used were acridine orange (Merck), ($\varepsilon = 54000\ M^{-1}\ cm^{-1}$ at 492 nm) and proflavine (Serva), ($\varepsilon = 42000\ M^{-1}\ cm^{-1}$ at 444 nm). For assessing variations in the absorbance of these dyes on binding to DNA, a DNA/dye ratio of 0.330—10 ($C_{dye} = 10\ \mu g/ml$) in a 0.1 M NaCl solution was used.

For acridine orange the excitation wavelength was $\lambda_{ex} = 490$ nm and the emission wavelength $\lambda_{em} = 530$ nm, and for proflavine $\lambda_{ex} = 440$ nm and $\lambda_{em} = 510$ nm. For assessing the fluorescence intensity of these dyes on binding to DNA a dye/phosphate DNA ratio of 0.04—0.8 ($C_{DNA} = 100\ \mu g/ml - 5\ \mu g/ml$, $C_{dye} = 10^{-5}M$) in a 0.1 M NaCl solution was used.

The nucleohistone complexes were reconstituted at a DNA/histone ratio of 0.5—8, according to the method decribed in (7). The absorption and emission spectra of the complexes were analyzed, as well as their behaviour on thermal transition.

DN-ase (Mann Resarch Lab.) activity was determined according to the method described in (8), following up absorbance variations at 260 nm.

Spectrophotometric measurements were carried out with a Pye Unicam spectrophotometer and the emission spectra recorded on an Aminco Bowman spectrophotofluorometer.

Results and Discussions

The DNA and histone extracts were pure and well complexed in the reconstituted nucleohistones; the absoption spectrum of the nucleohistones presented $\lambda_{max_1} = 210$ nm and $\lambda_{max_2} = 260$ nm, fluorescence spectrum $\lambda_{em} = 305$ nm at $\lambda_{ex} = 280$ nm and the thermal transition showed a biphasic aspect, parameters characteristic of nucleohistones.

In the acridine orange — DNA complexes, maximum absorbance at 492 nm, characteristic of the dye, decreased with increase in theDNA/dye ratio (Fig. 1A *a*). The $(E_0 - E)/E_0$ (the ratio of the difference between absorbance of the dye and of the DNA-dye complexes to dye absorbance at 492 nm) are represented as a function of the DNA/dye ratio (Fig. 1 A*b*).

Similarly, for the proflavine-DNA complexes, maximum absorbance at 444 nm, characteristic of the dye, decreased with increase of the DNA/

/dye ratio (Fig. 1 B*a*). The same relative absorbances as a function of the DNA/dye ratio are represented in Fig. 1 B*b*).

The absoption spectra of these dyes bound to the nucleohistone complexes were registered ; the DNA/dye ratio was 10 (Figs. 2 A *a* and 2 B *a*). The DNA/dye ratio, upon binding of the dye to DNA, corresponding to the same relative absorbances was determined for various DNA/histone ratios in nucleohistone complexes (Figs. 2 A *b* and 2 B *b*).

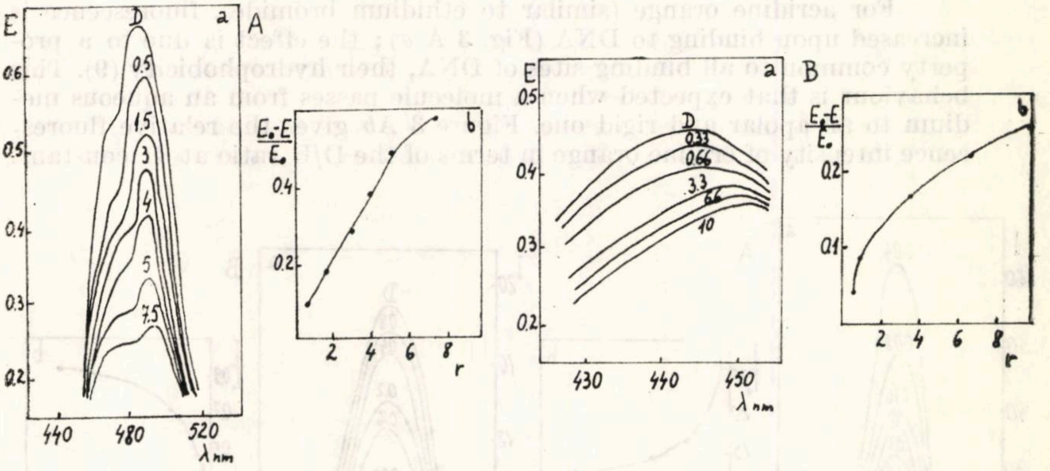

Fig. 1. — *a*. Absorption spectra of dye-DNA complexes, at different DNA/dye ratios (D : dye spectrum) ; *b*. Difference between dye absorbance and absorbance of the dye-DNA complexes refered to absorbance of the dye as a function of DNA/dye ratio ; A — acridine orange ; B — proflavine.

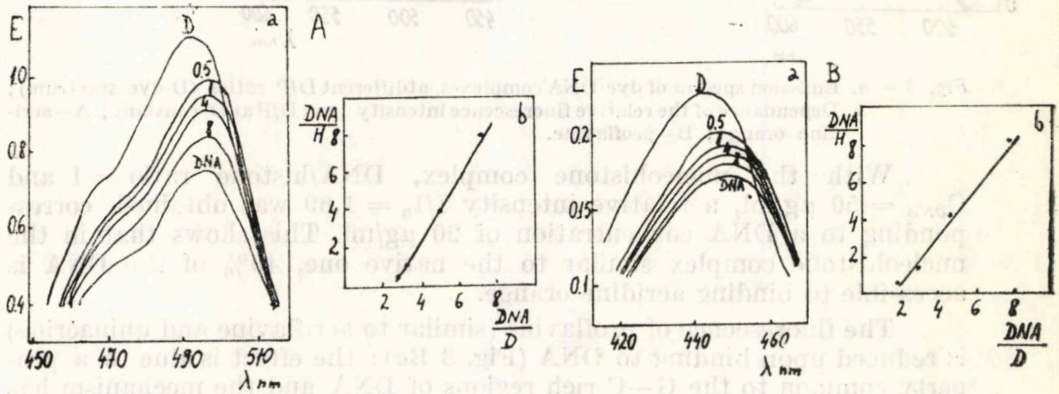

Fig. 2. a. Absorption spectra of dye — nucleohistone complexes at different DNA/histone ratios (D : dye spectrunm and DNA : dye-DNA complex spectrum) ; *b*. Correlation of DNA/histone with DNA/dye in dye-DNA complexes, corresponding to the same relative absorbance. A—acridine orange ; B—proflavine.

For different DNA/histone ratios corresponding DNA/dye ratios were obtained smaller than the actual one, DNA/dye = 10, explicable by the fewer effective binding sites of the dye in the nucleohistone complexes. In the nucleohistone complexes with different DNA/histone ratios, the DNA amounts available for binding the dye were in inverse proportion to the histone amounts in the complexes. From Figures 2 A *b* and 2 B *b* it may be seen that in the nucleohistone complex, similar to the native nucleohistone with DNA/histone = 1, 38 % of the DNA is available for binding one of the two dyes.

For acridine orange (similar to ethidium bromide), fluorescence is increased upon binding to DNA (Fig. 3 A *a*) ; the effect is due to a property common to all binding sites of DNA, their hydrophobicity (9). This behaviour is that expected when a molecule passes from an aqueous medium to an apolar and rigid one. Figure 3 A*b* gives the relative fluorescence intensity of cridine orange in terms of the D/P ratio at D constant.

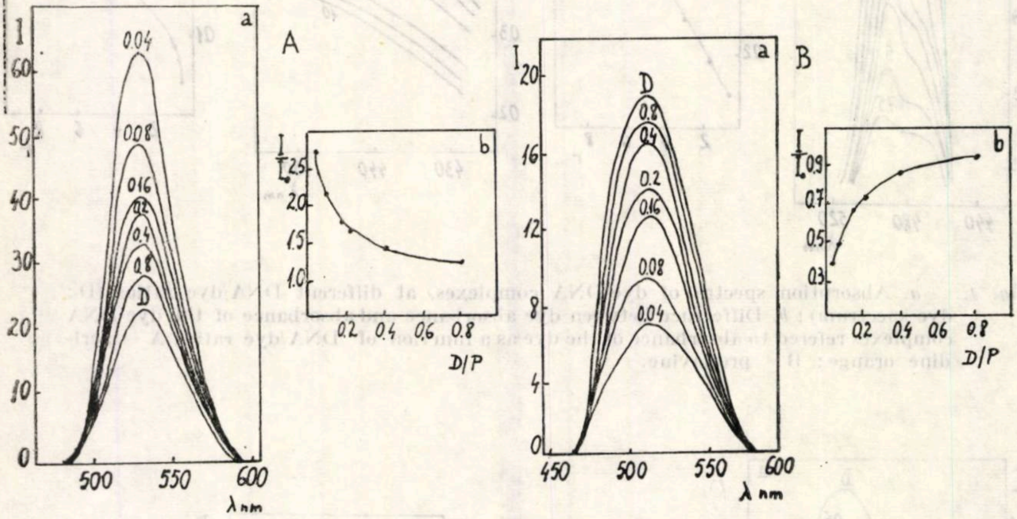

Fig. 3 — *a*. Emission spectra of dye-DNA complexes, at different D/P ratios (D-dye spectrum) ; *b*. Dependance of the relative fluorescence intensity upon D/P at D constant ; A—acridine orange ; B—proflavine.

With the nucleohistone complex, DNA/histone ratio = 1 and $C_{DNA} = 50$ μg/ml, a relative intensity $I/I_0 = 1.69$ was obtained, corresponding to a DNA concentration of 20 μg/ml. This shows that in the nucleohistone complex similar to the native one, 40% of the DNA is accessible to binding acridine orange.

The fluorescence of proflavine (similar to acriflavine and quinacrine) is reduced upon binding to DNA (Fig. 3 B*a*) ; the effect is due to a property common to the G—C rich regions of DNA and the mechanism has been related to the formation of a charge-transfer complex in the excited state (9). Figure 3 B*b* represents proflavine relative fluorecence intensity in terms of the D/P ratio at D constant.

With the nucleohistone complex, DNA/histone ratio = 1, $I/I_0 = 0.73$ was obtained, corresponding to $C_{DNA} = 19$ μg/ml, therefore 38% of DNA was available for binding proflavine.

DN-ase activity, acting upon the nucleohistone complexes was inversely proportional to the histone amounts in the complexes, the histones protecting DNA against the action of the enzyme (Fig. 4*a*). Figure 4*b* gives the correlation of DNA/histone ratio in the nucleohistone complexes with the DNA concentration corresponding to the same enzymatic activity, as when the enzyme acts upon DNA. From figure 4*b* it may be seen that in the nucleohistone complex, similar to the native nucleohistone, 40% of DNA is accessible to the action of DN-ase.

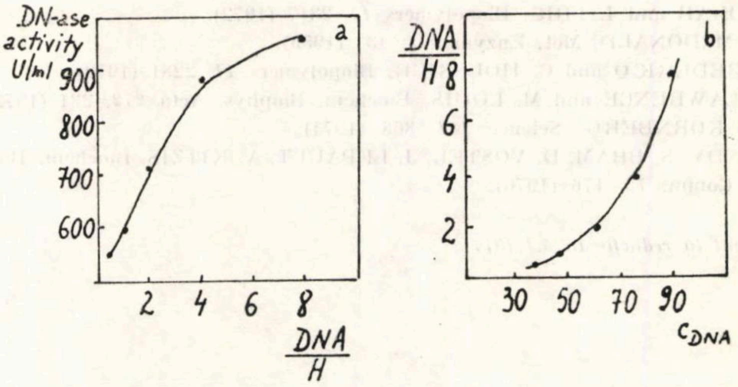

Fig. 4 — *a*. DN-ase activity of the nucleohistone complexes at different DNA/histone ratios. *b*. Correlation of DNA/histone ratios in the nucleohistone complexes with DNA concentration corresponding to the same enzymatic ctivity.

Conclusions

Characterization of the binding of dyes with affinity for DNA and of the susceptibility to DN-ase, are tests that permit estimation of the accessibility of DNA in nucleohistone complexes to be 38–40%. The accessible zones are to be found in DNA between the globular units, according to the model of repetitive subunits proposed by Kornberg (9), or this DNA plus part of the DNA on the surface of the repetitive substructures, the nucleosomes, according to the model of Bandy (10). These tests applied to partial nucleohistone complexes with histone fraction groups might reveal the sites at which accessible DNA exists in nucleohistone complexes.

REFERENCES

1. L. M. ANGERER, S. GHEORGHIU, E. N. MOUNDRIANAKIS, Biochem. *13*, 1075 (1974).
2. J. BONTEMPS and E. FREDERIQ, Biophys, Chem. *2*, 1 (1974).
3. R. CHALKLEY, Bioch. Biophys. Res. Comm., *64*, 587 (1975).
4. H. G. MARTINSON and B. J. MCCARTLY, Biochem. *14*, 1075 (1975).
5. J. MARMUR, J. Molec. Biol., *3*, 208 (1961).
6. J. A. SUBIRANA, J. Molec. Biol., *74*, 363 (1973).
7. J. SPONAR and I. FRIC, Biopolymers *11*, 2317 (1972).
8. M. R. MCDONALD, Met. Enzymol. *2*, 437 (1955).
9. E. FREDERICQ and C. HOUSSIER, Biopolymers *11*, 2281 (1972).
10. J. J. LAWRENCE and M. LOUIS, Biochem. Biophys. Acta *272*, 231 (1972).
11. R. D. KORNBERG, Science *184*, 868 (1974).
12. P. BANDY, S. BRAM, D. VOSTEL, J. LEPAULT, A. KITZIS, Biochem. Biophys. Res. Comm. *72*, 176 (1976).

Primit la redacție în 5.I.1977

ANALELE UNIVERSITĂȚII BUCUREȘTI, FIZICA, XXVIII, 1978, pag. 59—67

ATTENNUATION AND VELOCITY OF RAYLEIGH WAVES ON THE SURFACES OF SOME FERROUS MATERIALS

V. P. MIHU

Faculty of Physics, Bucharest University *

VETURIA RASZILLIER

INCREST—Bucharest

ABSTRACT

The paper presents experimental data on the behaviour of attenuation and velocity of Rayleigh waves propagating on three types of ferrous materials differing in composition, structure and degree of surface roughness.

The behaviour of Rayleigh waves has been investigated intensely, in view of applications in numerous fields, as defectoscopy /1—3/, communications /4/, geology /5/, with respect to their caracteristics of propagation in varous materials and conditions. In the present paper we investigate experimentally the attenuation and velocity of elastic surface waves on three types of materials differing in composition, structure and degree of surface roughness. The samples used for investigation were of dimension 250 × 45 × 45 mm., of unalloyed steel OL_{37} (denoted by O_i/3/), alloyed steel with 1.40% chromium and 0.30% manganese, annealing with pearlite-carbide structure, (denoted by R_{1-i}) and with a three phase structure of martensite-austenite-carbide (denoted by R_{2-i}). The third column of Table 1, indicates the various degrees of surface roughness, and Figs. 1—(O_i), 2—(R_{1-i}), 3—(R_{2-i}) show the structure of the samples, as obtained by X-ray diffraction and optically as well as the echos of Rayleigh waves at the frequencies of 2 and 4 MHz on the Beilby layers /6/ (samples with index zero) for all three types of structures investigated /7/.

The measurements were performed with an apparatus of type USIP 11 with a miniature palpator for emission-reception, equipped with a vibrator of barium titanate having dimensions 10 × 10 × 10 mm /3/. The working frequencies were 2 and 4 MHz.

---

* *National Center of Physics*, Măgurele, Bucharest, P. O. Box 5211.

Table 1

Nr.	Sample	Rmax. (μm)	Variation of velocity (%) 4 MHz	Attenuation (dB)		Observations
				2 MHz	4 MHz	
1	2	3	4	5	6	7
1	O_0^+	1	—	50	49	+ Reference samples – The results of attenuation measurement are mean values of at least eight individual measurements.
2	O_1	4,4	—	40,5	50	
3	O_2	30	−1	46	57	
4	O_3	97	−2	54,66	72	
5	R_{1-0}^+	1	—	39	44	
6	R_{1-1}	8,5	−0,8	35	45	
7	R_{2-0}^+	1	—	42	50	
8	R_{2-1}	10	−0,27	40	44	

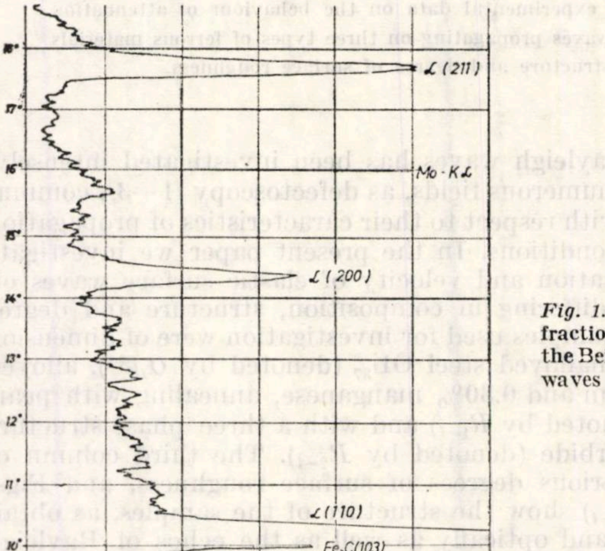

Fig. 1. **Unalloyed steel OL_{37} ; 1a. — Diffraction diagramm ; 1b. — Carbide in the Beilby layer, (x41) ;Echos of Rayleigh waves at the frequences of : 1c. 2 MHz and 1d. — 4MHz.**

In order to measure the attenuation an attenuator calibrated in dB has been used. The measuring procedure consisted in bringing the height of the echo signal to the reference level on the screen of the cathode-ray

1 b

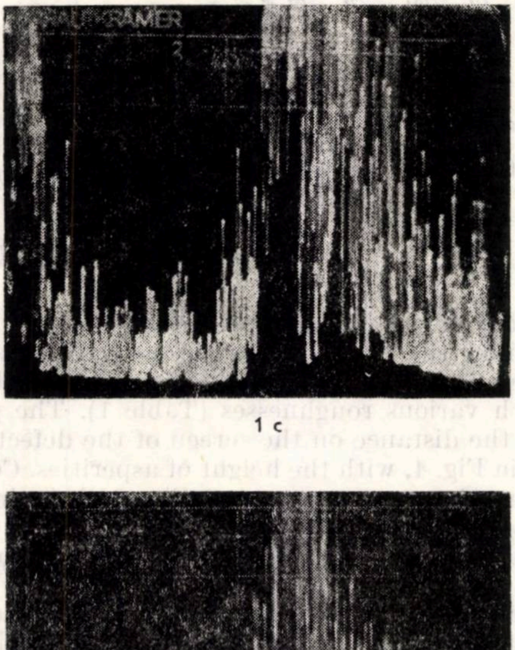

1 c

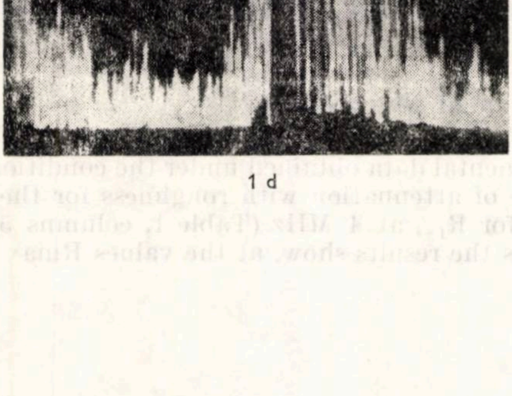

1 d

tube (Fig. 4a), for each sample separately, and in reading of the attenuation which has to be introduced with the calibrated attenuator.

The experimental results of the measurements of attenuation are shown in Table 1, columns 5 and 6, and their graphic representation as a function of Rmax. is given in Fig. 5.

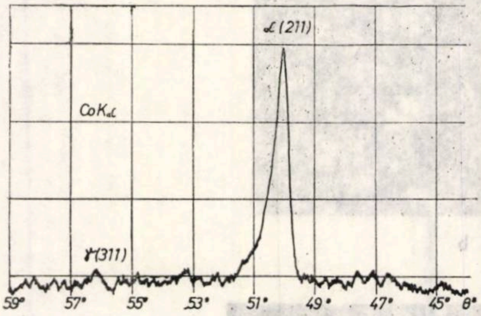

2 a

Fig. 2. Alloyed and annealing steel, R_{1-i}; 2a. — Diffraction diagramm; 2b. — Carbide in the Beilby layer, (x 41); Echos of Rayelgh waves at the frequences of: 2c. — 2 MHz and 2d. — 4 MHz.

Fig. 3. Alloyed and hardening steel, R_{2-i}; 3a. — Diffraction diagramm; 3b. — Carbide in the Beilby layer, (x41); Echos of Rayleigh waves at the frequences of: 3c. — 2 MHz and 3d. — 4 MHz.

3 a

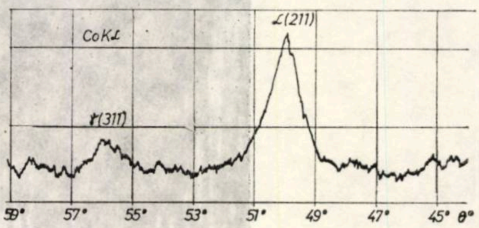

The behaviour of the velocity of Rayleigh waves has been investigated by determining the ratio of velocities as the inverse ratio of propagion time (at fixed distance and in arbitrary units) for the surfaces under investigation, with various roughnesses (Table 1). The propagation time as given through the distance on the screen of the defectoscope increases, as is exemplified in Fig. 4, with the height of asperities. Column 4 of Table 1 gives the values of measurements and Fig. 6 their dependence on the maximal height of the roughness.

Fig. 7.displays the dependence between ratio of velocities and attenuation.

Accidental errors of measurement, due to the position of the palpator, conditions of coupling and the pressing force of the palpator were eliminated by seeking the conditions to give the maximal echo, which was then taken into account. Sistematic errors from the determination of distances on the screen of the cathode-ray tube were of the order of 0.5% /3/.

Interpretation of the results

The experimental data obtained under the condition $2\pi \ R_{\max}/\lambda_R \ll 1$, show an increase of attenuation with roughness for the samples O_i at 2 and 4 MHz and for R_{1-i} at 4 MHz (Table 1, columns 5 and 6, and Fig. 6). For the others the results show, at the values Rmax used, a decrease.

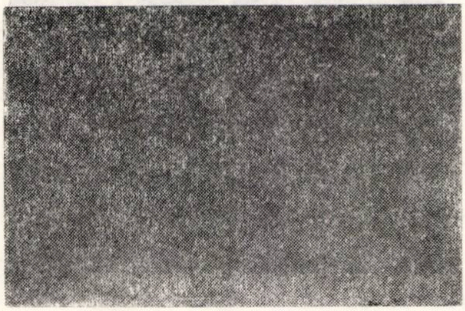

2 b

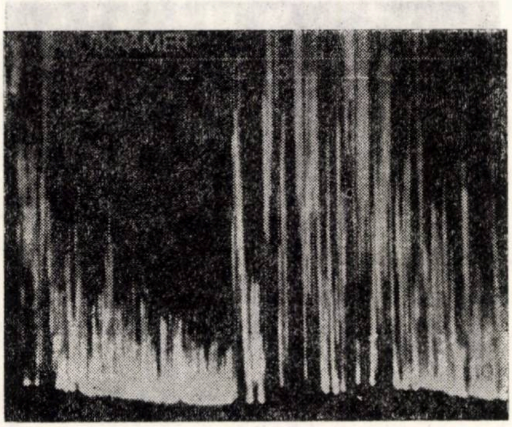

2 c

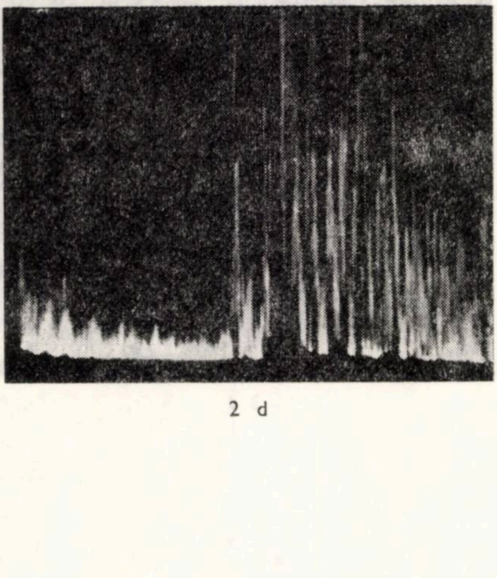

2 d

3 b

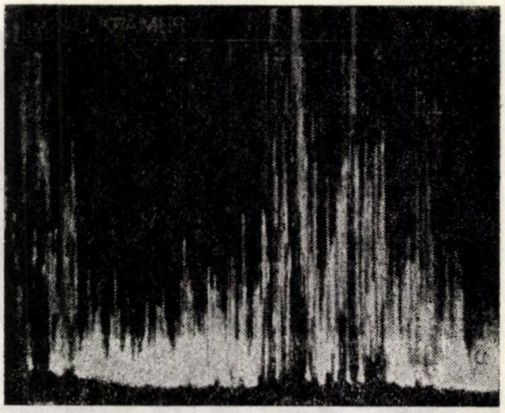

3 c

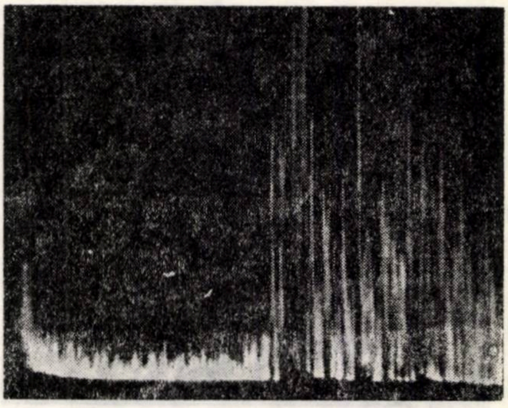

3 d

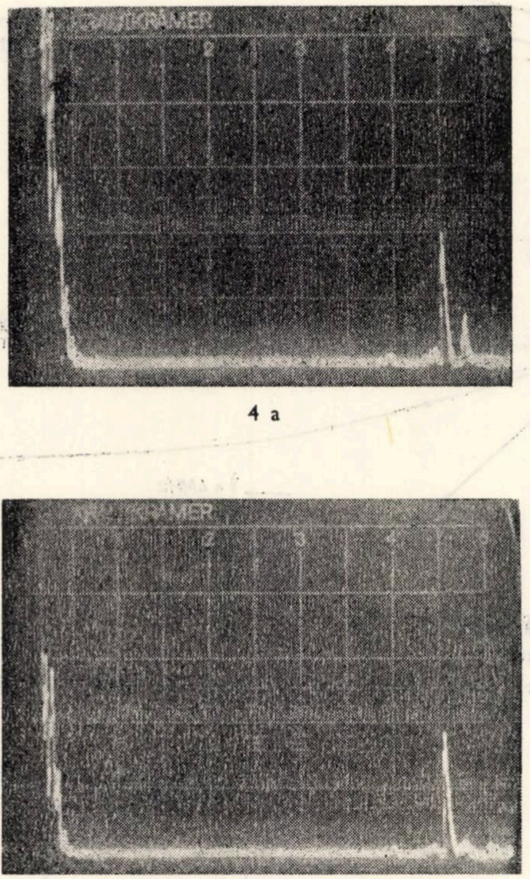

4 a

4 b

Fig. 4. Height of the echo signal on the screen of the cathode-ray tube for the reference line and behaviour of the velocity of Rayleigh waves for various Rmax. (the samples R_{1-i}, 4a—R_{1-0} and 4b—R_{1-1}, are taken as examples).

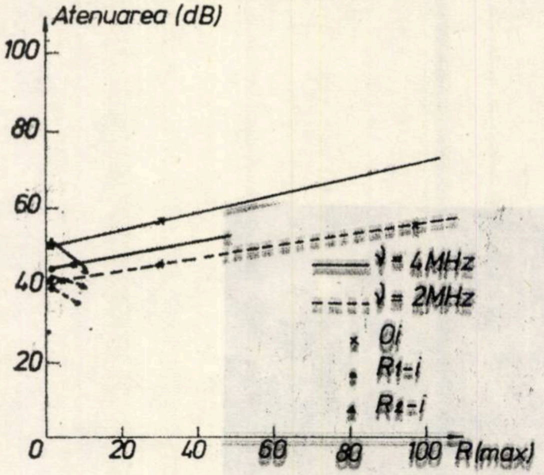

Fig. 5. Dependence of attenuation on the maximal height of the roughness.

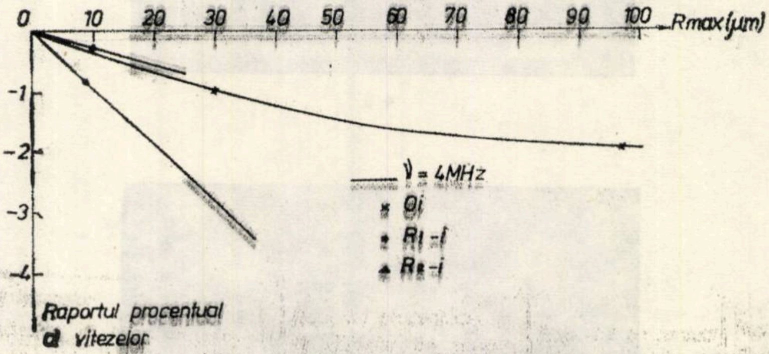

Fig. 6. Dependence of the velocity ratio (%) on the maximal height of the roughness.

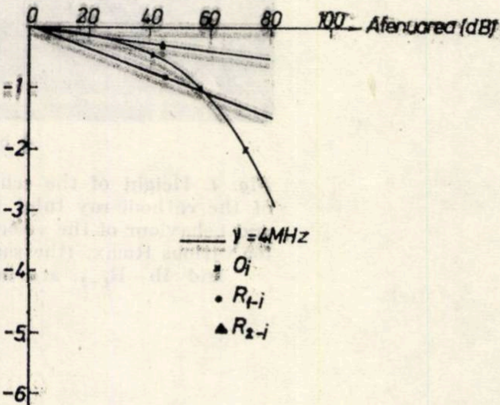

Fig. 7. Dependence between velocity ratio (%) and attenuation.

The increase of attenuation is in agreement with the opinion expressed in the papers /4/ and /5/, that asperities give rise to reflection of surface waves, as well as to their transformation into volume waves, thus increasing their attenuation with the increase of roughness.

The decrease of propagation velocity with the increase of roughness (column 4 of Table 1, and Figs. 4 and 6) may be interpreted as a dispersion phenomenon of Rayleigh waves due to the surface roughness. This dispersion may by attributed to the fact that the rough surface layer behaves as a layer of thickness Rmax and of propagation properties differing from those of the bulk material. Theoretical arguments in this sense have been given in /8/.

From Table 1 and Fig. 7 one observes that dispersion increases with the attenuation of Rayleigh waves for all three structures investigated.

As to the echos of Rayleigh waves, they appear as depending strongly on the composition and structure of samples, as shown in Figs. 1—3 (pictures c and d), for both frequencies, 2 and 4 MHz.

REFERENCES

1. I. A. VIKTOROV, *Physical foundations of the application of Rayleigh and Lamb waves in technology*, Nauka Publishers, Moscow, 1966.
2. D. A. CORDELLOS, *Material Evaluation*, *27*, 85 (1969).
3. VETURIA RASZILLIER, M. VLĂDESCU, St. Cerc. Mec. Apl. *35*, 299 (1976).
4. J. KLERK, *Elastic surface waves*, Physics Today, *11*, 32 (1972).
5. W. M. EWING, W. S. JARDETZKY, F. PRESS, *Elastic waves in layered media*, *McGraw-Hill*, New-York, 1957.
6. F. P. BOWDEN, D. TABOR, *Friction and lubrication of solids*, Oxford, 1964.
7. VETURIA RASZILLIER, *Investigation of the propagation of Rayleigh waves on the rough surface of some antifrictional materials*, Communication at the IV-th Conference on Mechanics, Bucharest, Romania, december 18—20, 1975 (to be published); — *Investigation of some antifrictional materials with elastic and electromagnetic waves*, Communication at the Scientific Session of the Academy of the S. R. R., Bucharest, december 13—14, 1976 (to be published).
8. V.P. MIHU, VETURIA RASZILLIER, Rev. Roum. Phys. *19*, 937 (1974).

Primit la redacţie la 4.V.1977

ANALELE UNIVERSITĂŢII BUCUREŞTI FIZICA, XXVII, 1978, pag. 69—75

EPR STUDY OF Cu^{2+} IONS IN MORDENITE – TYPE ZEOLITES

NICOLETA GRECU*
Institute of Physics and Technology of Materials, Bucharest

V. V. GRECU**
Physics Faculty, University of Bucharest, Bucharest

JANA BLUM***
Institute for Research Technologycal Ingineering and Design for Refineries — Ploieşti

ABSTRACT

The EPR spectrum of Cu^{2} ions in mordenite type zeolites is discussed. Comparison with X, Y and A zeolites is made showing that the Cu^{2+} sites in mordenite have a symmetry and crystal field intensity very similar to the other zeolites.

1. Introduction

Due to their catalytic properties there is a great interest in molecular sieve zeolites. Much attention has been paid to the cation exchanged zeolites with alkaline and alkaline earth ions as well as paramagnetic ions of the first transition period and rare earth ions. For such paramagnetic systems, the EPR technique proved to be a very efficient method to investigate the ion environment in the zeolite lattice, as well as their role in the catalytic process.

The EPR technique was first applied to a detailed study of the paramagnetic ions in an exchanged zeolite by Turkevich and co – workers [1]. Since then, several further investigations have been made mostly on transition metal ions as Cu^{2+}, Mn^{2+}, Co^{2+}, Fe^{3+}, Ni^{+}, Ti^{3+} and V^{4+}. Many of these studies have dealt with the cation site locations and atomic environment in the A—, X-and Y-zeolites. No systematic work has been carried out on the location of cations and molecules in mordenite

---

* *National Center for Physics*, Măgurele, Bucharest, P. O. B. 5207
** *National Center for Physics*, Măgurele, Bucharest, P. O. B. 5211
*** B-dul Republicii 291 A, Ploieşti

— type zeolites and the ammount of experimental data available on exchange cation sites in these zeolites is much less abundant.

As mordenite-type zeolites proved to be useful catalysts under acid conditions we will present the first EPR measurements on Cu^{2+} in synthetic H-mordenites for calcinated, hydrated and dehydrated samples over a wide temperature range.

2. Mordenite structure

The natural and synthetic modernites are zeolites with orthorombic structure and SiO_2/Al_2O_3 ratio more than 5. The approximate unit cell composition of mordenite group zeolites is

$$[Na_2, K_2, (NH_4)_2, Ca] \cdot (Al_8Si_{40}O_{96}) \cdot 28\ H_2O$$

The aluminosilicate framework of mordenite belongs to the Cmcm space group and is composed of a new type of chain, columns of linked 5-rings of tetrahedra [2]. These columns are cross-linked to give cylindrical channels, parallel to [001] (see fig. 1), having a free diameter of 7 Å bounded by near circular 12-rings. The channels are cross-linked by zig-zag interconected passages, parallel to [010] of 2,8 Å free diameter bounded by near circular 8-rings and flattened 10-rings.

The large pore — type mordenites have sorption properties consistent with 12-rings and the small pore-type ones have sorption properties consistent only with 8-rings [3]. The large pore mordenites are resistant to acid conditions and stable to high temperature. Small pore mordenites can be converted to large pore types by chemical treatment.

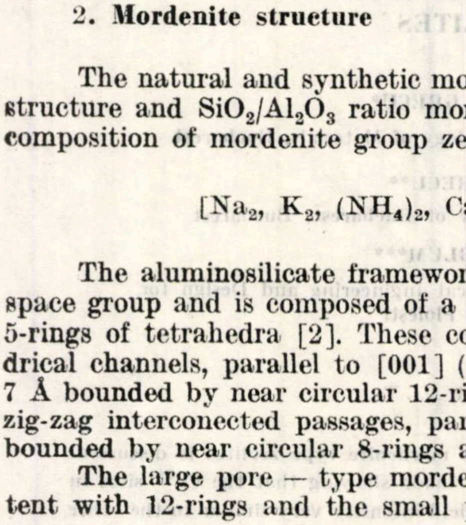

Fig. 1. Sieve structure of mordenite. The small ions (Na, Al, Si) are not shown.

3. Experimental

The H-mordenite was prepared by treating the Na—form at 90°C in aqueous solution of HNO_3 or HCl to obtain the desired Si/Al ratio; 95% exchangeble Na^+ ions were replaced by protons, H. Paramagnetic Cu^{2+} ions were introduced into these H-mordenites by ion exchange from an aqueous solution of copper chloride. Then, the samples are dried in air at 110°C and finally calcinated at 550°C.

Three samples of synthetic H-mordenite exchanged with 0,5% Cu having different Si/Al ratios were studied. These are: sample A with

$SiO_2/Al_2O_3 = 19$, sample B with $SiO_2/Al_2O\gamma_3 = 26$ and respectively sample C with $SiO_2/Al_2O_3 = 30$.

The EPR spectra of Cu^2 ions in mordenites were recorded with an X-band JES–3 X spctrometer with 100 kHz field modulation. Dehydrated samples were sealed in vacuo after calcination at different temperatures for 10 h and were measured over a wide temperature range from –196°C to 300°C.

4. Results

The observed EPR spectra are characteristic to Cu^{2+} ion in a polycrystalline sample. For all three hydrated samples at room temperature a broad asymmetric line with a poorly hfs of four components is observed. In the B and C samples, two spectra with different intensities appear (fig. 2). For the dehydrated samples the ratio of intensities of the two spectra depends on the temperature treatment and the hyperfine structure for both parallel and perpendicular components are resolved (fig. 3). By treating the samples in vacuo at temperatures higher than 450°C the EPR spectrum changes much, the signals becoming very weak (fig. 4).

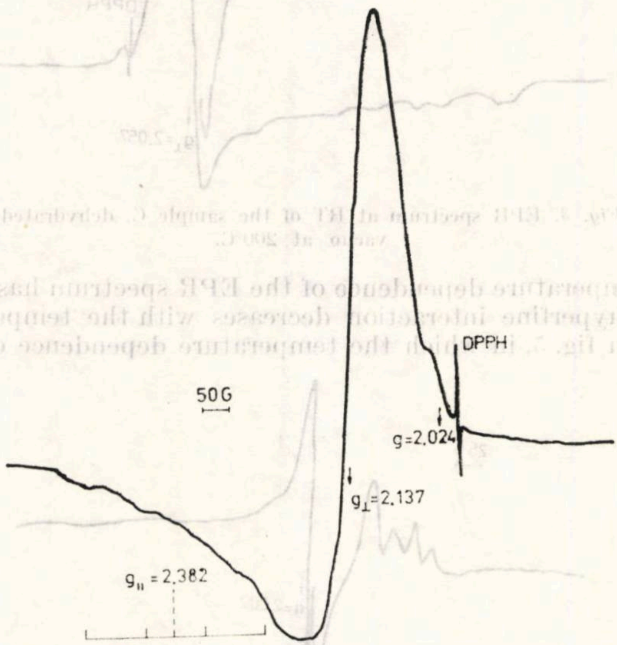

Fig. 2 EPR spectrum at RT of the sample C.

The observed spectra can be fitted to the usual spin-hamiltonian for a complex with axial symmetry,

$$H = \beta[g_\parallel \cdot B_zS_z + g_\perp (B_xS_x + B_yS_y)] + AS_zI_z + B(S_xI_x + S_yI_y)$$

The principal values of g and A tensors are obtained by the well known methods used for polycrystalline samples [4]. The Cu^{2+} spectrum parameters for the hydrated and dehydrated H-mordenite samples are listed in table 1.

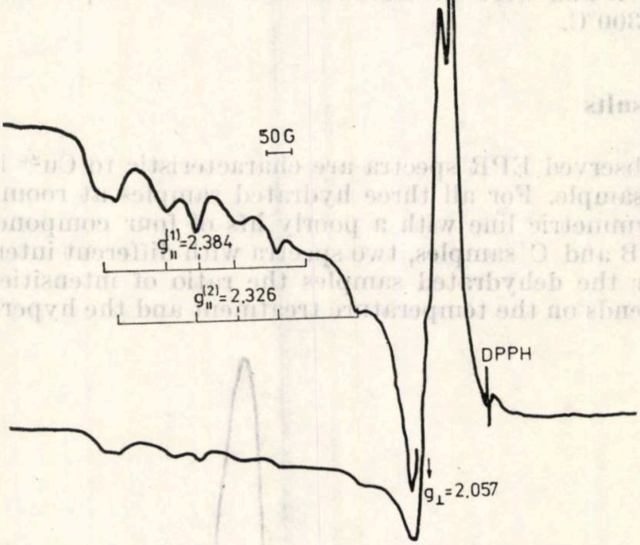

Fig. 3. EPR spectrum at RT of the sample C, dehydrated in vacuo at 200°C.

The temperature dependence of the EPR spectrum has been investigated. The hyperfine interaction decreases with the temperature, it can be seen from fig. 5, in which the temperature dependence of $A_{\parallel}$ is given.

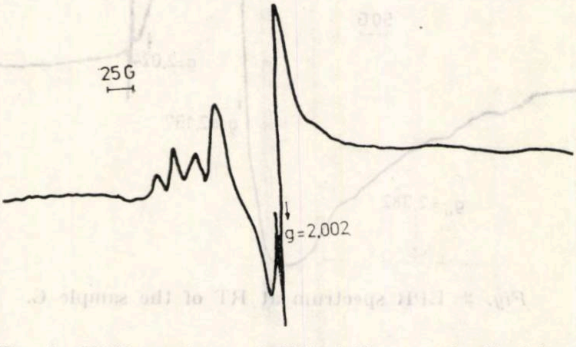

Fig. 4. EPR spectrum at RT of the sample C, dehydrated in vacuo at 500°C.

5. Discussion

These results for Cu^2 ions in synthetic mordenites have to be compared with the data for X-and Y-exchanged zeolites. Turkevich and coworkers [1] observed that the Cu^{2+} spectrum was a function of both the

Table 1

EPR parameters of Cu^2 in synthetic mordenites

Sample	Dehydrat. temperat.	Temp. of measu-rem.	Type	$g_{\parallel}$	$g_{\perp}$	A[G]	B[G]	ΔH]G]
A	—	RT	(1)	2.381	2.152	120	—	160
	200°C	RT	(1)	2.384	2.084	120	—	85
B	—	RT	(1)	2.377	2.09	123	—	75
	200°C	RT	(1) (2)	2.367 2.326	2.055 2.055	130 150	22 22	— —
	200°C	−196°C	(1) (2)	2.365 2.323	2.054 2.054	135 155	18 18	— —
C	—	RT	(1)	2.382	2.137	115	—	115
	200°C	RT	(1) (2)	2.384 2.326	2.057 2.057	125 149	28 20	— —
	200°C	−196°C	(1) (2)	2.376 2.321	2.056 2.057	132 157	18 18	— —
	400°C	RT	(2)	2.312	2.057	155	20	—
	400°C	−110°C	(2)	2.313	2.05	160	20	—
	500°C	RT	(2)	—	2.046	—	20	

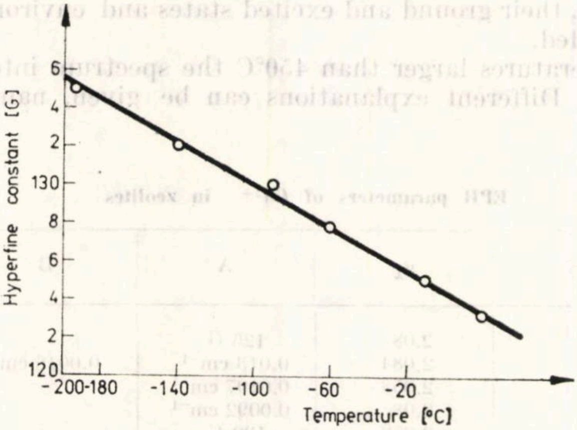

Fig. 5. Temperature dependence of Cu^{2+} parallel hyperfine constant in hydrated sample C.

dehydration conditions and the Cu^2 concentration. One interesting feature of the spectrum which was discussed later by Turkevich et al. [5], is the broad, rather symmetric line which appears in dehydrated zeolites containing sixteen Cu^{2+} ions per unit cell. It is attributed to a spin exchange phenomenon.

Tikhomirova and Nikolaeva [6] as well as Slot and Verbeck [7] have noted that in zeolites two different spectra can be resolved. It appears that this reflects the presence of Cu^{2} ions in two different sites. In addition, the relative intensities of the two sites may be varied by altering the other cation in the zeolite, suggesting that the different cations compete for the same site [8, 9].

A summary of data for zeolites is given in table 2.

By comparing the data from table 1 and table 2 one can see that the Cu^{2+} spin-hamiltonian parameters in X-, Y- and A-zeolites respectively mordenite type zeolites are very close each to other.

These results are quite surprising having in view the differences in structure of the two molecular sieves, in the Si/Al ratio, in the water content, etc. The conclusion which can be drawn is that the Cu^{2} ions are located in mordenites as well as in zeolites in sites which have the same symmetry and very similar local crystal fields.

By dehydration the type 1 center intensity decreases and consequently the intensity of type 2 center becomes larger. That is in accordance with the results obtained for zeolites and shows that at lower water content the Cu^{2+} ions move to the more stable position of the center 2.

Usually in zeolites the copper ions can occupy the position SI′, SII′ or SII sites. In mordenites more favorable positions in hydrated samples are VII and I sites (consistent with Smith's notation [10]) and positions VI and IV in dehydrated probes. Then we suppose that the type 1 spectrum, more intense in hydrated samples, is given by Cu^{2+} ions located in VII sites and the second one, which increases by dehydration, is due to Cu^{2+} ions in VII sites. For more precise conclusions further studies about Cu^{2+} ions, their ground and excited states and environment in mordenites are needed.

For temperatures larger than 450°C the spectrum intensity decreases very much. Different explanations can be given, namely a change

Table 2

EPR parameters of Cu^{2+} in zeolites

Spectra	$g_{\parallel}$	$g_{\perp}$	A	B	Ref.
Type 1	2,38	2.08	126 G	—	[1]
	2.386	2.084	0.013 cm^{-1}	0.0016 cm^{-1}	[5]
	2.350	2.058	0.0107 cm^{-1}	—	[7]
	2.38	2.08	0.0092 cm^{-1}	—	[11]
	2.350	2.058	120 G	—	[12]
Type 2	2.323	2.048	0.0176 cm^{-1}	0.0024 cm^{-1}	[5]
	2.326–2.33	2.056–2.067	0.015 cm^{-1}	0.0018 cm^{-1}	[7]
	2.32	2.05	162 G	22 G	[11]
	2.31	2.058	175 G	—	[12]

in Cu^{2+} valency, or larger fluctuations in the crystal field which determines the line broadening, and consequently a decrease of the signal beyond the limit of observation.

The temperature dependence of the hyperfine constant of the Cu^2 ions observed at lower temperature can be fitted with the expression

$$A = A(0) \cdot (1 - bT),\ b = (5{,}9 \pm 1{,}2)\,10^{-2}\ G/\text{degree}$$

Such a linear expression can be deduced by taking into account the vibronic properties of the hydrated ion [13]. Different mechanisms may be responsible for it. In order to differentiate between them, measurements at lower temperatures are necessary.

6. Conclusion

The Cu^{2+} EPR spectrum was studied for the first time in mordenite — type zeolites and compared with the data for A-, X- and Y-zeolites. In spite of the large differences in structure, the spin-hamiltonian parameters do not differ much, showing that the cation locations are very similar.

The temperature dependence of the hyperfine interaction allows the determination of vibronic properties of the ion complex.

REFERNCES

1. A. NICULA, D. STAMIRES, J. TURKEVICH, J. Chem. Phys. 42, 1965 (3684).
2. W. M. MEIER, Z. Kristallogr. 115, 1961 (439).
3. L. B. SAND, *Molecular Sieves* Soc. Chem. Industry, London p. 71, 1961.
4. CH. POOLE, *Electron Spin Resonance*, Inter. Public. N. Y. 1967.
5. J. TURKEVICH, Y. ONO, J. SORIA, J. Catal. 25, 1972 (44).
6. N. N. TIKHOMIROVA, I. V. NIKOLAEVA, Zh. Strukt. Khim. 10, 1965 (547).
7. H. B. SLOT, J. L. VERBEEC, J. Catai. 12, 1968 (216).
8. N. N. TIKHOMIROVA, I. V. NICOLAEVA, V. V. DEMKIN, E. N. ROSOLOVSKAYA, K. V. TOPCHIEVA, J. Catal. 29, 1973 (205).
9. L. E. ITON, J. TURKEVICH, J. Phys. Chem. 81, 1977 (435).
10. W. J. MORTIER, J. J. PLUTH, J. W. SMITH, Mat. Res. Bul. 10, 1975 (1037); 10, 1975 (1319); 11, 1976 (15).
11. I. D. MIKHEIKIN, V. A. SHVETZ, V. B. KAZANSKII, Kinet. Katal. 1970 (747)
12. V. KRUERKE, P. YUNG, Z. Phys. Chem. 58, 1968 (53).
13. J. C. VEDRINE, E. G. DEROUANE, Y. BEN TAARIT, J. Phys. Chem. 78, 1974 (53)

Primit la redacție la 28.XII.1977

ANALELE UNIVERSITĂŢII BUCUREŞTI FIZICĂ, XXVII, 1978, pag. 77—82

NON-OHMIC ELECTRICAL CONDUCTION IN POLYCRYSTALLINE SEMICONDUCTING CdS THIN FILMS

I. LICEA, V. RUXANDRA
Faculty of Physics, University of Bucharest*

ABSTRACT

The experimental non-ohmic current-field characteristics of polycrystalline semiconducting CdS thin films are obtained at various temperature. An interpretation of the results in the framework of a model considering the contribution of both intercrystalline barriers and hot electrons to the non-ohmic electrical conduction is made.

The studies on the electrical properties of semiconducting polycrystalline CdS thin films in strong electric field point out a non-ohmic behaviour of the current-field characteristics [1—9]. These studies haverevealed the close relationship between the electrical conductivity and the structure of the polycrystalline thin films consisting of a system of crystallites and intercrystalline barriers.

In this work we present some experimental results on the current-field characteristics of semiconducting polycrystalline CdS thin films at varions temperatures and we give an interpretation of the non-ohmic electrical condcution in these layers.

The j-E characteristics at dark have been obtained in a semi-automatic installation at various temperature using a pulse method to avoid the Joule heating of the samples [10]. The thin films have been obtained by thermal evaporation in vacuum with the deposition rate $V_d = 26 \frac{\text{Å}}{\text{s}}$ for a substrate temperature of 260°C. In Fig. 1 we present in a double-logarithmic scale a family of the j-E characteristics obtained between $-109°$C and 215°C. One may observe that the diagram for high temperature differs from those of low temperatures. In both cases the j-E curves present a non-ohmic behaviour. The curves 1—4 obtained for low temperatures express an exponential dependence of the electric current on the applied field. This fact can be easily seen in a semilogarithmic scale (Fig. 2).

---

* *National Center of Physics*, P. O. BOX 5211, Măgurele, Bucharest.

For strong electric field in this scale the curves are straigtht lines, according to an exponential dependence.

The behaviour of these j-E characteristics can be interpreted using a simple model of thin polycrystalline film consisting of a system of crystallites and intercrystalline barriers of the same type randomly oriented.

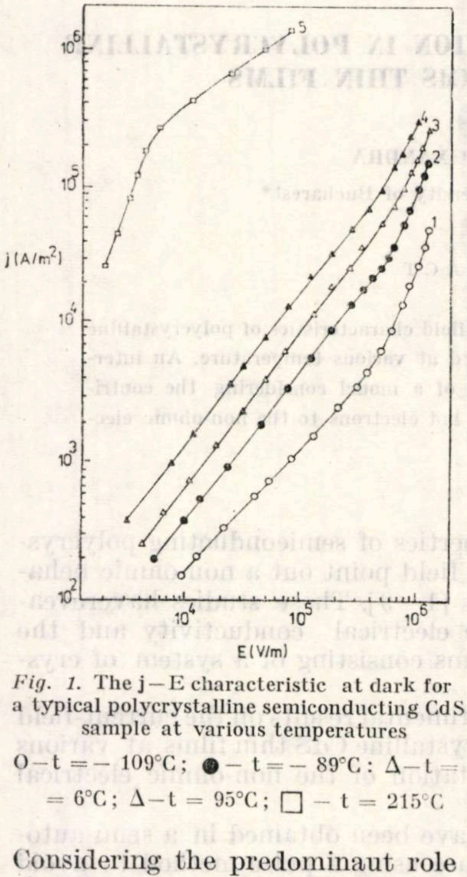

Fig. 1. The j – E characteristic at dark for a typical polycrystalline semiconducting CdS sample at various temperatures

O – t = – 109°C; ● – t = – 89°C: Δ – t = = 6°C; Δ – t = 95°C; □ – t = 215°C

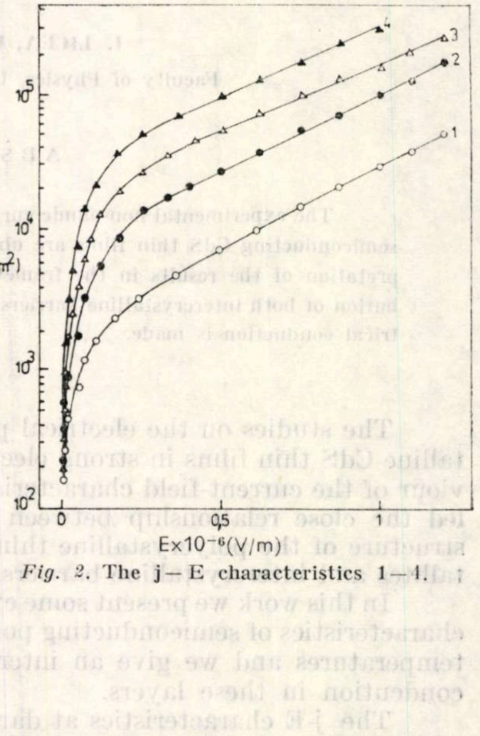

Fig. 2. The j – E characteristics 1 – 4.

Considering the predominaut role of the intercrystalline barriers on the electrical conductivity [8, 9] we can write the dependence between the current density and the field in the form

$$j = \frac{a e^{-Cx} \left(e^{bEx} - 1 \right)}{x^2} \tag{1}$$

where

$$a = \frac{qkm^*}{2\pi^2 h^3}, \quad b = \frac{qL}{kN}, \quad c = \frac{q\Phi + \varepsilon_c - \varepsilon_{Fn}}{k}. \tag{2}$$

j is current density, E is the macroscopic applied electric field and we denoted $x = \frac{1}{T}$. Here q and m^* are the charge and the effective mass of the electron, $2\pi\hbar$ is Planck's constant, $q\Phi$ the potential height of the barrier referred to the conduction band edge ε_c, ε_{Fn} is the electron Fermi level.

For high electric field and a given temperature the relation (1) in a semilogarithmic scale expresses a straight line given by

$$\ln j = \ln \alpha + \beta E \tag{3}$$

where

$$\alpha = \frac{a e^{-Cx}}{x^2}, \quad \beta = bx. \tag{4}$$

Therefore, the non-ohmic behaviour of the mentioned $j - E$ characteristics can be explained in the framework of the predominant role of the intercrystalline barriers. The slope of the straight lines gives the possibility to obtain the microscopic parameter b. We have $b = 6{,}2 \times \times 10^{-4} \frac{mK}{V}$ so that, defining the mean size of the crystallite by

$$D = \frac{L}{N} = \frac{kb}{q} \tag{5}$$

we obtain $D = (500-550)$ Å. This value agrees to that obtained experimentally by electronography and X-ray diffraction. The crossing point between the extension of the straight line and the ordinate gives the values of α. If we plot in a semilogarithmic scale the values of αx^2 for various given temperatures we obtain again a straigth line (Fig. 3), accordingly to the relation

$$\ln(\alpha x^2) = \ln a - Cx. \tag{6}$$

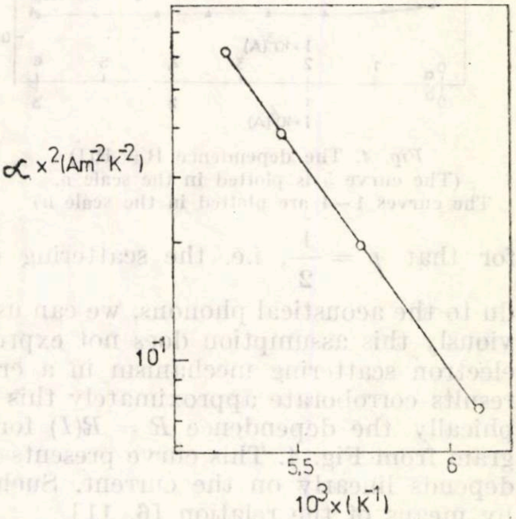

Fig. 3. The dependence $\ln(\alpha x^2) = f(10^3 x)$

The slope gives the constant C, i.e., the activation energy $\Delta\varepsilon$ [4, 6, 7]. We obtain $C = 2.36 \times \times 10^3 K$ and $\Delta\varepsilon = 0.22\ eV$. The value of the constant a can be obtained also as the crossing point between the extension of the straight line and the ordonate $\ln(\alpha x^2)$.

Obviously, the knowledge of the constants a, b and C gives the possibility to plot theoretically the $j - E$ characteristics using the relation (1). The agreement with the experimental data is suitable for the whole family of curves of the investigated samples.

In order to explain the behaviour of the $j-E$ characteristics at high temperature (the curve 5), the consideration of the intercrystalline barrier contribution only to the electrical conduction becomes unsatisfactory. Indeed, this curve do not maintains the shape of a straight line in a semilogarithmic scale, $\ln j = f(E)$, and the departure is for strong electric field. In this case the contribution of the crystallites at the electrical conduction must be considered [6, 11]. Such an assumption is reasonable also since at high temperature the influence of the barrier to the electrical conduction reduces [7].

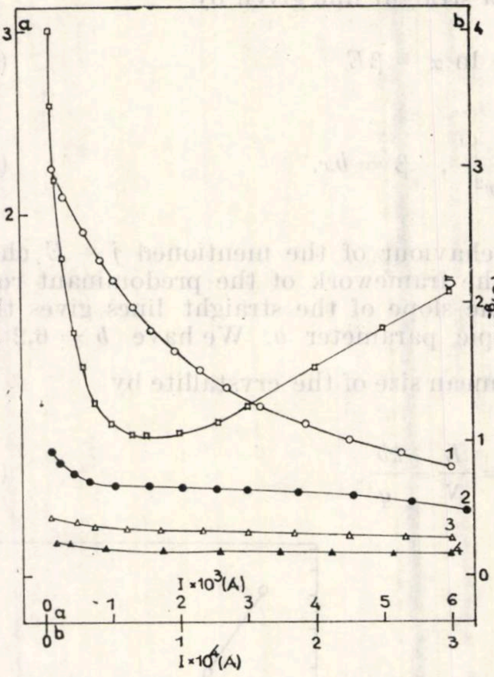

Fig. 4. The dependence R = R(I)
(The curve 5 is plotted in the scale a.
The curves 1–4 are plotted in the scale b)

In strong electric field we must consider also the electric heating in any crystallites. We assume the current-field relation in a crystallite in a strong electric field (for a range of values in which only the mobility depends on the field) given by $j = C'(x)\mathscr{E}_c^p$. Here $C'(x)$is a constant depending on the absolute temperature and on the scattering mechanismof hot electrons and $\mathscr{E}_c^p$ is the field in a crystallite. If we consider a field range for that $p = \frac{1}{2}$, i.e. the scattering of hot electrons is predominant du to the acoustical phonons, we can use the result of the work [11]. Obviously this assumption does not expresses entirely the complicated hot electron scattering mechanism in a crystal. However the experimental results corroborate approximately this dependence. Indeed plotting graphically the dependence $R = R(I)$ for the curve 5 we obtain the diagram from Fig. 4. This curve presents a minimum and for great current depends linearly on the current. Such an behaviour can be explained by means of the relation [6, 11]

$$R = \frac{K_1}{I}\ln\left(1 + \frac{I}{A'}\right) + K_2 I \qquad (7)$$

where

$$K_1 = \frac{L}{bx}, \quad K_2 = \frac{L}{g^2 d^2 C'^2_{(x)}}, \quad A' = gd\, ae^{-Cx} \qquad (8)$$

are some constant parameters for a given temperature, d is the width and g is the thickness of the sample. The parameters K_1, K_2 and A' can be obtained from the experimental curve and its knowledge allows to plot the theoretical curve $R = R(I)$.

In order to determine the parameters K_1, K_2 and A' we make use of the fact that the $R-I$ characteristic has a minimum corresponding to the value I_m of the electric current given by

$$\ln\left(1 + \frac{I_m}{A'}\right) = \frac{I_m}{I_m + A'} + \frac{K_2}{K_1} I_m^2 . \tag{9}$$

For large values $I > I_m$ the R$-$I characteristic may be approximated by a straight line with the slope K_2 corresponding to the predominant conduction mechanism through crystallites. For $I < I_m$ the shape of the $R-I$ characteristics corresponds to the predominant conduction mechanism through intercrystalline barriers. The following relation for the electrical resistance R_m

$$R_m = \frac{K_1}{I_m + A'} + 2K_2 I_m \tag{10}$$

at the minimum point is valid. If we know K_2 (approximated by the slope of the straight line), I_m and R_m from the experimental curve, the relations (9) and (10) represents a system of equations from which we obtain

$$\frac{I_m + A'}{I_m} \ln \frac{I_m + A'}{A'} = \frac{R_m - K_2 I_m}{R_m - 2K_2 I_m} \tag{11}$$

and

$$K_1 = (R_m - 2K_2 I_m)(I_m + A') \tag{12}$$

Relation (11) is a transcedental equation in A' which may be solved graphically or numerically. The knowledge of A' allows one to obtain K_1 from relation (12). The obtained values are $K_1 = 4.34 \times 10^{2}$ (Ω.A), $K_2 = 2.47 \times 10^5$ (Ω.A^{-1}) and $A' = 1.08 \times 10^{-9}$ (A).

We observe a satisfactory agreament between the theoretical curve and the experimental data especially for the minimum of the resistance. This fact indicates that the two types of conduction considered, through intercrystalline barriers and crystallites, act simultaneously and competitively. For small currents (small fields) there is an ohmic dependence and very good agreement between the theoretical curve and the experimental data.

In the same Figure 4 are plotted (in other scale) the curves $R = R(I)$ at the low temperature corresponding to the curves $1 - 4$ of $j - E$ characteristics. One may see that in this case the dependence $R = R(I)$ can be explained in the framework of the barrier mechanism, i.e. considering only the first term of the relation (7).

The above interpretation about the $j - E$ characteristics and the satisfactory agreement with the experimental data points out the close correlation between the structure of polycrystalline thin films and the non-ohmic electrical conduction.

REFERENCES

1. B. L. LUTZKI, YU. F. OGRIN, S. P. CHELNIKOV, in The Problems of Film Electronics, Moscou, 1966, p. 424 (in Russian)
2. A. NICOLAU, I. LICEA, I. SECAREANU, Rev. Roum. Phys., *13*, 471 (1968)
3. H. BERGER, G. JANICHE. N. GRACHOVSKAYA, Phys. Stat. Sol., *33*, 417 (1969)
4. N. PAVASKAR, C. MENEZES, Jap. J. Appl. Phys., *9*, 212 (1970)
5. J. I. B. WILSON, J. WOODS. J. Phys. Chem. Solids, *34*, 171 (1973)
6. I. LICEA, V. RUXANDRA, I. SECĂREANU, Acta Phys. Polon., *A 46*, 511 (1974)
7. A. M. PAVELET, S. YU. PAVELET, F. A. FEDORUS, Poluprovod. Teh. i Mikroelektr., *21*, 44 (1975)
8. I. LICEA, V. RUXANDRA, Analele Univ. Buc., ser. St. naturii, *25*, 39 (1976)
9. V. RUXANDRA, I. LICEA, N. BĂLTĂȚEANU, Analele Univ. Buc., Fiz., *26*, 97 (1977)
10. V. RUXANDRA, I. LICEA, B. POPESCU, Analele Univ. Buc., Fiz., *28*, 83 (1978)
11. I. LICEA, V. RUXANDRA, I. SECĂREANU, Acta Phys. Polon., *A45*, 511 (1974)

Primit la redacție la 20.XII.1977

ANALELE UNIVERSITĂȚII BUCUREȘTI FIZICĂ, XXVII, 1978, pag. 83—90

CURRENT-FIELD CHARACTERISTICS OF SMALL CONDUCTING THIN FILMS IN STRONG ELECTRIC FIELD

V. RUXANDRA, I. LICEA
Faculty of Physics, University of Bucharest*

B. POPESCU
Geological and Geophysical Prospection Center for Hidrocarbons, Bucharest

ABSTRACT

The current-field characteristics of semiconducting polycrystalline CdS thin films in strong electric field obtained in d. c. current and in pulse-regime are analyzed. An interpretation taking into account the Joule-heating in the framework of the barrier conduction mechanism is given.

1. Introduction

Electrical conduction in polycrystalline small conducting thin films in strong electric fields can be studied both in d.c. current and in pulse-regime. However, in sufficient strong fields, in these samples too, becomes necessary to use the pulse-method in order to avoid the Joule-heating. Indeed, this effect makes difficult the study of the non-ohmic behaviour of electrical conductivity in strong electric field.

In this work the current-field characteristics of semiconducting polycrystalline CdS thin films in strong electric fields are analyzed and an interpretation of the Joule-heating in the framework of the barrier conduction mechanism is made.

2. Experimental

Block-scheme of the Experimental Equipment

The block-scheme of the experimental measuring equipment is plotted in Fig. 1. The samples has been placed in the cryostat 1 connected to a vacuum assembly 3 and 4 allowing to obtain $10^{-5} \div 10^{-6}$ torr. (For some measurements in magnetic fields the cryostat can be placed between the poles of an electromagnet 2).

---

* *National Center of Physics*, P. O. BOX 5211, Măgurele, Bucharest.

For d.c. current measurements has been used an electromechanic generator as linear growing voltage source or time-base of an oscilloscope 6.

The sample temperature has been measured using a cooper-constantan thermocuple connected to a recording milivoltmeter 12 and 13.

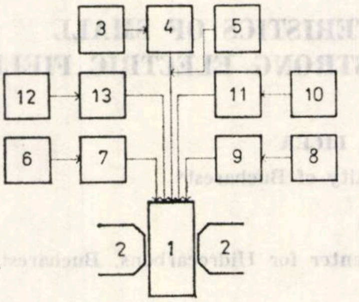

Fig. 1. The block-scheme of the experimental measuring equipment.
1 — Cryostat; 2 — Poles of the electromagnet; 3,4 — Vacuum assembly; 5 — Electronic vacuumetre; 6 — Oscilloscope; 7 — Measuring scheme in d. c. current; 8 — Pulse generator; 9 — Measuring scheme in pulse-regime; 10 — Sinusoidal voltage generator; 11 — Measuring scheme in sinusodal-regime; 12, 13 — Recording milivoltmeter.

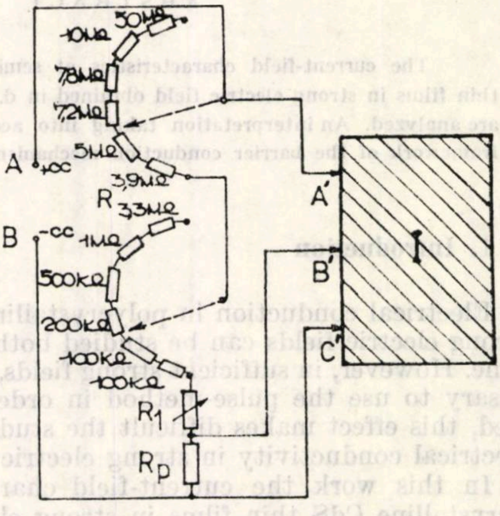

Fig. 2, *a*. The measuring scheme in d. c. current.

Measuring Scheme in D.C. Current. In the measuring scheme in d.c. current a standard resistence group (0—90 MΩ) has been placed in series with the sample (Fig. 2, a). The points *A* and *B* are the input bornes for linear growing d.c. voltage. The input X of the recorder X — *Y* is applied voltage *U* which comes from sample resistance and the input Y is applied voltage U_0, which comes from standard resistance.

Measuring Scheme in Pulse-regime. The pulse measure diagram is given in Fig. 2, b. It was necessary to introduce a switching system composed of switches $K_1 \div K_4$, because resistance, which gives measured voltage, must be placed to the generator and the oscilloscope table.

Input terminals of the oscilloscope have been connected just $\frac{1}{6}$ from measured voltage, using two voltage, dividers composed of resistances R_2 and R_3, respectively R_4 and R_5, because the used oscilloscope has been able to measure maximum voltage 120 V and impulses have had amplitude 500 V.

When switches $K_1 \div K_4$ are in position a it is measured $\frac{1}{6}$ from standard resistance voltage and when they are in position b it is measured $\frac{1}{6}$ from sample resistance voltage. Resistance R_1 adapts output impedance of the pulse generator and load impedance.

Fig. 2, b. The measuring scheme in pulse-regime.

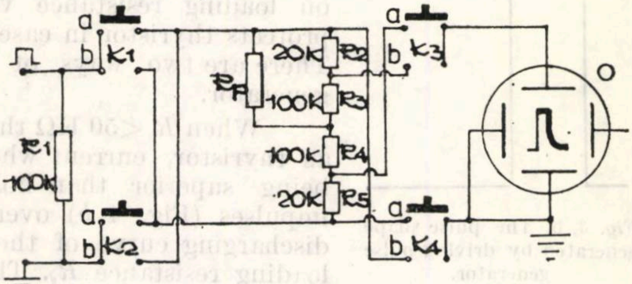
a
b
K1
20K
R2
RP
100K
R3
100K
R4
R1
100K
20K
R5
a
b
K2
a
b
K3
o
a
b
K4

Pulse Generator. The pulse generator is composed of two main parts : driving pulse generator and own pulse generator.

Driving pulse generator (Fig. 3, a) consists of a multivibrator made with transistors T_1 and T_2, a differentiating circuit consists of C_2, R_5, R_6 and EFD 108, a monostable flip-flop (T_3, T_4) which makes impulses, and an emiter repeater (T_5) for adaptation between driving pulse generator and own pulse genertor.

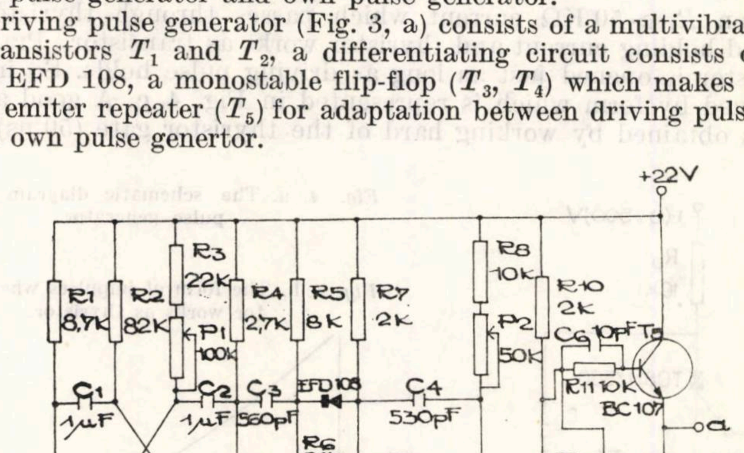
+22V
R3
22K
R1
8,7K
R2
82K
P1
100K
R4
2,7K
R5
8K
R7
2K
R8
10K
R10
2K
P2
50K
C6
10pF
T5
R11 10K
BC107
C1
1µF
C2
1µF
C3
560pF
EFD108
C4
530pF
R6
5,1K
T1
T2
T3
T4
R12
2K
a
BC107
BC107
BC107
BC107
R9 30K
C5 10pF
b

Fig. 3, a. The schematic diagram of the driving pulse generator.

In no-load work driving pulse generator is able to generate impulses with amplitude 22 V and with rectangular form (Fig. 3, b).

The schematic diagram of own pulse generator is given in Fig. 4, a. In the interval of driving pulses thyristor T 0,8 N/500 is turned on and has a very high resistance. At this moment the condenser C_2 is charged through resistance R_p with a voltage practically equal to the power unit voltage. The lory interval of driving pulses is sufficient that power unit charges completely condenser C_2. A given impulse of driving pulse generator open the thyristor, letting condenser C_2 discarge through loading resistance R_s. So impulses are obtained on resistance having amplitude practically equal to power unit voltage. Form and duration of impulses depend on loading resistance value R_s. Resistance R_p protects thyristor in case of output short-circuit. There are two ways of working of own pulse generator.

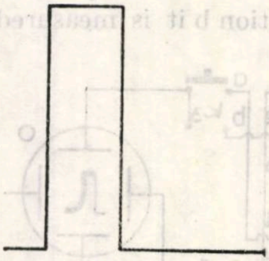

Fig. 3, b. The pulse shape generated by driving pulse generator.

When $R_s < 50$ KΩ thyristor *T* 0,8 N/500 works as thyristor, current which passes through it being superior than holding current. Form of impulses (Fig. 4, *b*) overlaps approximately over discharging curve of the condenser C_2 through loading resistance R_s. The condenser C_2 discharges through loading resistance R_s until current, which passes through thyristor, becomes equal to holding current. At this moment thyristor is turned on crude, producing an impulse with duration about milliseconds, which depends on power unit voltage value and loading resistance value.

When $R_s > 50$ KΩ current which passes through thyristor does not exceed holding current and thyristor works as transistor. Practically the thyristor is opened just as long as driving pulse holds. So impulses are obtained by form which is represented in Fig. 4, c. A good anterior front was obtained by working hard of the thyristor gate (50 ns). Horizontal front is also very good because duration of impulse represents just a fraction (10^{-5}) of duration of complete discharge of the condenser C_2 through loading resistance. Posterior front is not so good, but it is not important. Its form comes from recombination process in thyristor.

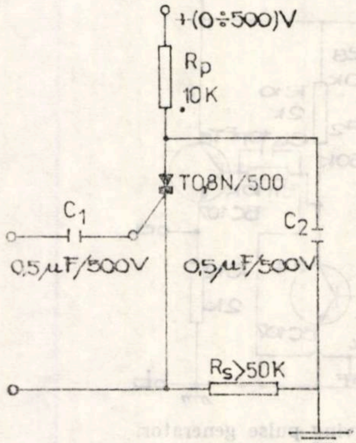

Fig. 4, a. The schematic diagram of own pulse generator.

Fig. 4, b. The form of impulses when thyristor works as thyristor.

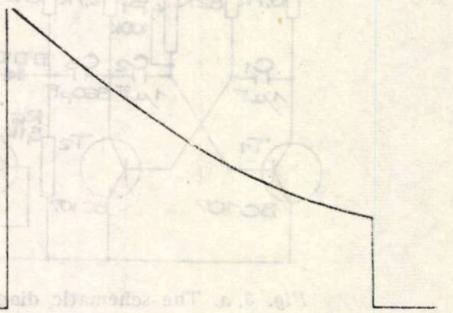

Impulse amplitude can be adjusted between 20 and 500 V through variation of supply voltage. Duration of impuls is also adjusten between 20 and 50 μs. Pulse repetition rate can be adjusted between 8 and 20 Hz.

In experimental dterminations, an oscilloscope well calibrated, with which has been measured accurately pulse amplitude.

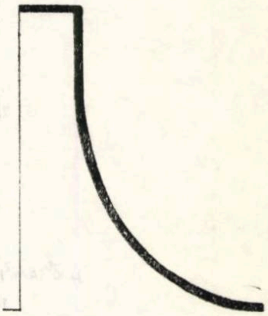

Fig .4, c. The form of impulses when thyristor works as transistor.

3. Results and Interpretation

A family of current-field characteristics obtained in the pulse-regime is plotted in Fig. 5. In Fig. 6 is plotted the family of current-field characteristics obtained in d. c. current measurements at the same temperatures as these corresponding to the characteristics from Fig. 5. The measurements have been made on a semiconducting polycrystalline CdS film obtaind by thermal evaporation in vacuum for a substrate temperature $t_s = 200°\mathrm{C}$ and the deposition rate $V_d = 16 \frac{\text{Å}}{\text{s}}$. The thickness and the width of the sample have been 1.5 μm and 7.5×10^{-9} m², respectively.

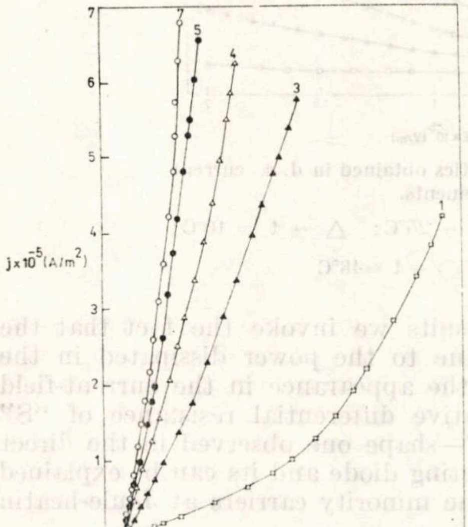

Fig. 5. Current-field characteristics obtained in the pulse-regime.

□ — t = — 135°C; ▲ — t = — 25°C; △ — t= 10°C; ● — t = 33°C; ○ — t = 48°C

By comparing the shape of the $j-E$ characteristics obtained in a pulse-regime and in d. c. current one observe that in the small fields range the behaviour of these curves is the same. On the contrary, in the strong fields range the behaviour of these curves differs. While the $j-E$ characteristics obtained in the pulse-regime present an exponetial dependence [1–5], those obtained in d.c. current have a region in "S" — shape with negative differential resistance. For higher temperatures the "S" — shape appears for smoller electric fields. If the field is further increased, the breakdown becomes.

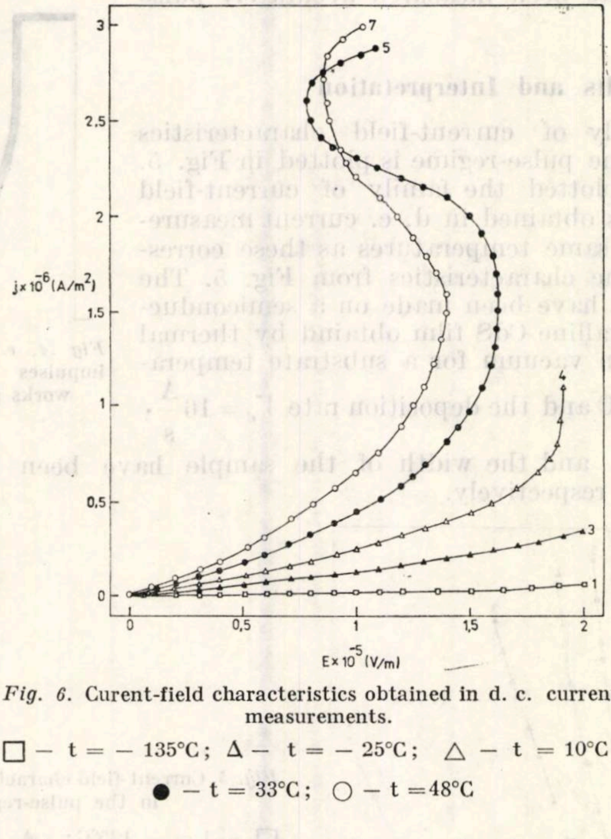

Fig. 6. Curent-field characteristics obtained in d. c. current measurements.

□ — t = — 135°C; Δ — t = — 25°C; △ — t = 10°C;
● — t = 33°C; ○ — t = 48°C

In order to interpret these results we invoke the fact that the Joule-heating in a semiconductor (due to the power dissipated in the sample) may lead in some cases to the appearance in the current-field characteristic of a region with negative differential resistance of "S" — shape. This, a such region in "S"—shape one observed in the direct and inverse brandres of a semiconducting diode and its can be explained as being due to the increasing of the minority carriers at Joule-heatin [6–8].

One may show that in a polycrystalline semiconducting film with predominant conduction mechanism through the intercrystalline barriers the Joule-heating may lead toa modification in "S"-shape of the $j-E$ characteristics in the strong field range. Let us consider the relationship for the $j-E$ characteristics in the barrier conduction mechanism [3, 5]

$$j = aT^2 e^{-\frac{C}{T}} (e^{\frac{bE}{T}} - 1) \tag{1}$$

where a, b and C are some constants with respect to the absolute temperature and the electric field E, depending on the microscopic film structure. This expression allows to explain satisfactorily the non-ohmic effects in polycrystalline semiconducting CdS thin films [3, 5].

Considering the power P dissipated in the sample, due to the Joule effect we can write

$$P = jE = \vartheta(T - T_0), \tag{2}$$

where T_0 is the medium temperature (i. e. the sample temperature in pulse regime) and T is the sample temperature (establised as a result of Joule-heating), ϑ is a coefficient depending on the thermal exchange and the sample geometry. As a result, the absolute temperature T in the $j - E$ dependence does not to be a constant parameter. It can be expressed by

$$T = T_0 + \gamma jE \tag{3}$$

where $\gamma = \dfrac{1}{\vartheta}$ and $j = j(E, T_0)$. Replacing (3) in (1) and taking into account that in the strong field range $e^{\frac{bE}{T}} \gg 1$, we obtain

$$j = a(T_0 + \gamma jE)^2 e^{\frac{bE - C}{T_0 + \gamma jE}}. \tag{4}$$

Considering (4) as a relation ship of the form $F[j(E), E] = 0$, and evoluating $\dfrac{\mathrm{d}j}{\mathrm{d}E} = -\left(\dfrac{\partial F}{\partial E}\right)\left(\dfrac{\partial F}{\partial j}\right)^{-1}$, we obtain after some transformations

$$\frac{\mathrm{d}j}{\mathrm{d}E} = j\,\frac{(T_0 + \gamma jE)(b + 2\gamma j) - \gamma j(bE - C)}{(T_0 + \gamma jE)^2 - \gamma E[2(T_0 + \gamma jE) - (bE - C)]}. \tag{5}$$

In this expression, accordingly to the experimental data [5], $bE - C < 0$, so that the numerator is positive. The second term of the denominator is positive also. Moreover, since $j = j(E)$ is a growing function it is necessary that $\dfrac{\mathrm{d}j}{\mathrm{d}E} > 0$. This condition implies

$$(T_0 + \gamma jE)^2 \geqslant \gamma E[2(T_0 + \gamma jE) - (bE - C)]. \tag{6}$$

If in (6) the equality is fulfiled, follows that $\dfrac{\mathrm{d}j}{\mathrm{d}E} = \infty$. In this point the curve $j = j(\mathrm{E})$ presents a modulation point leading to a "S"-shape of the characteristics. (We remember that the condition $\dfrac{\mathrm{d}j}{\mathrm{d}E} = 0$ may lead to a "N"-shape on the current-field characteristics [9]).

A similar behaviour presents also the dependence $P=P(E)$ since the condition (6) maintains and $\frac{\mathrm{d}P}{\mathrm{d}E}=E\frac{\mathrm{d}j}{\mathrm{d}E}+j$.

Therefore, considering the Joule-heating in the case of the conduction mechanism through the intercrystalline barriers one may explain the appearance of a region "S"-shape on the current-field characteristics obtained in d. c. current regime. It is easily to see also that for higher medium temperatures the negative differential resistance appears at smaller electric fields. The above considerations give on interpretation of the effect, but a concrete calculus implies also the knowledge of the coeficient γ (i. e. the thermal exchange) and this subject will be treated separately.

REFERENCES

1. B. L. LUTZKY, YU. F. OGRIN, S. P. CHELNIKOV, in *The Problem of Film Electronics*, Moscow, 1966, p. 424
2. A. NICOLAU, I. LICEA, I. SECĂREANU, Rev. Roum. Phys., *13*, 471 (1968)
3. I. LICEA, V. RUXANDRA, Analele Univ. Buc., ser. St. naturii, 39 (1976)
4. V. RUXANDRA, I. LICEA, N. BĂLTĂŢEANU, Analele Univ. Buc., Fiz. *26*, 97 (1977)
5. I. LICEA, V. RUXANDRA, Analele Univ. Buc., Fiz., *27*, 77, (1978)
6. S. BENZER, J. Appl. Phys., *20*, 804 (1940)
7. B. M. VUL, Jurn. Tehn. Fiziki, *26*, 2403 (1956)
8. J. I. ALFIOROV, A. I. UVAROV, Elektricestvo, *5*, 46 (1964)
9. V. P. SONDAEVSKI, V. I. SMIRNOV, *Fizika p-n perehodov*, Izd. „Zinatne", Riga, 1966, p. 83

Primit la redacţie la 22 I 1977

ANALELE UNIVERSITĂȚII BUCUREȘTI FIZICA, XXVIII, 1978, pag. 91—96

THE INFLUENCE OF SUPPORT ROUGHNESS ON THE OPTICAL CONSTANTS OF THE PbTe FILMS STUDIED BY INTERNAL REFLECTION ELLIPSOMETRY

G. G. BRĂTESCU, ELENA ZAMFIR

Faculty of Physics, University of Bucharest*

ZINCA MARIȘ

Institute for Physics and Technology for Radiation Devices**

ABSTRACT

This paper presents the results of an experimental study that conducted to obtain the exact values of optical constants of the PbTe film. These are quantitatively determined by measuring of the ellipsometer parameters on both interfaces, ambient-film and substrate-film, and taking into account the influence of the surface roughness of the glass substrate. The results are compared with the values of optical constants given by different autors, for $\lambda = 5893$ Å.

Introduction

The optical properties of PbTe were experimentally studied by absorption [1—3], reflection [4—7], electroreflectance [8—9] and interferometric [10] measurements. For spectral regions with the very high absorption coefficients, the optical constants were determined from the reflectivity using the Kramers-Kronig analysis [5—7, 11] and corelated with the measured absorption curves. The calculation of constants from the pseudopotential bands is complicated by the fact that transitions responsable for optical properties occur at quite low energies. Small errors in band energies are large procentage errors and result in large errors in the optical constants. The values of optical constants calculated by several autors are rather discordant. [5—7, 11, 12].

The ellipsometric method in the study of surface is a convenient technique for high sensitivity in direct determination of the optical constants. The major obstacles in obtaining of concordant experimental dates are surface contamination upon exposure to atmosphere and the influence of the substrate roughness which may complicate the interpretation of experimental results. Taking into account the factors which may influence of the measurements we studied experimentally the two surfaces of the film deposited on the glass surfaces with the well known roughness.

---

* *National Center of Physics*, P. O. Box 5211, Măgurele, Bucharest.

** *National Center of Physics*, P. O. Box 5206, Măgurele, Bucharest.

Basic relations

The optical constants, refractive index n and extiction coefficient k, depending on ellipsometer parameters ψ and Δ, which characterize the investigated surface, are given by following relations [13, 14]:

$$n^2 - k^2 = n_0^2 \sin^2\theta_0 + \frac{n_0^2 \sin^2\theta_0 \mathrm{tg}^2\theta_0 (\cos^2 2\psi - \sin^2 2\psi \sin^2\Delta)}{(1 + \sin 2\psi \cos\Delta)^2} \qquad 1.a)$$

$$2nk = \frac{n_0^2 \sin^2\theta_0 \mathrm{tg}^2\theta_0 \sin 4\psi \sin\Delta}{(1 + \sin 2\psi \cos\Delta)^2} \qquad (1.b)$$

where n_0 is refractive index of ambient medium and θ_0 is angle of incidence.

The ellipsometric formula, based on the model randomly rough surface by means the root-mean-square value tg β_0 of partial derivates (ξ_x', ξ_y') of random height surface irregularities $(\xi(x, y))$, is given by [15, 16]:

$$\mathrm{tg}\, \psi \exp (i\Delta) = \frac{\hat{R}_p(\theta) + \frac{1}{2} \mathrm{tg}^2\beta_0 [\hat{R}_{px}''(\theta) + \hat{R}_{py}''(\theta)]}{\hat{R}_p(\theta) + \frac{1}{2} \mathrm{tg}^2\beta_0 [\hat{R}_{sx}''(\theta) + \hat{R}_{sy}''(\theta)]} \qquad (2)$$

where $\hat{R}_{p,s}$ are the Fresnel amplitudes for an ideal smooth surface and $\hat{R}_{p,s}''$ are second order derivatives of them in ξ_x', ξ_y'. The indices p and s speciffie light polarisation parallel and perpendicular to the incidence plane respectivelly. $\hat{R}_{p,s}$ and $\hat{R}_{p,s}''$ are depending on n_0, θ, n and k [16, 17).

The method of internal reflection ellipsometry which gives the ellipsometric parameters ψ and Δ of the noncontamined film-substrate interface is schematically shown in figure 1 [18]:

The beam reflected upon the internal film surface is characterized by a set of measured parameters ψ_m and Δ_m. They are related to the ellipsometers parameters ψ and Δ of the investigated surface by the expression:

$$\mathrm{tg}\, \psi_m \exp (i\Delta_m) = \frac{t_p t_p'}{t_s t_s'} \mathrm{tg}\, \psi \exp (i\Delta_m) \qquad (3)$$

where $t_{p,s}$ and $t'_{p,s}$ are the Fresnel transmission coefficients of the air-glass and respectivelly galss-air surface. The complex refractive index of film $\hat{N}$, in the case of negligible absorption in glass, is given by [18].

$$\hat{N} = n_s\left[1 - \frac{4\hat{\rho}\sin^2\theta}{(1+\hat{\rho})^2}\right]^{1/2} \operatorname{tg}\theta' \qquad (4)$$

where $\hat{\rho} = \operatorname{tg}\psi \exp(i\Delta)$ and $\sin\theta' = \frac{\sin\theta}{n_0}$.

Experiment.

The samples were prepared by vacuum evaporation of the PbTe high purity at 10^{-5} Torr preassure, on the BK 7 glass supports with different roughness at room temperature.

The thickness of PbTe film measured by interferometric method is 8 600 Å.

The supports have parallel plane faces and a thickness of 8 mm. For beam with about Ø = 2 mm they permit to obtain a separation of reflected beams.

The glass surfaces were mechanically polished to a mirrorlike appearance where one interface of them shown optical precission of $\lambda/20$ and the other one has a known roughness. These supports were cleaned in alchool isopropilic vapor.

A conventional ellipsometer with a compensator for jellow Na line was used [14]. The ψ and Δ values for the glass surfaces were obtained as overage values of 16 measurements made in all four zones after the allignement of ellipsometer components and sample by the standard Mc Crackim method [19].

The ellipsometer parameters ψ_m and Δ_m on the both sample sides were measured in the same way.

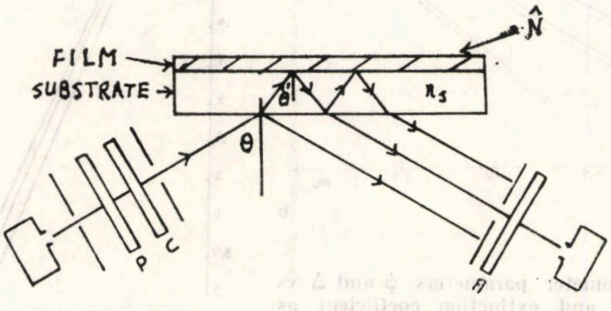

Fig. 1. The method of internal reflection ellipsometry.

Results and discussion.

The parameters of glass surfaces for two samples on $\psi_A = 5.345°$; $\Delta_A = -2{,}093°$ and $\psi_B = 5.446°$, $\Delta_B = -3.333°$.

Roughness of glass surface given by $\operatorname{tg}\beta_0$, was determined by means formula (2) only from ψ value in accord with [16–17]

The experimental results for PbTe film, obtained by conventional method for air-film interface and internal reflection ellipsometry method for glass-film interface, are shown in table I. Glass roughnesses on also specified by tg β_0.

Table I

Experimental dates and refractive indices of PbTe film ($\hat{N}=n+ik$) evaluated by the two different techniques for both surfaces

	sample	θ	ψ m	Δ m	tan β_0	n_a	k_a
Conventional method	A	60	31.48	−137.415	0.016	2.052	2.536
	B	60	31.50	−137.491	0.030	2.054	2.542
Internal reflection method	A	60	46.013	171.850	0.016	4.259	3.571
	B	60	45.901	−171.183	0.030	3.969	3.505

From the values ψ_m and Δ_m measured on both surfaces, pseudo-optical constants n_a and k_a were calculated by means formula (1) and respectivelly (4) supposing noncontamineted ideal smooth surfaces in both cases.

We see that results are differentiated only by internal reflection method on the galss-film interface. That is an obvious dependence by support roughness in accroding to the values of tg β_0.

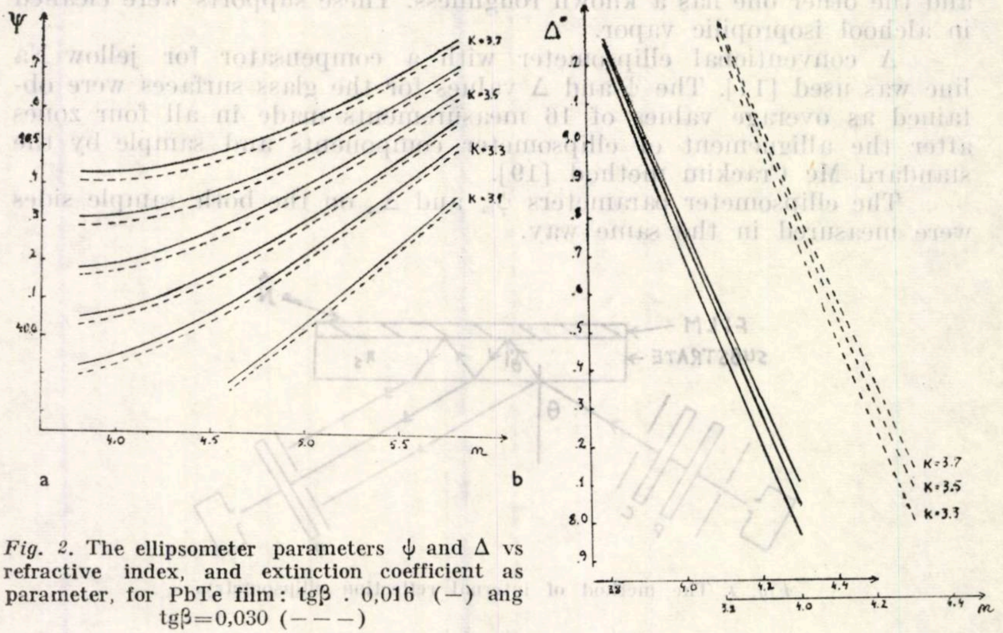

Fig. 2. The ellipsometer parameters ψ and Δ vs refractive index, and extinction coefficient as parameter, for PbTe film: tgβ . 0,016 (—) ang tgβ=0,030 (– – –)

The values obtained by the first method for the air-film interface are very differentiated comparatively with the others ones and this fact is determined by atmosphere contamination and it doesn't depend on the support roughness. This dependence appears in the case of metal surface with greater roughness [20].

Accounting of the support roughness, the exact constants are determined with a graphical method. For that we used the curves of the calculated values of ψ and Δ as function n and k as parameter, for glass refractive index $n_s = 1{,}5166$, and angle of incidence $\xi = 34{,}82°$.

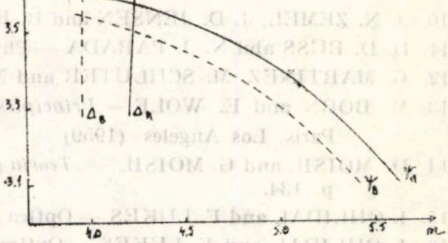

Fig. 3. **The extinction coefficient vs the refractive index for two surfaces with the different roughness: (A) tg $\beta_0 = 0{,}016$ and (B) tg $\beta_0 = 0{,}03$.**

These are given in figure (2) for two roughnesses. From the intersection of the experimental values with the two sets curves were determined some pairs of values n and k as plotted in fig. 3. From these curves was obtained a domain of values for which is possible to determine the true constants of PhTe values ($n = 4.15$ $k = 3{,}55$). For comparation, the our results and the values obtained by several authors in the Table II were shown.

Table II

The values of the optical constants for $\lambda = 5893$ Å

n	k	references
2,5	3,5	5
5,8	5.5	7
2,7	4,9	7 conform 11
4,15	3.55	present paper

The internal reflection ellipsometric method is found to be superior to conventional method because it avoids the contamination which may give the complete different values.

An important conclusion which follows from our work is that we may determine true optical constants of the film by rendering evident the surface roughness.

REFERENCES

1. A. F. GIBSON – Proc. Phys. Soc. (London), *B 863*, 756, (1950)
2 A. F. GIBSON – Proc. Phys. Soc. (London), *B 65*, 378, (1952)
3. T. S. MOSS – *Optical Properties of Semiconductors*, ,,Butterworths'' Sci. Publ. Ltd., London, (1959), p. 188.

4. M. LASSER and H. LEVINSTEIN – Phys. Rev., *96*, 1, 47, (1954)
5. M. CARDONA and D. L. GREENAWAY – Phys Rev., *133*, 6A, 1685, (1964)
6. S. E. KOHN, P. Y. YU, Y. PETROFF, Y. R. SHEN, Y. TSANG and M. L. COHENPhys. Rev. B, *8*, 4, 1477, (1973)
7. D. M. KORN and R. BRAUNSTEIN – Phys. Rev. B, *5*, 12, 4835, (1972)
8. D. E. ASPNES and M. CARDONA – Phys. Rev., *173*, 3, 714, (1968)
9. R. GLOSSER, R. KINOSHITA and B. REUNEX – Phys. Rev. Lett., *33*, 17, 1027, (1974)
10. J. N. ZEMEL, J. D. JENSEN and R. B. SCHOOLAR – Phys Rev., *140*, 1A, 330, (1965)
11. D. D. BUSS abd N. J. PARADA – Phys. Rev. B., *1*, 6, 2692, (1970)
12. G. MARTINEZ, M. SCHLUTER and M. L. COHEN – Phys. Rev. B, *11*, 2, 660, (1975)
13. M. BORN and E. WOLF – *Principles of Optics* Pergamon Press, London, New York, Paris, Los Angeles, (1959)
14. D. MOISIL and G. MOISIL – *Teoria şi practica elipsometriei* Ed. Teh., Bucureşti, (1973), p. 134.
15. I. OHLIDAL and F. LUKES – Optica Acta, *19*, 10, 817, (1972)
16. I. OHLIDAL and F. LUKES – Optics Commun., *5*, 5, 323, (1972)
17. G. BRATESCU, Z. MARIS and E. ZAMFIR – Comunicare Conf. Soc. Fiz. Chim., Tulcea aprilie 1977, to be published
18. E. C. CHAN, and J. P. MARTON – J. Appl. Phys., *43*, 10, 4027, (1972)
19. F. L. McCRACKIN, E. PASAGLIA, R. R. STRONBERG and H. STEINBERG – J. Res. Noth. Bur. Std. (US), 67A, 368, (1963)
20. G. G. BRĂTESCU, Z. MARIS and E. ZAMFIR – Anal. Univ. Buc., ŞtiinţeleNaturii, p. 31, (1975)

Primit la redacţie la 30 ianuarie 1978

ANALELE UNIVERSITĂȚII BUCUREȘTI, FIZICA, XXVII, 1978, pag. 97—101

THE INFLUENCE OF THE METEOROLOGICAL FACTORS ON THE CONCENTRATION OF ATMOSPHERIC AEROSOL

ELENA DECU, ȘT. LASCU
Faculty of Physics, University of Bucharest*
D. EȘEANU
The Institute of Meteorology and Hydrology, Bucharest

ABSTRACT

This paper analyses the concentration of the atmospheric aerosol in Bucharest using measurements covering a period of a year. It stresses out the influence of the auto-traffic and thermic inversions in increasing the concentration of particles as well as the role of thermic convection and of rain on the movement of particles concentration. The increasing of the relative humidity of air determines the enlarging of the dimensions of particles.

1. Introduction

The pollution degree can be considered as being the resultant of more tendencies that favours its increasing or decreasing. Taking into account this point of view we can classify the meterological conditions thus [1]:

— conditions that determine the dispersion of polluants: wind, ascendent movings and precipitations,

— conditions that determine the accumulation of polluants: wind, wind absence and thermic inversion,

— conditions that determine the chauging of polluants: the acid smog producing and the oxidating smog producing.

This paper presents a part of the results of the determinations concerning the atmospheric aerosol concentration in Bucharest — covering the period November 1974 — November 1975. This analysis refers to the influence of meteorological factors specially.

2. Experimental Data

The sizeson which measurements were made were: the Aitken nucleus concentrations C_A $(0,01\ \mu \leqslant \Phi \leqslant 0,1\ \mu$, with Scholtz counter), the concentration with big and buge nuclei C_G $(0,1\ \mu \leqslant \Phi \leqslant 5\mu$, with

---

* *National Center of Physics,* P. O. BOX 5211, Măgurele, Bucharest.

Zeiss conymeter), both of them being expressed in particles/cm^3 and meteorological parameters: the wind velocity on the soil V(m/s), the relative humidity of the air U(%), the air temperature t(°C), atmospheric pressure P(mm Hg) and the machines that the were going in the moment of test making which were expressed by the number of machines per hour (m/h).

The measurements were simultaneously made in different points of the town: the University Square, the Romană Square, the North Sattion Square, the Muncii Square, the Chibrit Square, the Moghioroş Square keeping as reference station the Village Museum (in the park).

The determinations were made on more days chosen in such a way as to characterize all the seasons of the year and to cover all the day long (06—16 TMG). The informations on atmospheric stratification were taken from the radiosoundings at the aerological station of Bucharest.

3. The Results Debating and Interpreting

As the absolute values of the concentrations differend much from a station to another, the necessity of representing all the stations on same graph imposed the measurements representing in relative dimensions towards the daily medium for each station ($C_A/\bar{C}_A$, $C_G/\bar{C}_G$).

Due to the close interdependence between the meteorological factors and the meteorological factors — the concentration of the particles, the isoplatar representations were preferred [4, 5]. These ones have the advantage of pointing out the varition of the concentration at the same time, as a function of two parameters, the curves on izoplatar representations expressing either the intensifying or the weakening of pollution towards the medium value.

The daily variations of the following parameters have been taken into consideration: the air temperature, the relative humidity of it and the auto-trafic.

We present as an examplu of debating the day of Dec. 7 1974 out of the multitude of analysed days, as it is characterized by important enough variations of meteorological conditions, leading to a detailed analysis of their influence on the concentration of particles in atmosphere.

During morning there exists a strong thermic inversion on soil (fig. 1a) accompanied by transparent fog. In the afternoon the ensemble of the meteorological conditions favours the developing of a very pronounced convective movement, the thermic inversion being disipated (fig. 1b).

Due to this fact we have expected to get higher concentrations during morning and a weaking of these during noon. These are very evidenced by the isoplatar representations (fig. 2 and 3), that show obviously the existence of some strong maximas during morning (the effect of thermic inversion combined with an intense auto-traffic and in the afternoon too (the effect of convection disappearance and the same intense traffic) as well as the existence of some minimas concentrations near 9—12 o clock TMG (the convection effect) as we can see in figures 2 and 3.

The medium concentrations, but not too high, of Aitken nuclei $119.10^3-248.10^3$ particles/cm^3 and big nuclei 405—811 particles/cm^3, towards other days noticing compared to the refference station of the

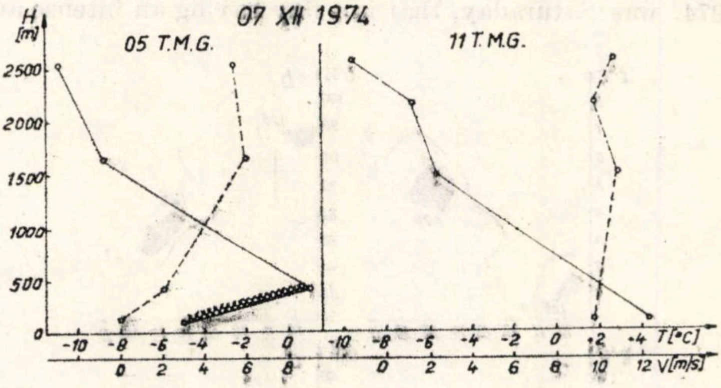

Fig. 1. **The profile of air temperature and wind velocity with the altitude; continuous line — the temperature, discontinuous line — velocity.**

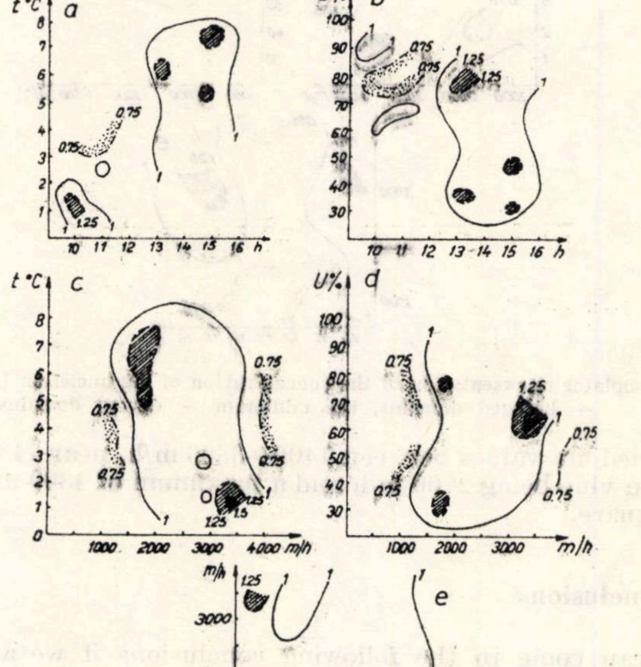

Fig. 2. **The ipsolatar representation of the Aitken nuclei concentration on Dec. the 7th 1974; the maximum — hatched domains, the minimum — dotted domains.**

Village Museum 39.10³, 540 particles/cm³ respectively, represent another proof of the important effect of convection for purifying the urban atmosphere. The convection effect is strenghened by the fact that Dec. the 7th 1974, was Saturaday, that is a day having an intense auto-traffic

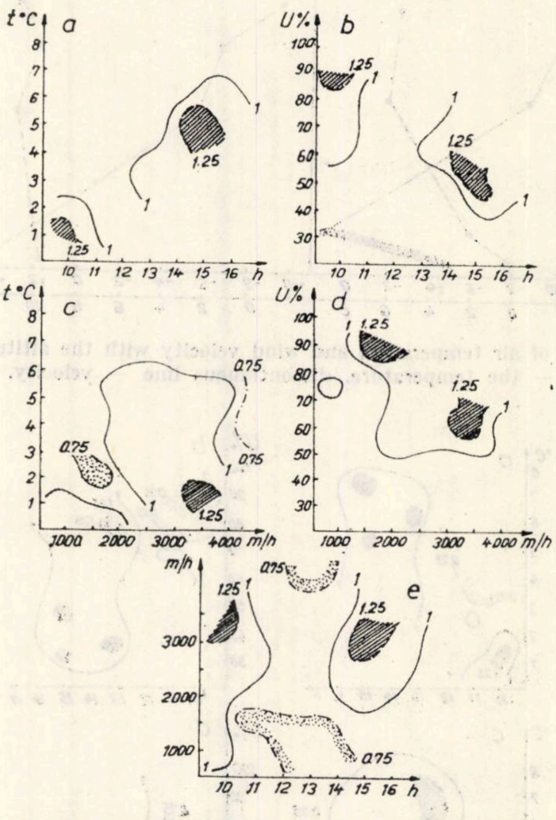

Fig. 3. The isoplatar representation of the concentration of big nuclei on Dec. the maximum — hatched domains, the minimum — dotted domains.

havin its medium values between 1400—3800 m/h, near 11 o clock TMG, the medium vlue being 2700 m/h and a maximum of 4300 m/h in the University Square.

4. Conclusions

We can come to the following conclusions if we analyse all the made determinations in the above mentioned period, in different meteorological stations :

a) The auto-trafic influence on the increasing of particles concentration in atmosphere.

b) Thermic inversions are opponent to the dispersing of the polluants ; the ascension of the air stratum from the soil being stopped, and the polluatns vechiculating being blocked under the inversion stratum. The asecendent movements are also stopped at the level of the inversion stratum and are counterballanced by the descendent movements. The thermic inversions that persisted one or more days determined an atmospheric calm that leads to the concentration of the polluants in the stratum of air that was very near to the soil.

c) The role of the thermic convection and of the „warmth isle" effect of the town, as important factors in destraying the thermic inversions, and respectively in their raising at higher altitudes lead to the dispersing of the polluants.

d) The role of the relative humidity of air in increasing the dimensions of the particles : at high humidity, very small particles which could not be detected become Aitken particles, while some Aitken particles enter the measurement domain of big particles, this effect is pointed out by the measurements made either before or during the precipitations, in accordance with [2, 3].

e) The effect of rain on the movement of the particles in atmosphere fixes the particles on soil, washes and moistens the soil, which removes, for a time, the raising of the particles at altitude, and dissolves certain polluants.

REFERENCES

1. CHOVIN P. et ROUSSEL A., *Physicochimie et Physiopathologie des polluants atmosphériques*, Masson et Cie Éditures, Paris, 1973.
2. RAYNOR S. G., SMITH E. M. and SINGER A. I., Atmospheric, Environment, vol. 8, 1974.
3. SINCLAIR D., COUNTESS J. R. and HOOPES J. G., Atmospheric, Environment, vol. 8, 1974.
4. WINTER V. et al., Rev. Roum. Géophys., 16, 1, 1972, 109–121.
5. WINTER V. et al., St. Cerc. Geofiz., 10, 2, 1972, 259–274.

Recevied et redaction on 5th Ian. 1978.

[illegible]

[illegible]

[illegible]

[illegible]

REFERENCES

1. [illegible]
2. [illegible]
3. [illegible]
4. [illegible]
5. [illegible]
6. [illegible]

ANALELE UNIVERSITĂŢII BUCUREŞTI FIZICĂ, XXVIII, 1978, pag. 103—107

SOME NOTICES ON INTERMEDIATE EARTHQUAKES PRODUCING IN VRANCEA

ŞT. LASCU
Faculty of Physics, University of Bucharest*

ABSTRACT

This paper stresses out an asymetry of the propagation velocity with the direction, there existing a decreasing of this one on the direction of fault-plan, a plan that coincides with the Benioff plan for the region under study. It confirms that the earthquake of March the 4 1977, was a multiple phenomenon of dislocation consisting of four shochs in an interval of 19 seconds.

1. Introduction

It has already been demonstrated by many authors that in Vrancea region, numerous earthquakes occur, being characterized both by the persistency of their geographical coordinates and by their depth.

The statistics of the noticed data within the last five centuries suggests the idea that the number of earthquakes hawing their magnitude over 7 is very small, too; about 2—3 each century. We have at out disposal instrumental notices for two strong earthquakes only (that one on the 10th of Oct., 1940, $M = 7{,}4$ and on the 4th of March 1977, $M = 7{,}2$) because the world seismic system, based on such instrumental data is quite new.

We shall try to come to some conclusions regarding the way this kind of earthquakes take place as well as regarding their particular characteristics of propagation of their waves by analizing their recording pointing out those of the last earthquake because notices on this one are more numerous and certain too.

2. The Material Used and the Way of Work

For the study under disscussion we have used the recordings of aproximately 400 seismic stations of the earthquake on March 4th 1977, having an homogeneous distribution in epicentral distance as well as

---

* *National Center of Physics*, P. O. BOX 5211, Măgurele, Bucharest

in azimuth, in comparison with other earthquakes, the registerings of the strong earthquake of Oct. 10th 1940, included.

The analysis of the seismograms registered at a series of seismic stations pointed out the fact that the earthquake of March 4 1977, was a multiple seismic phenomenon that consisted of at least four shocks that succeded at invervals of some seconds, the time duration between the first and the last ons being aproximately 19 seconds [7]. Although the number of seismic stations that registered the earthquake of Oct. 10th 1940 was very reduced, the presence of more shocks on its seismograms has not been noticed at all.

The distribution of time differences between the recorded travel time of longitudinal waves P_0 and the same travel time calculated P_c has been repretented as a function of epicentral distance and as a function of azimuth, for the earthquake on March 4th 1977.

In figures 1, we represented the differences $P_0 - P_c$ as function of azimuth. In figure 1-a the points on the graphs are mediated keeping a constant interval for the azimuth, while in the figure 1-b the mediation was made in such a way as each point is the medium of the same number of individual values. Both figures stress the absence of registering the azimuth interval for 120°—150°.

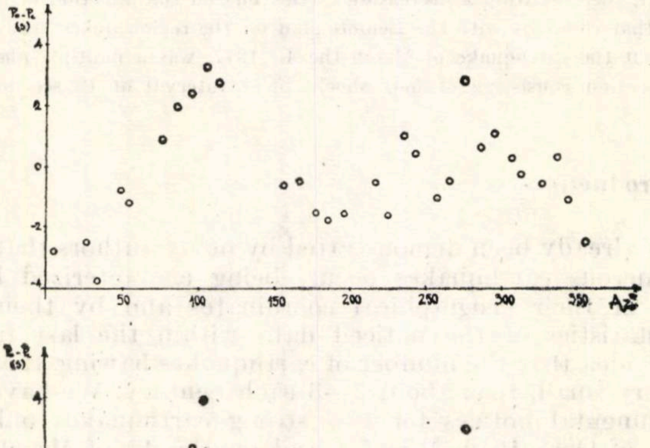

Fig. 1. $P_0 - P_c$ as a function of azimuth, for1977 III 4; 1_a — = δAz = constant, 1 — δN =constant.

In figures 2 the same differences $P_0 - P_c$ are represented as a function of epicentral distance, following the above procedure; in figure 1-a the mediations have been made keeping the interval of epicentral distance constant, but in figure 1-b the number of individual values, has been kept equal. Although the distribution of the points on graph is not perfect homogeneus, and this is obviously to be seen in figure 2-b, within the interval 30°—65° the number of registerings being much more reduced, we can easily state that the whole epicentral distance comprised between 0° and 100° is very well covered.

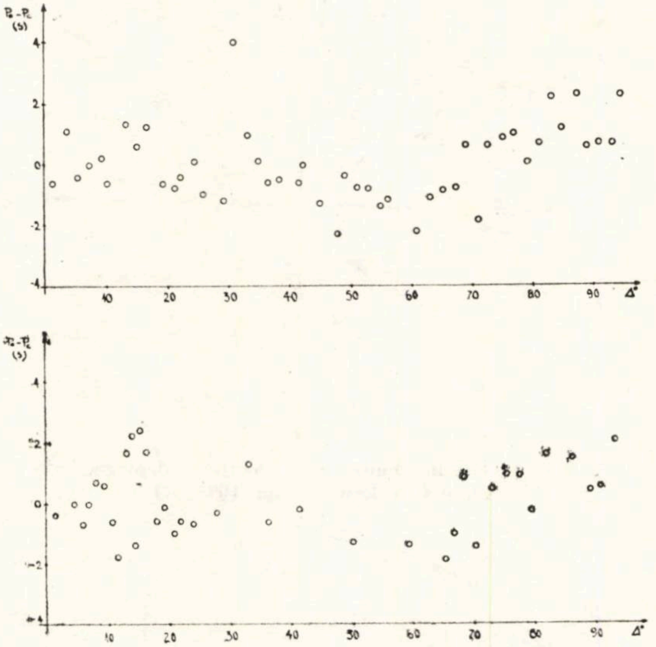

Fig. 2. $P_0 - P_c$ **as a function of** $\Delta°$, **for 1977 III 4;** 2_a — $-\delta\Delta$ **= constant,** 2_b — δN **= constant.**

Figure 3 reprezents the distribution of the displacement vector in P wave in seismic station that their epicentral distance below 12°; the continuons segments stand for sure signs, whereas the discontinuous segments stand for contestable signs. The long continuous arrows represent the distribution of compressed and dilated tensions in focus.

In figure 4 a solution of the fault plan for the earthquake on March the 4 1977 is represented, the seismic stations in which the signs of the first displacement have been identified in P wave, these ones are represented in Wulff proiection on the inferior semispace, the two possible fault plans a and b being traced by a continuous line, whereas we used a discontinous one for the traced plan that comprises the compressed and dilated tensions P and T.

3. The Analysis of the Results and Conclusions

Figures 1-a and 1-b point out a variation of the propagation velocity with the direction, there fore it's an asymmetry of it. For the azimuth directions of aproximately 180° and 360° there is a superior velocity to that foreseen for an homogenuous earth but for the directions whose azimuth is to be found near 100° and 280° there is a reduced velocity in relation with the given one for an earth having an homogeneous stratification. We point out the fact that the velocity reducing in relation

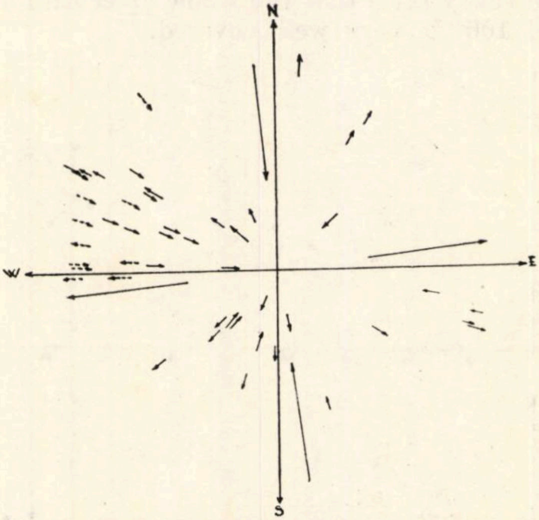

Fig. 3. The horizontal components of deplacement vectors of P waves for 1977 III 4.

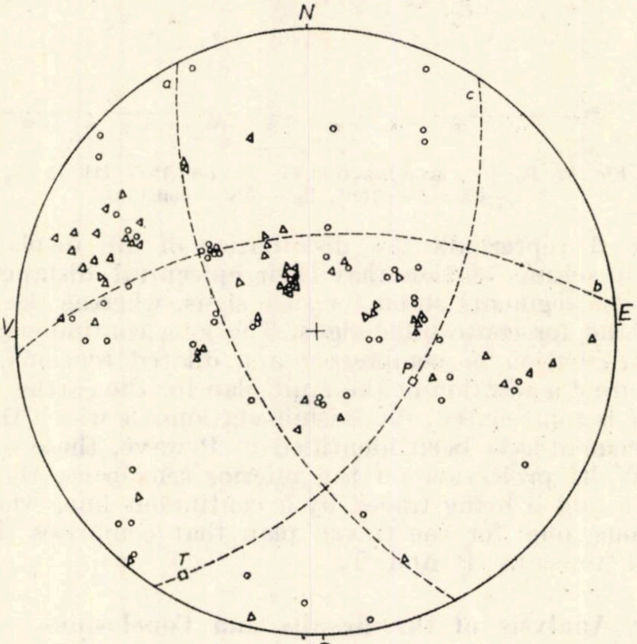

Fig. 4. Facult-plane solution for 1977 III 4.

with the tandard one is much more pronounced towards its increasing. The P_0-P_c negative values go up to -2 seconds and the pozitive values $P_0 - P_c$ come to $+4$ seconds.

If it is compared with figure 4, it leads to the idea of choosing the plan b as a fault, plan, the velocity of longitudinal waves decreasing in the breaking plan. This leads to the conclusion that the direction of the breaking plan had been outlined before the earthquake took plance [5]. As we can easily noticed the fault plan is tangent to the mountains curvature having an inclination of 34° in the inferior semispace both the direction and the inclination being in a perfect concordance with the parametres of the Benioff plan established in [4, 8].

The results of figure 4 strenghten the conclusions regarding the elements of the fault plan demonstrating that the earthquake of March 4th 1977, was of a compressional type, very like all the earthquakes in this region [2, 9, 11].

If the compressional type of earthquake is the same for the majority earthquakes in this region, irrespective of their magnitude, this one being a characteristic given by the general motion of tectonic microplates that co-operate to the generation of these earthquakes, the parameters that define the fault plan and the principal tensions P, T, vary within the weak earthquakes [2, 11]; it demonstrates that the strong earthquakes can't be described by the weak ones; and consequently the possibility of strong earthquakes prediction through those weak ones can't be successfull.

By comparing the way of manifesting of the two strong earthquakes we can come to the conclusion that these ones manifest themselh as a process of multiple dislocation, for the earthquakes having a reduced depth ($h \approx 80$ km), the interval between the shocks being of the seconds order, and for those having a bigger depth ($h \approx 130$ km) the interval being of the days order, the earth is much more homogeneous at this depth.

Figures 2 a and 2 b confirm the existence of an astenospheric canal, not too developed for the P wave whose inferior limit is to be found at a depth of 220—250 km ($\Delta \approx 15°$) as well as the existence of a second stratum of reduced $\frac{dt}{d\Delta}$ at depths over 600 km [1, 3, 6, 10].

REFERENCES

1. BOTT H. P. MARTIN, *The Interior of the Earth*, Lonodn, 1972.
2. CONSTANTINESCU LIVIU, ENESCU D., Probleme de Geofizică, vo.II, 1963, 45—77.
3. HALES L. ANTON ,*Developments in Geotectonics*, 4, The Upper Mantle, 1972, 447—483.
4. IOSIF T., Revue Roumaine de Géophysique, Tome 12, N 1, 1968, 23—38.
5. LASCU ȘT., Analele Univ. Buc., Științele naturii 1974, 45—52.
6. LASCU ȘT., Analeie Univ. Buc., Științele naturii 1975, 41—48.
7. MÜLLER G., BOYLER K-P., STÖCKL H., ENESCU D., The Romanian earthquake of March 4 1977 (I), Karlsruhe, 1977.
8. PETRESCU G., RADU C., Analele Univ. ,,Al. I. Cuza'' Iași, Tom VI, 1960, fasc. 3, 757—782.
9. PETRESCU G., RADU C., LASCU ȘT., Studii și Cercetări de Geofizică Nr. 1, Tomul 3, 1965, 18—29.
10. PETRESCU G., RADU C., LASCU ȘT., Revue Roumaine de Géophysique, N 1, Tome 9, 1965, 35—47.
11. RADU C., Revue Roumaine de Géophysique, Tome 11, N 2, 1967.

Recevied at redaction on 5th Ian. 1978

ANALELE UNIVERSITĂŢII BUCUREŞTI, FIZICĂ, XXVII, 1978, pag. 109—119

CONSIDERATIONS SYNOPTIQUES ET STATISTIQUES SUR LES CHUTES DE GRÊLE EN ROUMANIE

ELENA DECU
Faculté de Physique, Université de Bucarest*

D. VRAPCEA, GH. STĂNCĂLIE
Institut de Météorologie et Hydrologie, Bucarest*

RÉSUMÉ

Les données recueillies des archives de l'Institut de Météorologie et de Hydrologie de Bucarest, concernant les chutes de grêle enregistrés dans la période 1961—1975 à 137 stations à service permanent en Roumanie ont permis dé mettre en évidence la distribution, en pourcentage, des dimensions des grêlons et du temps d'apparition (saison, mois, décade, jour et durée de la chute). Ces données ont été analysées et comparées avec celles d'autres pays (notamment la France). Des aspects géographiques sont discutés aussi.

1. Introduction

En raison de sa position géographique, tout le territoire de la Roumanie est exposé aux chutes de grêle. Les dégâts produits par ce phénomène en agriculture ont déterminé des études aussi bien théoriques que pratiques visant a en réduire les effets nocifs. C'est ainsi que certaines chutes de grêle ayant détruit divers types de cultures ont été analysés [5], [12] et qu'on a tenté de rechercher les processus synoptiques et thermodynamiques expliquant les chutes de grêle [1], [2], [6].

Une approche statistique des chutes de grêle est apparue nécessaire sur le plan théorique, pour connaître le spectre de la distribution dimensionelle des grêlons et sur le plan pratique pour combattre le phénomène. Il existe des régions dont la géographie et l'orographie favorisent les chutes de grêle, ainsi que des périodes où il grêle plus fréquemment, et c'est seulement en approfondissant ces facteurs qu'une activité efficiente peut être menée pour prévenir la grêle.

---

* *Centre National de Physique,* Bucarest, Măgurele, P. O. Box 5211.

II. Distribution dimensionnelle des grêlons

Les grêlons tombes aux stations de Păltiniș—Sibiu et Fundata—Brașov ont été mesurés. A Păltiniș—Sibiu (1454 m d'altitude) la taille moyenne des grêlons en 71 cas pedant un intervalle de 15 ans était de 1 à 14 mm, des grêlons de 5 cm de diamètre n'étant observés qu'exceptionneilement. La figure 1 présente la distribution de la fréquence des grêlons suivant leur taille (en pourcentage). A Fundata—Brașov (1371 m d'altitude) les grêlons ont été mesurés dans 67 cas. La figure 2 en montre la variation dimensionnelle entre les limites donnés, avec un histogramme du pourcentage des dimensions possibles dans une série de chutes de grêle. Elle diffère de la figure 1 qui ne présente que la fréquence de certaines dimensions moyennes. On y peut remarquer toutefois l'allure similaire des courbes.

Les grêlons de petite taille ont une fréquence beaucoup plus grande, mais il n'est pas exclu qu'on ait pris pour de la grêle des chutes de grêsil (surtout au début du printemps), ou que, ce qui est plus probable, au moment de l'observation, les grêlons en fondant, eussent réduit leur taille. Ces deux stations ont enregistré des grêlons géants, arrivant à 5 cm de diamètre. Une chute de grêle du 1-er Juillet 1975 à Bucarest—Afumati a produit des grêlons d'une taille exceptionnelle, à savoir d'un diamètre de 6—7 cm.

La comparaison de nos résultats avec ceux d'une étude similaire faite en France [8] (fig. 3) a montré que les grêlons de grande taille sont moins fréquents en Roumanie.

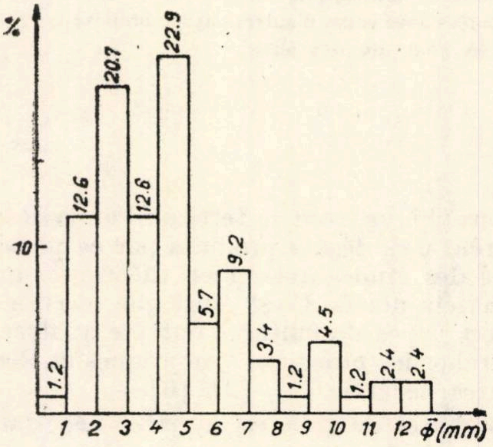

Fig. *1.* La distribution des diamètres moyens pour les granules observés à la station de Păltiniș—Sibiu (1 454 m).

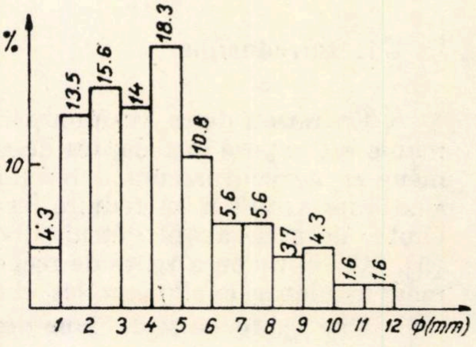

Fig. *2.* La distribution des diamètres des granules d'une série de chutes à la station Fundata—Brașov (1 371 m).

III. Distribution temporelle

En analysant les données sur 15 ans (1961—1975) à 137 stations à service permanent il en a résulté 3334 jours avec 3585 chutes de grêle.

1. *Distribution saisonniere.* L'histogramme de la figure 4 représsente la distribution saisonnière (par critère astronomique) des jours

ou il a grêlé. On y remarque un pourcentage maximum (54,2 %) en printemps. La figure 5 montre la distribution par saisons suivant le calen. drier. Le pourcentage maximum y est déplacé vers les mois d'été (55,3 %), avec une nette prédominance de l'intervaile 1-er — 20 Juin. Ce pourcentage suggère donc que ces mois s'associent à une fréquence plus élevée des cas de grêle.

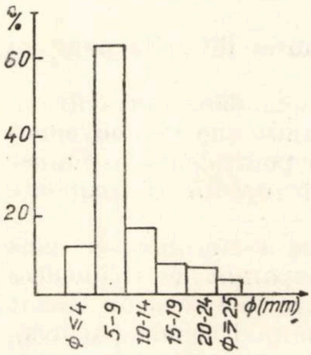

Fig. 3. La distribution dimensionnelle des granules en France.

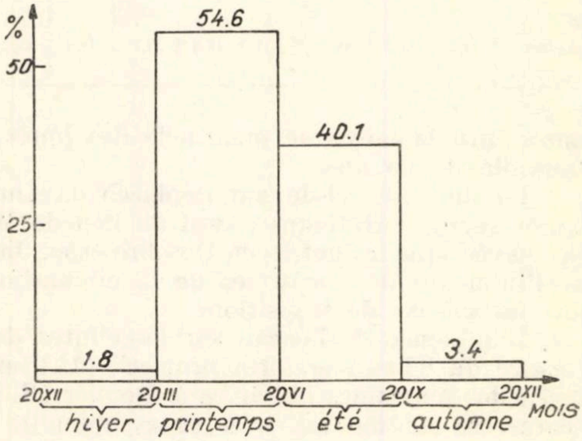

Fig. 4. La distribution saisonnière (astronomique) des jours à chutes de grêle sur le territoire dela Roumanie

2. *Distribution mensuelle.* L'histogramme de la figure 6 présente la distribution prépondérante des chute s de grêle en Mai (28,0 %) et leur fréquence plus grande dans la saison chaude (Avril—Septembre : 95,5 %) que dans celle froide (Octobre — Mars : 4,5 %).

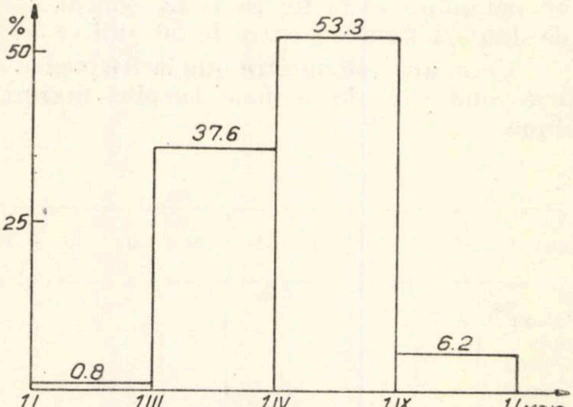

Fig. 5. La distribution saisonnière (selon le calendrier).

La distribution mensuelle des jours avec chute de grêle a été étudiée par Besson [3] aussi, mais il a utilisé pour ceci seulement les données de l'Observatoire météorologique de Paris—Montsourise Le tableau 1

Tableau 1

Mois	J	F	M	A	M	J	J	A	S	O	N	D	par an
Fréquence	0,7	0,3	0,8	1,0	0,8	0,3	0,2	0,1	0,2	0,8	0,2	0,2	4–5

donne ainsi la moyenne mensuelle des jours à chutes de grêle pour un intervalle de 60 ans.

La moyenne ci-devant déplacée davantage que dans notre distribution vers la printemps (Avril au lieu de Mai) ainsi que les moyennes plus élevées que les notres en Octobre et en Janvier pourraient s'expliquer par l'influence de l'océan et de la circulation subtropicale si fréquente dans les saisons de transition.

L'influence de l'océan sur les chutes de grêle a été analysée dans le cadre du "Thunderstorm project" [11], en comparant les fréquences mensuelles moyennes obtenues à Denver (E. U. A.), viile sous un climat à caractère continental, avec ceiles obtenues à Ponta Delgada (Açores), ville sous un climat océanique. Les deux localités se trouvent à peu près sous la même latitude. Le tableau 2 met nettement en évidence ces différences, qui expliquent les chutes de grêle se produisant en saison froide dans les régions océaniques. La Roumanie étant située sous une zone de climat continental tempéré, son régime est à peu près comme celui de la ville de Denver (voir tableau 2 et figure 6).

La distribution mensuelle considérée du 20 au 20 du mois suivant (donc une distribution mensuelle plutôt astronomique) apparaît dans l'histogramme de la figure 7. La courbe s'élève de façon plus accentuèe que dans la figure 6 entre le 20 Mai et le 20 Juin (30,1 %).

Cette analyse montre que la fréquence maximum des chutes de grêle correspond avec la période la plus marquée d'instabilité thermodynamique.

Tableau 2

Mois	J	F	M	A	M	J	J	A	S	O	N	D	par an
Station Ponta-Delgada (Açores), 51 ans (fréquence)	0,6	0,7	0,8	0,3	0,1	0	0	0	0	0,1	0,3	0,5	3–4
Denver (E.U.A.) 40 ans (fréquence)	0	0	0,1	0,5	1,1	0,8	0,3	0,3	0,2	0,1	0	0	3–4

3. *Distribution par {cades*. Elle apparaît dans la figure 8. La distribution mensueile n'a montré aucune oscillation statistique. Par décades (15 ans) la résolution paraît toutefois plus grande, ainsi que le nombre de jours à chute de grêle (3334). Il y a donc plusieurs oscillations dint la plus importante se situe entre les 1-er et 10 Juin, quoique celle-ci n'ait pas été interprétée synoptiquement d'une manière différente des autres.

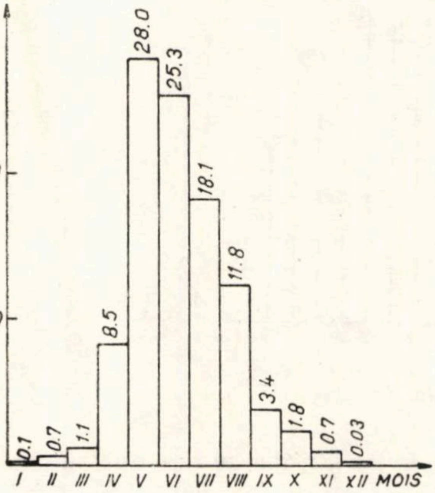

Fig. 6. La distribution mensuelle (selon le calendrier).

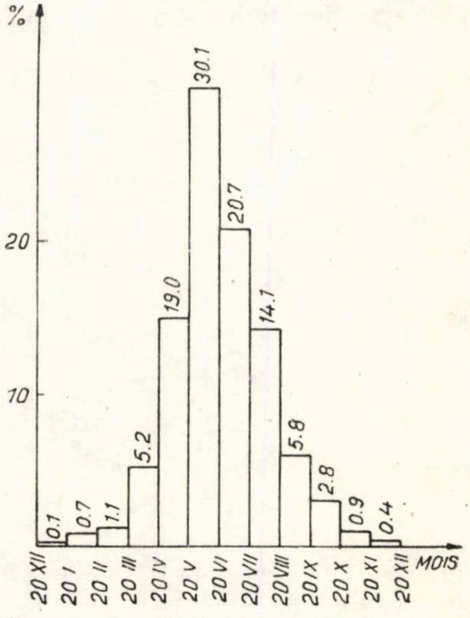

Fig. 7. La distribution mensuelle (astronomique).

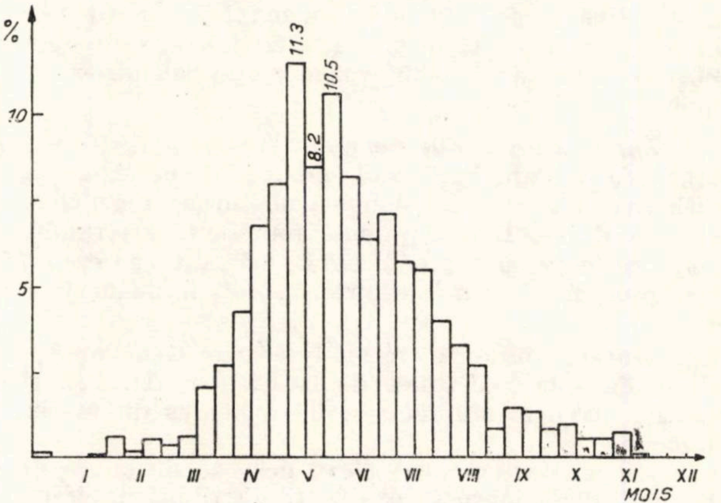

Fig. 8. La distributionpar décades des cas de chutes de grêle pendant 15 ans sur le terri- toire de la Roumanie.

Pendant l'intervalle de 15 ans analysé à cette station aucune chute de grêle n'a été signalée entre les 10 Décembre et 31 Janvier, et les quelques chutes enregistrées du 1-er Décembre au 10 Février n'étaient peut-être que des chutes de grésil ou le résultat d'une activité frontale sur un fond de circulation tropicale. En Janvier il n'y a eu que quatre chutes, le 1-er Janvier 1971 à 10^{36} heures à Călăraşi, a 14^{48} heures à Feteşti, à 11^{54} heures à Jurilovka et à 12^{48} heures à Sulina.

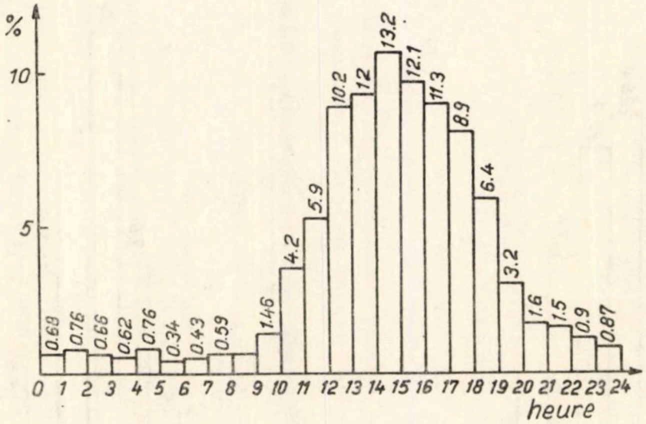

Fig. 9. La distribution diurne.

Les décades ou les chutes ont dépassé la valeur moyenne se situent entre le 21 Avril et la 20 Aout, avec un maximum entre le les 21 et 30 Mars et un autre entre les 11 et 20 Juin, ce qui est en concordance avec les distributions mensuelles (conformément au calendrier et au critère astronomique).

4. *Distribution diurne.* Elle est montrée par la figure 9. Nous avons dit plus haut que pendant l'intervalle analysé il ont été enregistrés 3334 jours de grêle avec 3585 chutes, dont 65 nocturnes, mais on n'en connaît ni l'heure ni la durée. L'histogramme représente les résultats obtenus en anylsant le reste de 3520 cas. Il est intéressant que dans 7% des cas environ, il a grêlé deux ou même plusieurs fois le même jour et dans le même lieu.

La distribution diurne a été analysée par Genève [8] aussi, pour les mois d'été dans le Sud-Ouest de la France (fig. 10). Il en résulte une distribution avec le minimum a 5–6 heures du matin, de même qu'en Roumanie.

Le nombre particulièrement élevé des cas de chute de grêle aux heures "chaudes" de la journée dans notre distribution, c'est à dire entre midi et 17 heures (58,8%) s'explique par la temperature qui attenit en mêmme dépasse le niveau de cumulisation, favorisant ainsi les phénomènes convectifs. Le maximum se situe entre 14 et 15 heures, donc à 2 heures de différence du maximum mis en évidence par Genève. Pour l'expliquer il faudrait tenir compte du fait que la distribution présentée dans la figure 10 ne concerne que les mois d'été.

Le maximum atteint pendant la nuit entre 23 et 01 heures dans la figure 10 n'apparaît pas dans la distribution que nous avons obtenue.

La littérature introduit un rapport R entre le nombre des cas d'orages à grêlons et le nombre total d'orages. La forme de la distribution horaire est dictée par la distribution horaire des orages ainsi que par la possibilité de distinguer, grâce au coefficient R, un nuage orageux capable d'engendrer une chute de grêle (Fig. 10).

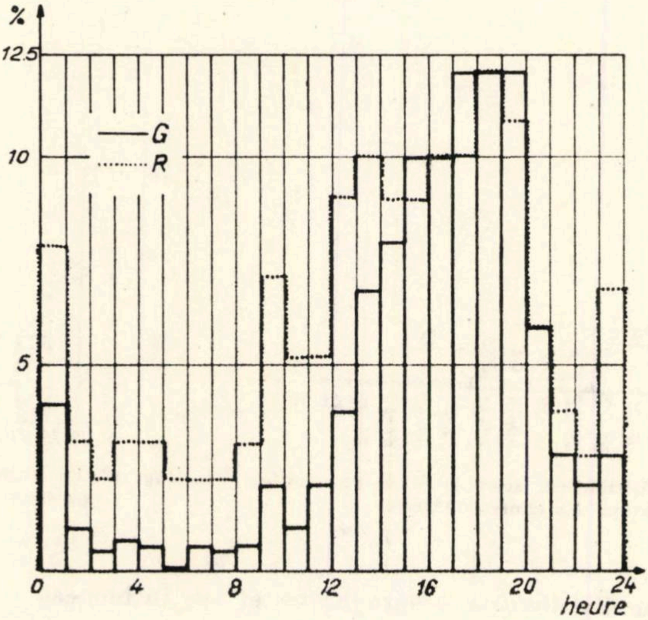

Fig. 10. La variation diurne des cas de grêle en France.
G = grêle ; R = coefficient grêligène.

5. *Distribution de la durée des chutes de grêle.*

Une dernière analyse temporelle se rapporte à la durée de la chute de grêle. Les résultats sont illustrés dans la figure 11, avec le même nombre de cas analysés que pour la distribution ci-devant.

L'analyse a utilisé les tableaux climatologiques des archives de l'Institut de Météorologie et de Hydrologie de Bucarest ou les intervalles ont été fixés suivant les critères climatologiques. Ainsi les plus fréquentes des chutes (48%) sont celles durant entre 4 et 8 minutes ; on a également noté que 85% des chutes ont une durée jusqu'à 15 minutes.

L'allure de la courbe et la distribution des valeurs rappellent celles qui ont été obtenues en France (Fig. 12) [8].

Les durées maximum des chutes de grêle signalées en Roumanie sont 1 heure et 45 minutes au pic Lăcăuţi, 1 heure et 30 minutes à Apa

Neagră (le 19 Juillet 1975) et au pic Omul (le 24 Juillet, 1973), dont la longueur dépasse donc la durée, considérée très longue aussi, d'une chute de grêle observée à Kansas City (E. U. A.) le 3 Juin 1959 [10]. Dans la littérature ces valeurs apparaissent possibles.

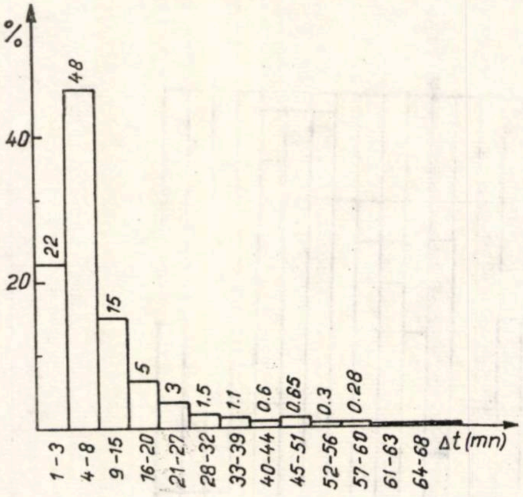

Fig. 11. La distribution selon la durée de manifestation des chutes de grêle.

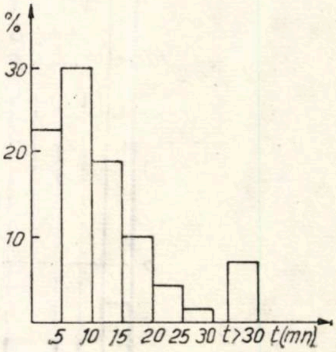

Fig. 12. La durée des cheuts de grêle en France.

IV. La distribution géographique et ses influences

La grêle est un phénomène local. Dans l'ensemble, la latitude et l'altitude en sont des facteurs déterminants. La Roumanie en est assez fréquemment affectée dans toutes ses regions, en raison de sa position géographique (45° latitude N). Il existe cependant des zones de fréquence diverses pour les chutes de grêle, suivant les particularités de la surface sous-jacente. Le nombre de jours de grêle enregistrés par 137 stations à service permanent en Roumanie, représenté dans la figure 13, offre une vue d'ensemble de la période considérée. Cette carte permet de constater quelques traits particuliers.

Ainsi, la Mer Noire, le Delta du Danube ainsi que les lacs du littoral (Razelm, Sinoe etc.) ont une action protectrice grâce à laquelle en Dobrogea il n'y aeu pendant15ans que 6 à 8 chutes de grêle. Près deces régions, la température assez basse de l'eau à la surface pendant les mois chauds réduit la convection thermique. Le même phénomène a été constaté dans la région de la Mer Caspienne, du lac Baïkal et dans la région des grands lacs canadiens [7] [9].

Dans la littérature il a été montré que le facteur grêligène R d'une région à influence maritime ne diffère pas de celui d'une région colatitudinaire à influence contientale. Les chutes de grêle y seraient donc plus rares tout simplement en raisond e nombre plus petit d'orages [7] [9].

Sur le cours de certaines rivières à vallée plus profonde telles que Siret, Olt etc. il y a eu moins de chutes de grêle en 15 ans grâce à la

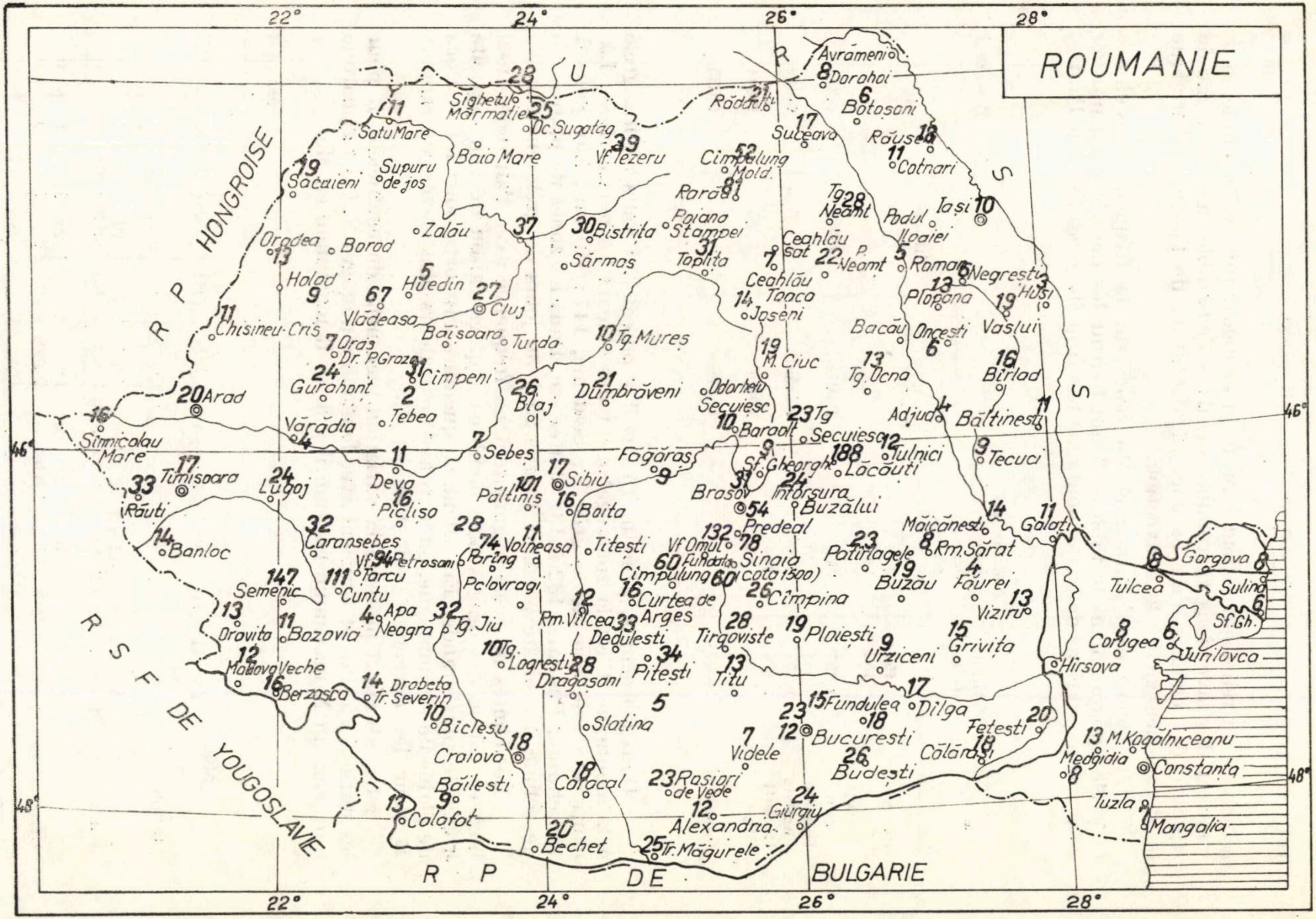
ROUMANIE
22°
24°
26°
28°
46°
48°
R P HONGROISE
U R S S
R S F DE YOUGOSLAVIE
R P DE BULGARIE
8 Avrameni
8 Dorohoi
6 Botoșani
18 Răuseni
11 Cotnari
24 Rădăuți
17 Suceava
52 Cîmpulung Mold.
81 Rarău
28 Tg Neamț
10 Iași
Podul Iloaiei
5 Roman
22 P. Neamț
7 Ceahlău sat
Ceahlău Toaca
14 Joseni
31 Poiana Stampei
Toplița
30 Bistrița
Sărmaș
39 Vf. Iezeru
25 Sighetul Marmației
28
25 Oc. Sugatag
Baia Mare
11 Satu Mare
19 Săcăieni
Supuru de jos
37
Zalău
13 Oradea
Borod
9 Holod
5 Huedin
67 Vlădeasa
27 Cluj
Băișoara
Turda
10 Tg. Mureș
11 Chișineu-Criș
7 Oraș Dr. P. Groza
24 Gurahonț
31 Cîmpeni
2 Tebea
20 Arad
4 Vărădia
16 Sînnicolau Mare
33 Răuți
17 Timișoara
24 Lugoj
11 Deva
16 Picliso
7 Sebeș
26 Blaj
21 Dumbrăveni
Odorheiu Secuiesc
19 M. Ciuc
13 Tg. Ocna
Bacău
6 Onești
13 Plopana
6 Negrești
3 Huși
19 Vaslui
16 Bîrlad
4 Adjud
11 Băltinești
10 Baraolt
23 Tg Secuiesc
9 Sf. Gheorghe
188 Lăcăuți
12 Tulnici
9 Tecuci
17 Sibiu
101 Păltiniș
16 Boița
9 Făgăraș
31 Brașov
24 Întorsura Buzăului
54 Predeal
132 Vf Omul
78 Sinaia (cota 1500)
60 Fundata
60 Cîmpulung
14 Măicănești
11 Galați
23 Pătîrlagele
8 Rm. Sărat
19 Buzău
4 Făurei
13 Viziru
15 Grivița
14 Banloc
32 Caransebeș
28
74 Voineasa
11
94 Vf. Petroșani
Parîng
Polovragi
111 Tarcu
147 Semenic
Cuntu
4 Apa Neagra
32 Tg. Jiu
12 Rm. Vîlcea
Titești
16 Curtea de Argeș
26 Cîmpina
33 Dedulești
28 Tîrgoviște
19 Ploiești
9 Urziceni
13 Oravița
11 Bozovici
12 Moldova Veche
16 Berzasca
14 Drobeta Tr. Severin
10 Tg. Logrești
28 Drăgășani
34 Pitești
13 Titu
5
17
15 Fundulea
18 Dîlga
20 Fetești
18 Călărași
10 Bicleșu
18 Craiova
Slatina
7 Videle
23 București
12
26 Budești
9 Băilești
13 Calafat
18 Caracal
23 Roșiori de Vede
12 Alexandria
24 Giurgiu
20 Bechet
25 Tr. Măgurele
8 Gorgova
8 Sulina
6 Sf. Gh.
Tulcea
8 Cerugea
6 Jurilovca
Hîrșova
13 M. Kogălniceanu
8 Medgidia
Constanța
Tuzla
Mangalia

Fig. 13. **La Carte de la Roumanie avec le nombre de jours à chute de grêle pendant la période de 1961 à 1975, à 137 stations permanentes.**

BUDAPESTI MŰSZAKI EGYETEM * 1848 KÖZPONTI KÖNYVTÁRA

concavité du relief qui retient l'air froid et dense qui s'y accumule, provoquant des inversions thermiques et, dans l'ensemble, une plus grande stabilité des ciuches d'air et une augmentation de l'énergie thermique de déclenchement de la convection.

L'influence de l'altitude et du relief sur la fréquence des chutes de grêle apparaît dans le tableau 3 qui fournit les donnée comparatives de plusieurs stations de basse montagne pas trop éloignées l'une de l'autre.

Tableau 3

Station	Altitude (m)	No. des cas enregistrés pendant 15 ans
Păltiniş	1 454	146
Sibiu	452	17
Pic Vlădeasa	1 837	67
Huedin	558	5
Fundata	1 371	139
Lăcăuţi	1 176	188
Dîlga	95	17
Urziceni	55	9
Fundulea	67	18

Tableau 4

Station	Altitude (m)	R
Păltiniş	1 454	0,385
Lăcăuţi	1 176	0,849
Dîlga	95	0,044
Urziceni	55	0,025

Dans l'ensembie, pendant 15 ans il y plus de 50 jours ou il a grêlé à la montagne. C'est la zone également des valeurs les plus élevées : Lăcăuţi, 188 ("le pôle de la grêle") ; Semenic, 147 ; Păltiniş, 101 jours à 146 chutes ; Fundata, 132 à 139 chutes etc. Dans les zones de plateau ou de colline il a eixsté pendant 15 ans 25 à 30 jours de grêle environ.

Les chutes de grêle augmentent en fréquence avec l'altitude aussi bien en raison des orages plus nombreux, qu'en raison de leur capacité grêligène plus grande. En calculant quelques rapports pour les stations de plaine de et montagne, on a trouvé des valeurs plus élevées du rapport R pour les dernières (voir tableau 4).

Le tableau 5 présente la variation mensuelle du coefficient R pour les stations Păltiniş et Urziceni avec le nombre d'orages N. On y remarque que pour un N maximum en Juin il y a un R maximum en Mai.

Tableau 5

Station	Mois	I	II	III	IV	V	VI	VII	VIII	IX	X	XI	XII
Păltiniş	N	6	2	2	12	73	95	76	78	19	2	1	0
	R	0	0,5	0	0,41	0,47	0,23	0,24	0,18	0,31	0	0	0
Urziceni	N	0	2	2	20	64	96	85	51	23	13	1	0
	R	0	0	0	0,1	0,08	0,02	0,01	0	0	0	0	0

V. Conclusions

1. Aux stations Păltiniş—Sibiu et Fundata—Braşov il a grêlé avec des grêlons ayant une taille de 4—5 mm environ en diamètre dans la plupart des cas. La taille maximum jamais observée à une station de Roumanie a été 7 cm, le 1-et Juillet 1975 à Bucarest—Afumaţi.

2. Les données statistiques montrent qu'en Roumanie entre les 1-er Décembre et 1-er Février il n'y a pas eu de chute de grêle alors qu'il y en a eu en abondance entre Avril et Septembre (95,5%), entre les 20 Mai et 20 Juin (30,1%) et entre les 20 Mai et 1-er Juin (11,3%).

3. Le minimum de variation diurne se situe entre 5 et 6 heures du matin (0,34%) et le maximum entre 14 et 15 heures (13,2%). Des chutes de grêle a moins de 1% par heure, d'origine frontale, se produisent pendant toute la journée sans une fréquence prédominante et sur celles-ci se superpose entre 9 et 22 heures l'effet de la convection diurne. Les pourcentages cumulatifs sont entre 9 et 22 heures plus de 1% par heure et 92% du total, entre 11 et 19 heures plus de 5% par heure et 80% du total, entre 12 et 17 heures plus de 10% par heure et 59% du total.

4. 48% des chutes de grêle durent entre 4 et 8 minutes. Une durée maximum de 105 minutes a été enregistrée à la station de montagne de Lăcăuţi.

5. La carte présentée démontre l'influence protectrice de la Mer Noire, du Delta du Danube et des lacs du littoral. De même, il en ressort la grande capacité grêligène des orages qui se produisent à la montagne, surtout à la station Lăcăuţi (188 chutes pendant 15 ans, R = 0, 849).

BIBLIOGRAPHIE

1. I. O. BĂLCESCU, MILITARU FLORICA, in *Culegere de lucrări de meteorologie ale I. M.H. pe anul 1964*, 95, 1966.
2. I. O. BĂLCESCU, MILITARU FLORICA, in *Culegere de lucrări de meteorologie ale I.M.H. pe anul 1965*, 47, 1967.
3. BESSON, Ann. des serv. techn. d'hygiène de la ville de Paris, 14, 148, 1932.
4. C. CĂPUZ, in *Culegere de lucrări de meteorologie ale I.M.H.* pe anul 1972, 253, 1974.
5. GH. CIUMAC, Revista Pădurilor, 1, 32, 1952.
6. ELENA DECU et collab. *Grindina, condiţii de producere şi metode de combatere*, Facultatea de Fizică, Bucureşti, 1976.
7. R. GENÈVE, LE SAOUT, *Note E.E.R.M.*, 5, *Météorologie nationale*, Paris, 1959.
8. R. GENÈVE, *La grêle, Memorial de la Météorologie Nationale*, 48, 1961.
9. POSTUK, SOKHRINA, *Trudi G. G. O.*, Leningrad, 74, 3, 1958.
10. F. H. LUDLAM, Nubila, 1, 12, 1958.
11. R. K. SOUTER, J. B. EMERSON, N. A. C. A., Tech. note 2734, 162, 1952.
12. N. ZAMIFRESCU, GH. CONSTANTINESCU, GH. BÎLTEANU, Probleme agricole, 11, 70, 1959.

Recu le 8-I-1978

ANALELE UNIVERSITĂŢII BUCUREŞTI, FIZICA, XXVII, 1978, pag. 121–130.

THE INVESTIGATION OF THE THREE-DIMENSIONAL LIGHT DISTRIBUTION NEAR FOCUS WITH LASER BEAM

G. G. BRĂTESCU and T. TUDOR
Faculty of Physics, University of Bucharest*

ABSTRACT

The main results of the scalar theory of the optical field in the neighbourhood of the focus are rewieved. It is presented a laser beam arrangement for the experimental investigation of the intensity distribution near focus, and some experimental results obtained with this arrangement.

Introduction

The three-dimensional light distribution near the focus of a well corrected lens is esentially the diffraction distribution on the aperture of the lens.

On the basis of Kirchhoff theory of diffraction[1], Lommel[2] and in dependently Struve[3] calculated the light distribution near focuses. Especially Lommel's works offer a clear analyses of the problem; he expressed the intensity in terms of convergent series of Bessel functions, so-called Lommel functions. Lommel and Struve's works did not quite call the attention at that time and the problem was treated again over more than twenty years, by Debye[4] who introduced on this occasion the field integral representation which carries his name.

Finally, during the up-to-date development of the undulatory optics, the light distribution near focus is treated theoretically exhaustively by Zernike and Nijboer[5] and later independently by Linfoot and Wolf[6]; diagrams were published which show in detail the field in this complex region[6–9].

Experimental confirmations of the theory previsions were obtained first in microwaves range by P. A. Mathews and A. L. Cullen[10] for the case of rectangular aperture and by M. P. Bachynski and G. Bekefi[11] for circular aperture. C. A. Taylor and B. J. Thompson[12] perform the first comprehensive check of the theory results in the optical range, working the thermical light of a mercury vapor lamp so that to present a coherence degree enough for coformity with the theory. Such an exigency has as reverse the weakening of intensity in the diffraction picture, fact which imposed the limits of the method, making impossible the raising of intensity maps on the basis of quantitative photometrical measurements.

---

* *National Center of Physics, P.O. Box* 5211, Măgurele, Bucharest

The optimum frame — natural in the present — of complete, experimental approach of the problem is offered by laser radiations. This supplies, on one hand, the coherent wave fronts which the above mentioned theoretical treatments suppose, and, on the other hand, the intensity necessary for quantitative photometrical determinations.

Theory

1. *General formulas of intensity distribution near focus.*

Especially, the case of circular aperture was treated in details due to its simple symmetry, as weil as it reffers to usual situations of practical interest.

Let Σ be a spherical monochromatic coherent wave, supplied by a well corrected optical system with exit aperture of radius a, converging towards the axial focal point 0 (fig. 1). We shall be interested by the complex amplitude and, particularly, the intensity in some P point in the neighbourhood of the geometrical focus 0: we shall denote $\vec{R}$ the position vector of this point and $\vec{q}f$ the position vector of a current point of wave front, relative to 0.

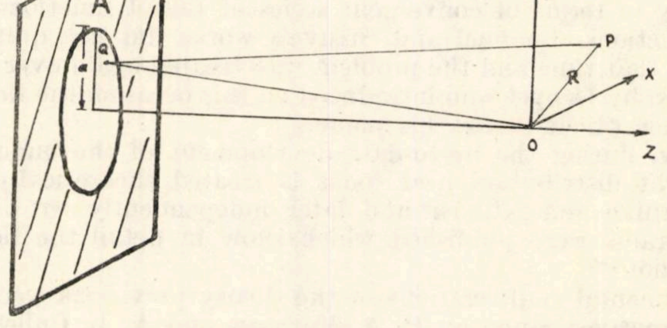

Figure 1. Diffraction of a converging, spherical wave at a circular aperture: notation.

If $f \gg a \gg \lambda$, $f \gg R$ we are in the conditions of Kirchhoff's approximation and the amplitude at P may be written as a superposition of contributions of plane waves that are propagated in the directions of the geometrical rays, from all Q points of the aperture towards P point according to Fresnel -Kirchhoff diffraction integral:

$$U(P) = -\frac{i}{\lambda}\,\frac{A\mathrm{e}^{-ikf}}{f}\iint_{\Sigma}\frac{\mathrm{e}^{iks}}{s}\,dS \qquad (1)$$

where $s{=}PQ$ and A/f is the amplitude at Q of the incident wave. As

$$s - f \approx -\vec{q}\vec{R}$$

the diffraction integral may be written under the form given by Debye:

$$U(P) = -\frac{i}{\lambda}A\iint_{\Omega}\mathrm{e}^{-ik\vec{q}\vec{R}}d\Omega \qquad (2)$$

where $d\Omega = dS/f^2$ is the element of the solid angle that subtends at O the surface element dS around Q point: the integration is extended over the solid angle Ω which the aperture subtends at the focus.

To evaluate the diffraction integral (2) we shall pass, adequately to the problem symmetry, from the Cartesian coordinates of $P(x, y, z)$ and $Q(\xi, \eta, \zeta)$ points at the cylindrical coordinates (r, ψ, z) respectively $(a\rho, \theta, \zeta)$

$$\xi = a\rho\sin\theta \qquad x = r\sin\psi$$

$$\eta = a\rho\cos\theta \qquad y = r\cos\psi$$

ρ being the polar radius normalized to the unit of Q point. Since Q lies on the spherical wave-front:

$$\zeta = -\sqrt{f^2 - a^2\rho^2} \approx -f\left(1 - \frac{1}{2}\frac{a^2\rho^2}{f^2} + \ldots\right)$$

With these:

$$\vec{q}\vec{R} = \frac{x\xi + y\eta + z\zeta}{f} = \frac{a\rho R\cos(\theta - \psi)}{f} - z\left(1 - \frac{1}{2}\frac{a^2\rho^2}{f^2} + \ldots\right) \qquad (4)$$

It is useful to introduce for the characterisation of the position of the observation point, the dimensionless variables u and v defined as follows:

$$u = \frac{2\pi}{\lambda}\left(\frac{a}{f}\right)^2 z \qquad (5)$$

$$v = \frac{2\pi}{\lambda}\left(\frac{a}{f}\right)r = \frac{2\pi}{\lambda}\,\frac{a}{f}\sqrt{x^2 + a^2} \qquad (6)$$

u and v are some standard variables which, as we shall see, have a striking physical significance: in the intensity chart $u/4\pi$ represents the number of fringes of defocusing and v/π the number of fringes of lateral displacement of P from the axis. In the intensity chart (fig. 3) minima (i. e. fringes of defocusing) may be seen along the u axis at 4π, 8π, etc; along the v axis the minima (i. e., fringes of lateral displacement) occur at intervals of π. It is also to mention that the point lies in the direct beam of light or in the geometrical shadow, according as $\left|\frac{v}{u}\right| < 1$ or $\left|\frac{v}{u}\right| > 1$, indeed, for instance if $\left|\frac{v}{u}\right| < 1$ i. e. $\left|\frac{r}{z}\right| < \left|\frac{a}{f}\right|$, the observation point is in direct light (fig. 2).

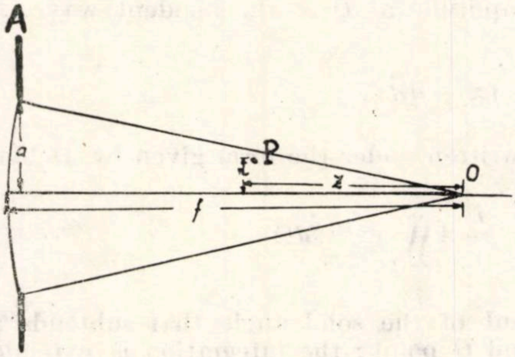

Figure 2. The observation point situated in the direct illuminated region; the condition $\left|\frac{u}{v}\right| > 1$

With these dimensionless variables, in the second order approximation relatively to ρ/f, we obtain:

$$k\vec{q}\vec{R} = v\rho\cos(\theta - \psi) - \left(\frac{f}{a}\right)^2 u + \frac{1}{2}u\rho^2 \tag{7}$$

and expressing the element of the solid angle

$$d\Omega = \frac{dS}{f^2} = \frac{a^2\rho d\rho d\theta}{f^2}$$

Debye's integral (2) becomes:

$$U(P) = -\frac{i}{\lambda}\frac{a^2A}{f^2}\,e^{i\left(\frac{f}{a}\right)^2 u}\int_0^1\int_0^{2\pi} e^{-i\left[v\rho\cos(\theta-\psi)+\frac{1}{2}u\rho^2\right]}\rho d\rho d\theta \tag{8}$$

With the integral representation of Bessel's functions,

$$J_n(x) = \frac{i^{-n}}{2\pi}\int_0^{2\pi} e^{-ix\cos\alpha}\,e^{in\alpha}\,d\alpha$$

the integral with respect to θ in (8) is written as $2\pi J_0(\mathrm{v})$ so that the complex amplitude at the observation point P, is :

$$U(P = -\frac{2\pi i a^2 A}{\lambda f^2}\, \mathrm{e}^{\,i\left(\frac{f}{a}\right)^2 u} \int_0^1 J_0(v\rho)\,\mathrm{e}^{-\frac{1}{2} i u \rho^2}\, \rho d\rho \tag{9}$$

where

$$\int_0^1 \mathrm{J}_0(v\rho)\,\mathrm{e}^{-\frac{1}{2} i u \rho^2}\, \rho d\rho \tag{10}$$

is the so-called Lommel 's integral. The calculation of this integral is based on a iterative procedure and the result is given as a sume of series of Bessel's functions, the so-called Lommel's functions. Writting

$$U_n(u, v) = \sum_{j=0}^{\infty} (-1)^j \left(\frac{u}{v}\right)^{n+2j} J_{n+2j}(v) \tag{11}$$

and

$$V_n(u, v) = \sum_{j=0}^{\infty} (-1)^j \left(\frac{v}{u}\right)^{n+2j} J_{n+2j}(v) \tag{12}$$

the Lommel's functions U and V of order n, the intensity in the neighbourhood of the focus is expressed finally, in the forms :

$$I(u,v) = I_0 \left(\frac{2}{u}\right)^2 [U_1^2(u, v) + U_2^2(u, v)] \tag{13}$$

and

$$I(u, v) = I_0 \left(\frac{2}{u}\right)^2 \left[1 + V_0^2\,(u,v) + V_1^2(u,v) - 2V_0(u,v)\cos\frac{1}{2}\left(u + \frac{v^2}{u}\right) - \right.$$
$$\left. -2V_1(u, v)\sin\frac{1}{2}\left(u + \frac{v^2}{u}\right)\right] \tag{14}$$

were

$$I_0 = \left(\frac{\pi a^2 A}{\lambda f^2}\right)^2 \tag{15}$$

is the intensity in the geometrical focus ($u = 0$, $v = 0$). The formulas (13) and (14) are equivalent and valid at all points in the neighbourhood of the focus ; but the first is only convenient for computation for $\left|\frac{u}{v}\right| < 1$ — i. e. when the point of observation lies in the geometrical shadow — and the second for $\left|\frac{u}{v}\right| > 1$ — when the observation point lies in the illuminated region.

Based on these formulas, it has been calculated the intensity distribution in the neighbourhood of the focus and diagrams of this distribution have been represented[7,5,6,1]. In fig. 3, we show the most spread out representation in the speciality literature, of the intensity distribution near the focus calculated according to the scalar theory. The focus represents the contour lines of the intensity (isophotes) in a meridional plane near focus. The three-dimensional intensity distribution is obtained by rotating this figure around the optical axis. It is simmetrical about the geometrical focal plane.

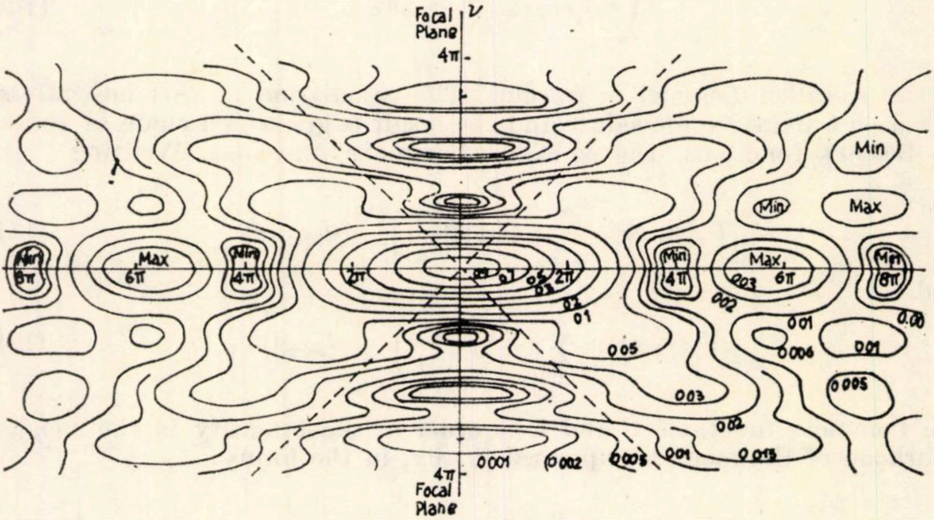

Figure 3. Isophotes (lines of equal intensity) near the focus of a converging spherical wave diffracted at a circular aperture.

Of particular interest is :

a). The intensity distribution in the geometrical focal plane.

For this case $u=0$, and it is obtained from (13) :

$$I\,(0,\, v) = 4I_0 \left\{ \lim_{u \to 0} \left[\frac{U_1(u,\, v)}{u} \right]^2 + \lim_{u \to 0} \left[\frac{U_2\,(u,\, v)}{u} \right]^2 \right\}$$

and using the definiting relation (15) for U functions

$$I\,(0,\, v) = I_0 \left[\frac{2J_1(v)}{v} \right]^2 \tag{16}$$

The intensity distribution consists of a bright disc, centered on the geometrical focus, surrounded by concentric bright and dark rings. According to table I, the distance in v scale beween two successive minima of the intensity, is aproximately equal to π and tends asymptotically to π with the increasing of minima orders. This justifies the denomination or $\frac{v}{\pi}$ as number of fringes of lateral displacement of P from axis and the role of dimensionaless variable v in the calculus.

Table I

v	$\left[\frac{2 J_1(v)}{v}\right]^2$	
0	1	Max
$1{,}220\pi$	0	Min
$1{,}635\pi$	0,0175	Max
$2{,}233\pi$	0	Min
$2{,}679\pi$	0,0042	Max
$3{,}238\pi$	0	Min
$3{,}699\pi$	0,0016	Max

b). The intensity distribution along the optical axis:

For this case $v=0$; from (12) $V_0(u,0)=1$, $V_1(u,0)=0$, and from (14)

$$I(u,v)=I_0\left(\frac{\sin\frac{u}{4}}{\frac{u}{4}}\right)^2 \qquad (17)$$

Thus the intensity distribution along the axis is characterized by the function $\sin\frac{u}{4}$: as it is well known, the interval between two successive minima (except those bordering the central maximum) of this function is $\frac{u}{4}=\pi$: this justifies the denomination of the quantity $\frac{u}{4\pi}$ as number of fringes of defocusing of P, and the role of dimensionless variable u, in the calculus. The first two minima of intensity are obtained at $\frac{u}{4}=\frac{\pi}{\lambda}\left(\frac{a}{f}\right)^2 z=\pm\pi$ thus at a distance $z=\pm\lambda\left(\frac{f}{a}\right)^2$ from the focus.

Experimental method. Results

The use of laser radiation has here — as in any interference or diffraction experiments — all the advantages connected to the coherence of such a radiation and its high energy density. The experimental arrangement which we used is shown in figure 4.

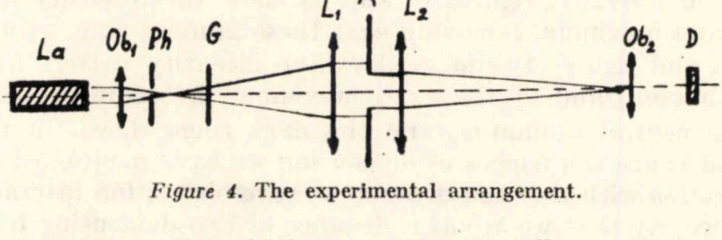

Figure 4. The experimental arrangement.

We have worked with a Spectra Physics 133 laser, which supplies an unpolarized beam; this allows us to be placed in the conditions of the above mentioned scalar theory. Because laser works in TEM_{00} mode, the intensity distribution in the cross section is a gaussian one. In order to become closer to the conditions of the theory, which implies a uniform intensity distribution on the wave front, the beam is passed through a suitable gaussian attenuator, G, which is obtained by impressing a photographic plate in the beam and by replacing it after development in the beam in the same position where the impressing was done.

The objective Ob_1(x 10) and the lens form an afocal system of expending: in their common focus is placed a pinhole *Ph*, for filtering. The circular aperture *A* with a 4 cm diameter, is placed in the parallel beams of coherent light, and the intensity distribution from the neighbourhood of the geometrical focus of the lens $L_2(f=$ cm) has been projected on the screen *E* by means of the objective Ob_2 (x 10).

The well known difficulties connected to the use of thermical light in such an experience (the very weak light flow in the arrangement, as a consequence of the prealable diaphragmation, imposed by the exigency of a highly enough coherence of the wave front at the aperture) are overcome by the use of the laser beam.

The intensity distributions near focus may be projected by the objective Ob_2 at distances of several meters with waste of illumination.

Another essential advantage of the use of laser beam in the investigation of the intensity distribution near focus is the possibility to perform quantitative photometrical determinations.

In this paper we shall deal only with the rising of some photographical recordings of the intensity distribution in several planes paralle to the focal plane (fig. 5).

The intensity distribution — formulae (13) or (14) and figure 3 — is simmetrical about the optical axis; particularly in planes parallel with the focal plane it shows up as a succesion of concentrical alternatively bright and dark rings. A minimum or a maximum of intensity will arise at the center according to $u=n.4\pi$, or $u = 0$; $(2n+1)2\pi$ respectively (where $n \geqslant 1$, integer)

The figures a) and c) show the intensity distribution in planes parallel to the focal plane at the second and the third axial minimum respectively ($u=8\pi$ and $u=12\pi$); figures b) and d) show the intensity distribution at the axial maximum following next these minima (i. e. at $u=10\pi$ and $u=14\pi$); and figures f) and e) show the intensity pattern at the fifth axial minimum, and at the axial maximum preceeding this minimum.

The central minimum, and the dark rings shown in the figures a), c) and f) are the fringes of defocusing we have mentioned previously in connection with the signification of variable u; for instance if $n=2$ (fig. a), we say that we are at a distance of two defocusing fringes from the geometrical focus. As the observation plane is moved further away from the focal plane new rings arise from the center, filling the optical field.

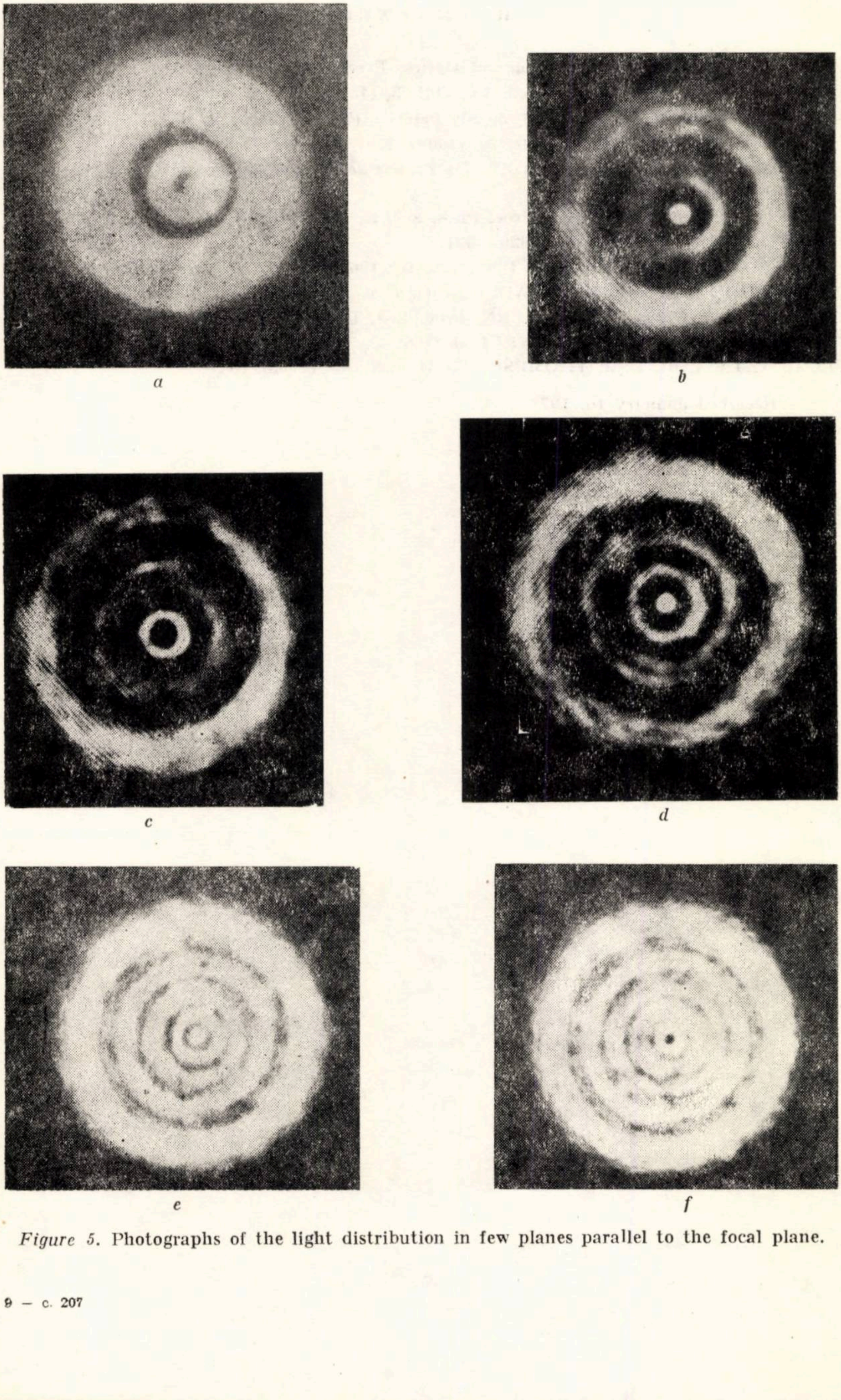

a b c d e f

Figure 5. **Photographs of the light distribution in few planes parallel to the focal plane.**

REFERENCES

1. M. BORN, E. WOLF, Principles of Optics, Pergamonn Press, 1970.
2. E. LOMMEL, Abh. Bayer Akad. 15, Abtl. 3, (1886), 531.
3. H. STRUVE, Mém. de l'Acad. de St. Petersb. (7), 34, (1886), 1.
4. P. DEBYE, Ann. d. Physik (4), 30, (1909), 775.
5. F. ZERNIKE, B. R. A. NIJBOER, *La Théorie des Images Optiques* (Paris, Revue d'Optique), 1949.
6. E. H. LINFOOT, E. WOLF, Proc. Phys. Soc. B, 69, (1956), 823.
7. M. BEREK, Z. Phys. 40, (1926), 421.
8. A. BOIVIN, E. WOLF, Phys. Rev., 138, B, (1965), 1561.
9. A. BOIVIN, J. DOWW, E. WOLF, J. O. S. A., 57, (1967), 1171.
10. P. A. MATHEWS, A. L. CULLEN, Proc. Inst. Electr. Engrs., Pt. C., 103, (1956), 449.
11. M. P. BACHYNSKI, G. BEKEFI, J. O. S. A., 47, (1957), 428.
12. C. A. TAYLOR, B. J. THOMPSON, J. O. S. A., 48, (1958), 844.

Received January 16, 1978

Abonamentele în ţară se pot contracta la oficiile P.T.T.R., agenţii poştali şi factorii poştali.

Cititorii din străinătate se pot abona, adresîndu-se la ILEXIM Departamentul Export-Import Presă, P.O.Box 136 — 137, telex: 11220, Bucureşti, str. 13 Decembrie nr. 3.

I.P.I. 207

BUDAPESTI MŰSZAKI EGYETEM
KÖZPONTI KÖNYVTÁRA
1848

Lei 22